Surface residue: eliminating a source of disorder in carbon nanotube devices

Delft, 2007

Johan van den Berg
Supervisor: Gary Steele

Summary

When devices are created on a silicon sample with carbon nanotubes, residue is left behind on the surface from this fabrication process. Because this has a negative impact the devices, methods were investigated to eliminate this residue.

First several samples without any devices were used to determine how a clean surface could be obtained. These experiments showed that while immersing the samples in dichloroethane was ineffective, heating them was shown to completely remove the residue, and created a surface that was in most cases almost identical to that before any resist had been applied. This method of cleaning the surface was highly effective, and can be explained by the decomposition of the polymer into volatile products.

The effect of this heating on the electrical properties of devices was also investigated by perfoming room temperature measurements on both nanotube devices and Aluminium Single electron transistors (Al-SETs).

Because our CNT devices also often include an Al-SET, it was important to characterize the effect of heating on the junction resistance of the Al-SET. An Al-SET initially showed a significant drop in resistance, but after additional heating this seemed to stabilize. This suggests that the heating method of residue removal is potentially compatible with Al-SETs.

To characterise the effect on CNT devices, metal contacts were deposited on CNTs to create a large number of CNT transistors. Initially (before baking) their properties already varied widely. After they were heated on a hotplate, the electrical properties of the devices changed significantly, although it was difficult to find a common trend. A second heating in an inert environment gave a similar result.

As a recommendation for the future, systematic low temperature methods should be performed to determine the exact effect of the removal of the residue on quality of carbon nanotube devices.

Contents

Summary 2
Contents 3
1 Introduction 4
2 Theory 5
2.1 Carbon nanotubes 5
2.2 Quantum dots 9
2.3 PMMA 10
3 Removing residue from samples 11
3.1 Non-fabricated samples 11
3.2 Fabricated samples 15
4 Effect on the electrical properties of devices 18
4.1 Single Electron Transistors 18
4.2 Nanotube devices 19
5 Conclusion 24
References 25
Appendix 26
AFM scans before and after cleaning 26
Design for cvd4g 41
Probestation measurements 43

1 Introduction

Nowadays a lot of research is going into quantum mechanical systems. This research happens using a wide range of materials, from biochemical molecules to semiconductors. Ultimately we would of course like to create a quantum computer. This is however still quite far away and for now research is focussed on more fundamental systems.

One material that shows interesting quantum mechanical properties are carbon nanotubes (CNTs). Because most carbon is ^{12}C, there are few nuclear spins that can interact with electrons as opposed to GaAs for example, where the nuclear spins cause short decoherence times. Therefore, CNTs could make a suitable material for creating quantum dots.
However, it is still difficult to actually create good quantum dots. After devices have been fabricated they tend to show disorder, which is believed to be caused largely by the interaction of the nanotube with the substrate surface. One possible source of this disorder is residue that is left on the substrate from the fabrication process. This project was focussed on removing this residue and thus trying to improve device quality.

2 Theory

This chapter covers the theoretical background on nanotubes and quantum dots. A section on the polymer PMMA has also been added, since this plays an important role in fabrication. Removal of PMMA residue is a main focus of this project. Most of the theory presented in the first two sections of this chapter is based on [1] and [2].

2.1 Carbon nanotubes

The first carbon nanotubes were discovered in 1991 by the Japanese scientist Sumio Iijima. These tubes were multiwalled, consisting of 2 to 50 graphene sheets [3]. About two years later, he also discovered single walled carbon nanotubes. With a typical diameter of around 1 nm they were even smaller than the multiwalled tubes [4].

Such single walled nanotubes can be thought of as graphene sheets which have been rolled up into a cylinder along a certain axis. Since there are many ways to construct a cylinder in this way, there are also many different types of carbon nanotubes.
A nanotube can be conveniently described by a vector in the crystal lattice of a graphene sheet. By looking at figure 2.1 it can be easily seen how this works. The vector $\mathbf{C} = n\mathbf{a}_1 + m\mathbf{a}_2$ uniquely defines the nanotube, where $\mathbf{a}_1$ and $\mathbf{a}_2$ are the unit vectors of the graphene lattice. Rolling up the graphene along the vector **C** so that the vector circles around the tube exactly once will form the (n, m) nanotube. For every (n, m) pair we can now find a specific chiral angle φ and a diameter d:

$$\phi = \arccos\left(\frac{\sqrt{3}(n+m)}{2\sqrt{n^2+m^2+nm}}\right) \tag{2.1}$$

$$d = \frac{a}{\pi}\sqrt{n^2+m^2+nm} \tag{2.2}$$

where $a = \left|\vec{a}_i\right| = 2.46\text{Å}$ is the lattice constant. For the vector C in the figure, which is the (12, 4) direction, this gives an angle of 16.1° and a diameter of 1.13 nm. The vector **T** is perpendicular to **C** and points from (0, 0) to the first lattice point along this direction. The area $\left|\vec{T}\times\vec{C}\right|$ is the primitive unit cell from which the nanotube can be constructed.
There are two special directions in the graphene, which result in a nonchiral tube. One of them is the (n, 0), the so-called zigzag direction, and the other is (n, n), the armchair direction. These directions differ by a 30° angle and are also indicated in the graphene lattice on the left of figure 2.1. On the right side in the image these two types of nonchiral nanotubes as well as a chiral tube can be seen.

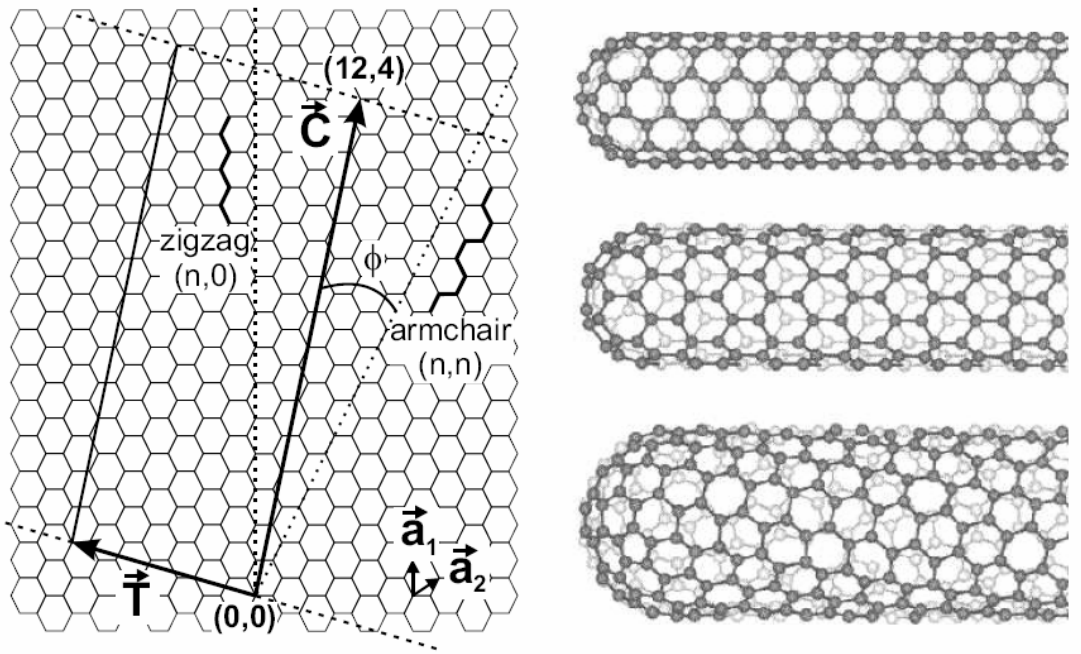

figure 2.1 Construction of a nanotube by taking the graphene between the dashed lines and wrapping it along the vector C. On the right an armchair (5, 5), a zigzag (9, 0) and a chiral (10, 5) nanotube can be seen. Image taken from [2].

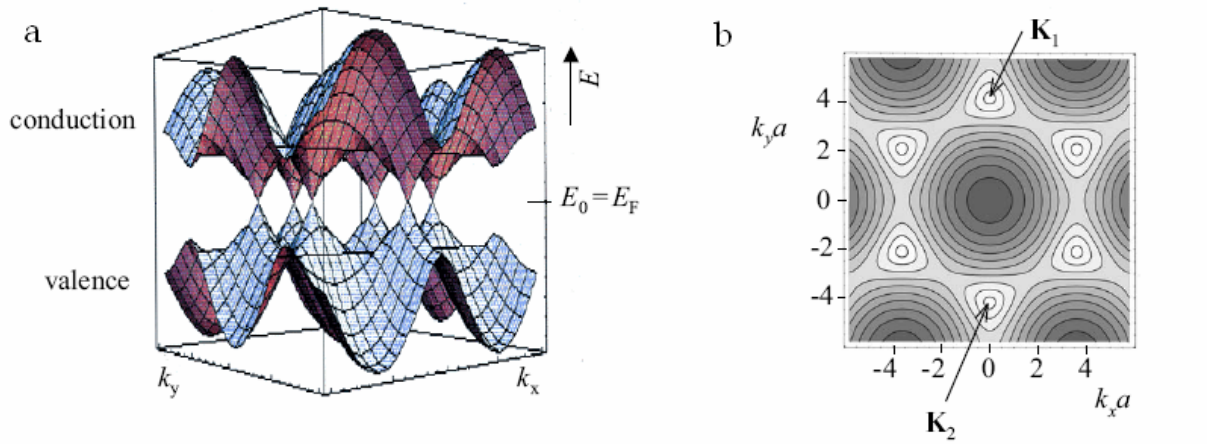

figure 2.2 (a) Energy dispersion relation for graphene. The conduction and valence band meet at six points called K-points, around which the dispersion is conical. (b) Contour plot of the valence state energies in (a). The six white points (darker means lower energy) are the K-points which define a hexagon that is the first Brillouin zone. Image reproduced from [5].

Because a carbon nanotube is a rolled up graphene sheet, its bandstructure can also be derived from the bandstructure of graphene. Therefore the bandstructure of graphene will first be discussed.

In a graphene sheet the carbon atoms are covalently bonded together. Since each atom has three nearest neighbours, each of the atoms forms three sp^2 'σ-bonds'. The fourth valence electron of each carbon atom occupies a p_z orbital. These orbitals mix together to form delocalized electron states ('π-bonds'). It is these states that determine the electrical conductivity properties of graphene.

The energy dispersion relation for graphene is shown in figure 2.2. It can be seen that there six points at which the conduction and valence band meet each other. These points are called 'K-points'. Only two of them are inequivalent, indicated by K_1 and

K_2 in figure 2.2b, the other points can be reached from K_1 or K_2 by a reciprocal lattice vector translation. Near the K-points the dispersion relation is conical, which is reflected by the circular contours around them.
It is important to know the shape and position of the cones near the K-points to understand electrical transport in graphene, because the electronic properties of a conductor are determined by electrons near the Fermi energy. The K_1 and K_2 points have coordinates $(k_x, k_y) = (0, \pm 4\pi/3a)$ and the slope of the cones is $\left(\sqrt{3}/2\right)\gamma_0 a$, where $\gamma_0 \sim 2.7$ eV is the energy overlap integral between neighbouring carbon atoms.

By imposing boundary conditions along the circumference of a CNT, the nanotube's bandstructure can be derived from the graphene bandstructure. Because the length of a CNT is generally much larger than its diameter, the spacing between the quantized values of the wavevectors is much larger in the direction perpendicular to the tube's axis, $k_\perp$, than in the parallel direction $k_\parallel$. If we consider infinitely long CNTs, the spacing between the allowed values for $k_\parallel$ vanishes, so then only the quantization due to the small nanotube diameter has to be taken into account. Imposing periodic boundary conditions along the circumference of the nanotube gives the allowed values for $k_\perp$:

$$\vec{C} \cdot \vec{k} = \pi d k_\perp = 2\pi j \,, \tag{2.3}$$

where d is the nanotube diameter and j is an integer. The spacing in $k_\perp$ is 2/d, which is quite large, because CNTs have a small diameter. Each allowed $k_\perp$ value creates a so-called one-dimensional subband in the longitudinal direction as shown in figure 2.3.

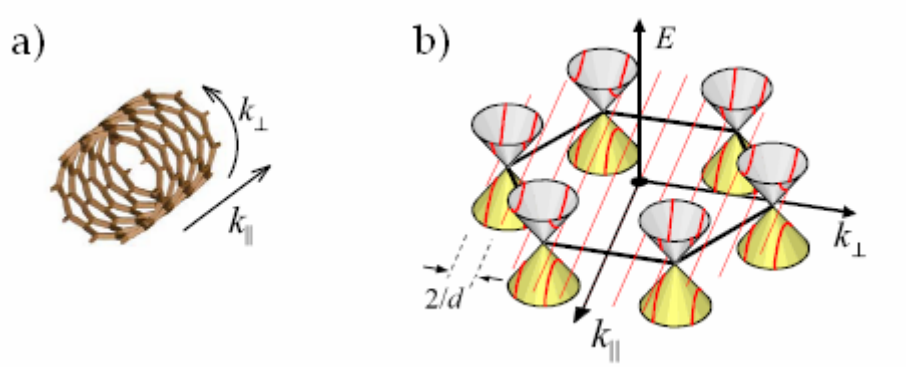

figure 2.3 (a) Section of a nanotube and the parallel and perpendicular directions. (b) Intersection of allowed k values with the dispersion cones define the electron states near E_f. These 1D subbands are obtained by imposing periodic boundary conditions along the CNT circumference. Image adapted from [5].

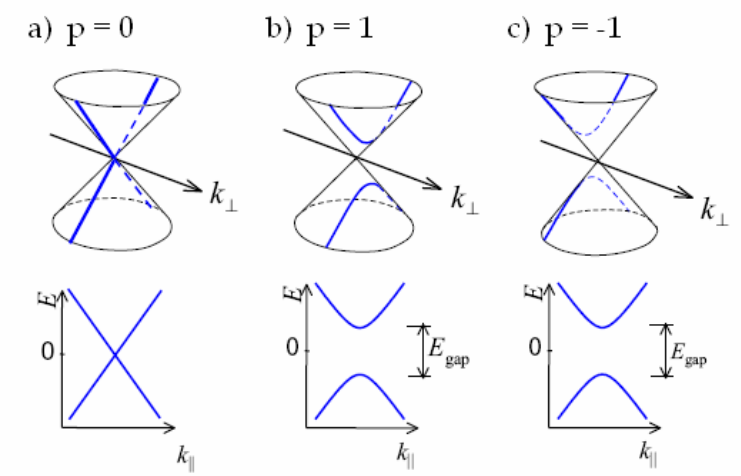

figure 2.4 Different band diagrams resulting from the different alignment between allowed k values and the dispersion cone.

What now determines the electrical properties of a CNT is the exact alignment between the dispersion cones and the allowed $k_\perp$ values. If one of those values goes exactly through the centre of a cone, we have a metallic tube, displayed in figure 2.4a. If not, there will be a gap between the valence and conduction band, as in figure 2.4b and c. Whether a given tube is metallic or conducting can be determined by calculating $n - m = 3q + p$, with q an integer and p -1, 0 or 1. For $p = 0$ the CNT will be metallic, for $p = 1$ and $p = -1$ the tube will be semiconducting. The bandgap of a semiconducting CNT is independent of its chirality. The $k_\perp$ value closest to the K-points misses them by $\Delta k_\perp = \pm 2/3d$ respectively for $p = \pm 1$. This leads to a bandgap value of $E_g = 2\hbar v_F \Delta k_\perp = 2\gamma_0 a / \left(\sqrt{3}d\right)$ ~0.8 eV/d[nm].

2.2 Quantum dots

A quantum dot (QD) is a small structure that has a discrete set of energy levels. Electrons in an object of finite size have a discrete energy spectrum according to quantum mechanics. So a small structure behaves like a quantum dot in an experiment, if the temperature is low enough to distinguish between different energy levels. Furthermore the electron must be at least partially confined to ensure a long enough lifetime of the energy levels.
Because in a CNT the momentum is quantized in the direction perpendicular to the axis, it usually considered a 1D object. In a real life experiment we will off course never have an infinitely long nanotube. Instead we will be dealing with only a section of the CNT, because metal contacts are created on the CNT. At the interface between the tube and the metal a tunnel barrier will naturally develop, confining the electrons and creating a zero dimensional structure. The distance between the metal contacts determines the length of the tube, whereas the height of the barriers determines how well the electrons are confined in the structure. A schematic picture of a CNTQD can be seen in figure 2.5.

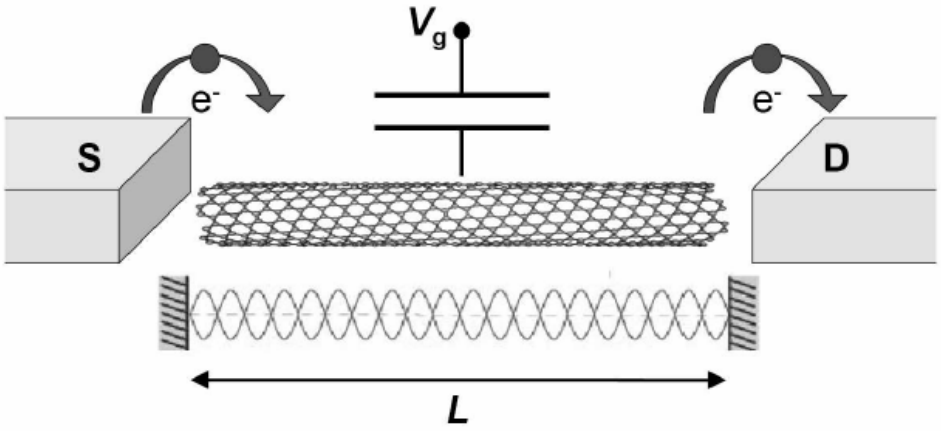

figure 2.5 Schematic overview of a CNT quantum dot. Two metal contacts deposited on the tube define the QD length. There is also a capactive coupling between the CNT and a gate electrode.

2.3 PMMA

Fabricating samples consists of several steps. First a set of markers is created to later determine the CNT location and for the fabrication of electrodes. This happens with electron beam lithography. Secondly, the nanotubes are grown on the sample from a deposited catalyst. The location of the nanotubes is then determined with AFM and a design is made for the sample. Finally, the sample goes through another e-beam cycle to create the designed electrodes.
The electron beam lithography involves spinning a layer (or actually two layers) of resist on the sample. For this resist normally the polymer polymethyl methacrylate (PMMA) is used. The structure of PMMA is as follows:

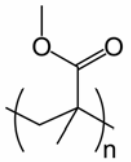

The two different layers used in fabrication differ in their molecular weight. This means that a polymer chain in one layer is on average longer than in the other layer. The typical length of a chain can be calculated with a model like the freely jointed chain or wormlike chain model. Using a value of 2.3 nm as the monomer length [7], this leads to a typical length of 136 nm for PMMA 350K and 224 nm for PMMA 950K.

After fabrication some of the used resist is left on the surface. Since this residue can cause disorder in a device, it should be removed. One way of trying to achieve this, is by baking the sample. An extensive review of burning PMMA has been made by W.R. Zeng, S.F. Li and W.K. Chow [6]. The relevant results will be summarized here.

PMMA decomposes in the absence as well as in the presence of oxygen when it is heated. Even though the mechanisms are different, the main decomposition product in both cases is the monomer MMA. The MMA can then further decompose into small gaseous products, which can burn if oxygen is present.
In the absence of oxygen there are two main processes of decomposition for radically polymerized PMMA (containing C=C bonds at the end). The first is terminal C=C bond scission in which the group at the end of chain breaks off, from where the polymer can then 'unzip' to create monomer. This stage starts around 220°C. The second process is random C-C bond, which starts around 300°C.At this temperature it is also the dominant process of decomposition. What happens is that a polymer chain breaks somewhere in the middle, creating two ends from which monomer can break off. Apart from these main-chain scissions there are also the minor process of random side-group scissions, which form methane and methanol.
In the presence of oxygen the reactions that occur are much more complicated. Macroradicals react with oxygen to create unstable hydroperoxides, which then quickly break down to create more free radicals. As mentioned, even though the mechanism is different, the main decomposition product is still monomer MMA. Also products such as 2-methyl-oxirane carbonic acid methyl ester, methyl pyruvate and dimethyl itaconate are produced, but only in small amounts.

3 Removing residue from samples

Because any contamination in the vicinity of a quantum dot can affect this dot, it is desirable to have a sample that is as clean as possible. However, after fabrication there will always be some residue on the surface. This is because the fabrication is done by e-beam lithography, which involves depositing resist on the surface. At the end of the fabrication the resist is removed again. This lift-off process doesn't actually remove all the resist, so that small amounts are still left on the sample surface.
In this chapter the experiments are discussed that were performed to determine a viable method for cleaning the surface of a sample.

3.1 Non-fabricated samples

In order to determine a proper cleaning method, first non-fabricated samples were considered. Four silicon samples (cut from the same wafer) were taken that had not undergone any fabrication step yet. Their surface therefore still had to be very clean. For every sample a couple of AFM scans were made of the surface. To get an accurate scan, a 2µm scan was made using the 12.8 µm 'E-scanner' with a scanning frequency of approximately 1 Hz. This provided a reference for later on. The Nanoscope software which controlled the AFM scanner also included image analysis functions. With this software a planefit and then a flattening operation were performed on every scan. Two examples of the resulting images are displayed in figure 3.1. The roughness function was then used to determine the RMS height of the silicon surface. To get an accurate value, a section without any obvious bumps or glitches was selected in every image. This resulted in an RMS value of 0.2 – 0.25 nm for the silicon surface.

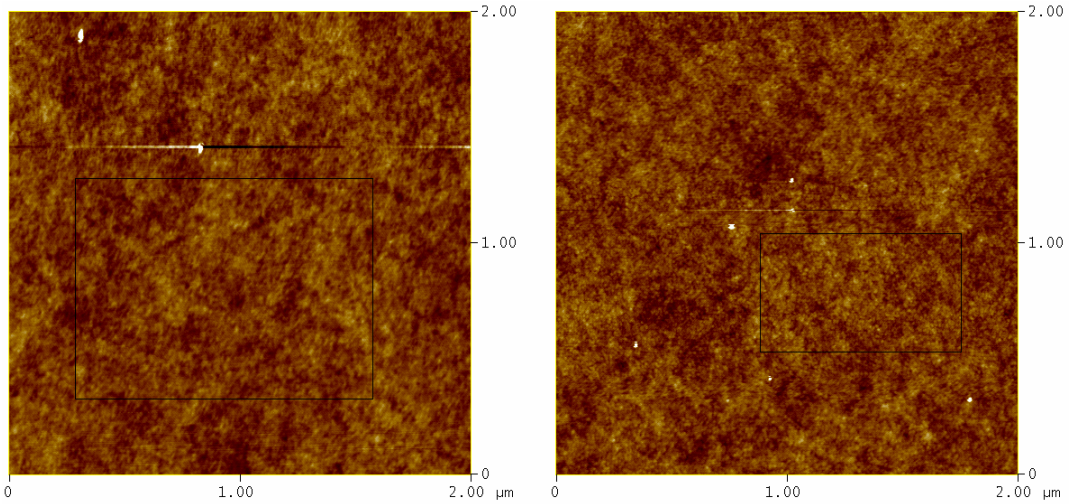

figure 3.1 Two AFM scans of the samples, taken before any treatment. The RMS of the silicon oxide surface is 0.2 to 0.25 nm.

When these scans were finished, resist was spun on each of the samples. Three of the samples all got a different, single layer of resist deposited on them. The used resists

for these were PMMA (poly-methyl methacrylate) 350K, PMGI (polymethylglutarimide) and a copolymer of MAA (methacrylic acid). The fourth sample was spun with two layers of resist; PMMA 350K and PMMA 950K, which is also used in actual fabrication.
The resist was then removed again from the samples in the usual way, without any further steps. Removing the resist is done by immersing the sample in hot acetone (60°C) for about half an hour. The sample is subsequently rinsed with cold acetone and iso-propyl alcohol and finally it's dried by blowing nitrogen over it.
After spinning and removing the resists, the samples were once again scanned with the AFM. A scan of each sample after planefitting and flattening is shown in figure 3.2. All the AFM scans made can be found in the appendix.
With the roughness function the RMS was again determined. For sample a (PMMA 350K) the RMS is 0.4 – 0.5 nm and for b (PMGI) it is also about 0.4 nm. In these samples the silicon surface is still visible. In the third sample (MAA) this is clearly not the case. This is also reflected in the RMS value, which is about 2 nm. Finally sample d (PMMA 350K + PMMA 950K) had an RMS value of 0.6 – 0.8 nm.

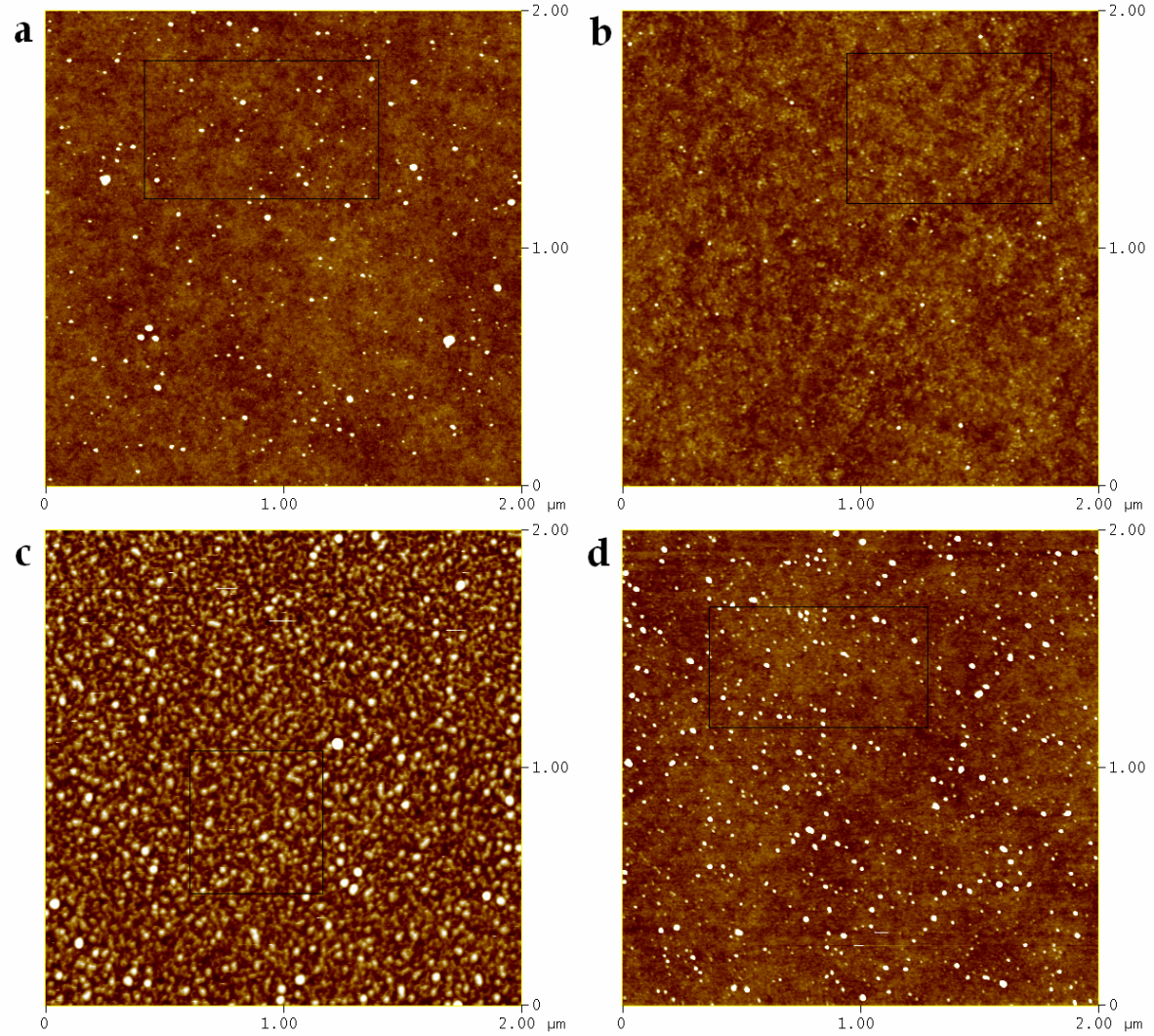

figure 3.2 AFM scans of the silicon surface after resist has been spun on and removed again. The used resists are PMMA 350K (a), PMGI (b), MAA (c) and for d two layers were used, one layer of PMMA 350K and one of PMMA 950K. Their RMS values are respectively 0.4-0.5 nm, 0.4 nm, 2 nm and 0.6-0.8nm.

Now the samples were ready to be cleaned. First every sample was cut into smaller pieces, so that different cleaning methods could be tried with a separate sample. The difficulty in finding a proper cleaning method is that it should not harm the device. For example, plasma is capable of removing the resist, but because it also destroys the carbon nanotubes, it can not be used to remove the residue.

The first method that was investigated, was trying to dissolve the residue in dichloroethane. This was chosen, because it has been observed in marker fabrication that immersing the sample in dichloroethane after the lift-off helps to remove small amounts of PMMA residue ([1], [2]). Just as with the lift-off in acetone, the samples were immersed in hot dichloroethane (60°C) for about 30 minutes. To determine the effect this cleaning procedure had, the samples were again scanned by AFM in the usual way. Figure 3.3 shows the images of these scans on the left side. The scans look very similar to those obtained before the cleaning procedure, so it seems that this method had little to no effect. This also can be concluded from the RMS values obtained from the scans, which were approximately equal to the RMS values before cleaning.

For the second set of samples we would simply try to get rid off the residue by baking the samples. This was done by putting the samples on a hotplate set to a temperature of 250°C for half an hour. Again AFM images were taken just as with the other samples, which can be seen on the right of figure 3.3.
This time a significant difference can be observed between the before and after images. If we look at the first sample, which was the one treated with PMMA 350K, we can see there is only a few bits of residue left. The RMS value of an area between those small amounts of residue is the same as that of the silicon surface before any treatment. Even if the entire scan is considered, the RMS of 0.34 nm is still lower than before the cleaning. For the second sample (PMGI), the result is similar. There is a bit more residue left than the PMMA sample and the blobs are a bit bigger. In between the residue the surface is again as clean as the untreated silicon. For the entire scan the RMS is comparable to the value before cleaning.
The third sample (MAA) shows an interesting image. It is clearly different from the ones before cleaning and after cleaning with dichloroethane. The RMS for this scan is about 1.2 nm, which is considerably lower than before the cleaning. However, this is still much higher than for a clean surface. What could be the case, is that heating the sample is indeed effective, but that the amount of residue on this sample is so big, that time the sample was left on the hotplate was not sufficient.
The last sample with the two layers of PMMA is again similar to the first sample with only a single layer of PMMA. Only very small amounts of residue are still left on the surface. A value of 0.23 nm for the RMS between these bits indicates that it really is just the silicon surface. For the entire image the value is only 0.26 nm, which is only slightly higher than that for the silicon surface. So the amount of residue left behind is indeed rather small.

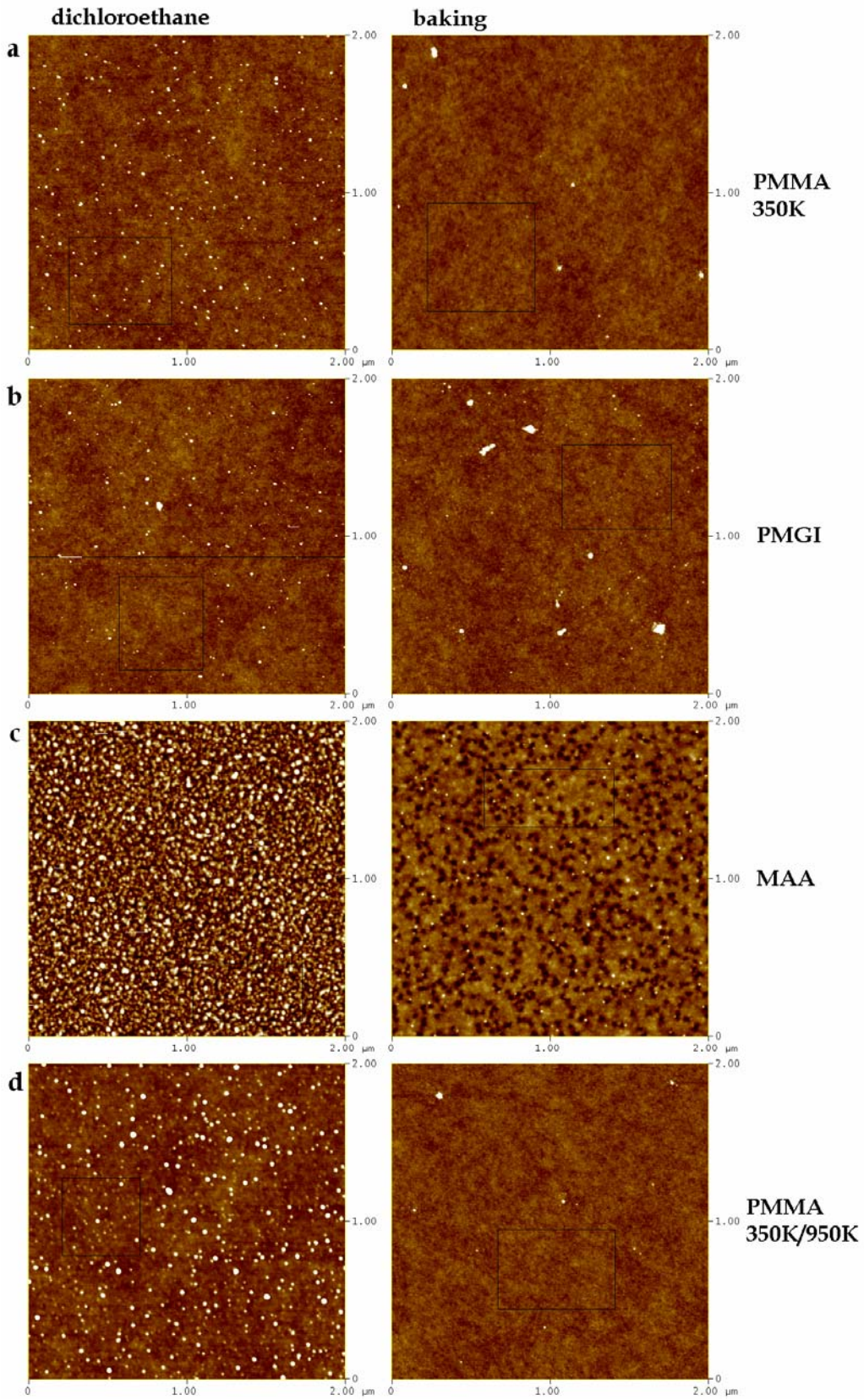

figure 3.3 AFM scans of the silicon after cleaning. The samples on the left were immersed in hot dichloroethane, while those on the right were put on a hotplate for 30 minutes at 250°C. The RMS values for the samples cleaned with dichloroethane are 0.4 nm, 0.4 nm, 2nm and 0.4-0.8nm respectively. For the heated samples these values are 0.34-0.38 nm, 0.36 nm, 1.2 nm and 0.26 nm for the entire scans. For the PMMA and PMGI samples the areas between the residue have an RMS of 0.2 to 0.25 nm, indicating that it really is the silicon surface.

3.2 Fabricated samples

Having determined that heating does a very good job in cleaning the surface of the non-fabricated samples, some more experiments were conducted on fabricated samples. A sample was available that had already been fabricated. Because the designed patterns were made too large by the lithography machine, there was no useful device on the sample. However, it was still well suited for examining the surface of a fabricated sample and the effect of heating on it.
To obtain a reference, first AFM scans were taken of the surface. The images obtained were rather remarkable. In the areas where according to AFM scans taken before fabrication, there should have been a nanotube, none were observed. Moreover, the metal contacts *did* show where a nanotube was, or at least where one had been, but at the edge of the metal there was no nanotube on the surface. In figure 3.4 this can be seen in the two left images. The chosen contrast makes it hard to see where the CNT runs under the metal, so in the middle image this is indicated by a black line just above it. On the silicon surface the tube should have been easy to spot, especially in the amplitude image (not shown), but that was clearly not the case. The explanation of this peculiar fact is that there was so much residue on the surface, that the nanotubes were completely buried under it. This became clear after the cleaning of the surface.
For determining the roughness a 2 micron scan (as with the non-fabricated samples) was taken between the devices and markers on the sample. This scan can be seen on the right of figure 3.4. From it an RMS value of 1.3 nm was determined for the fabricated sample before cleaning.

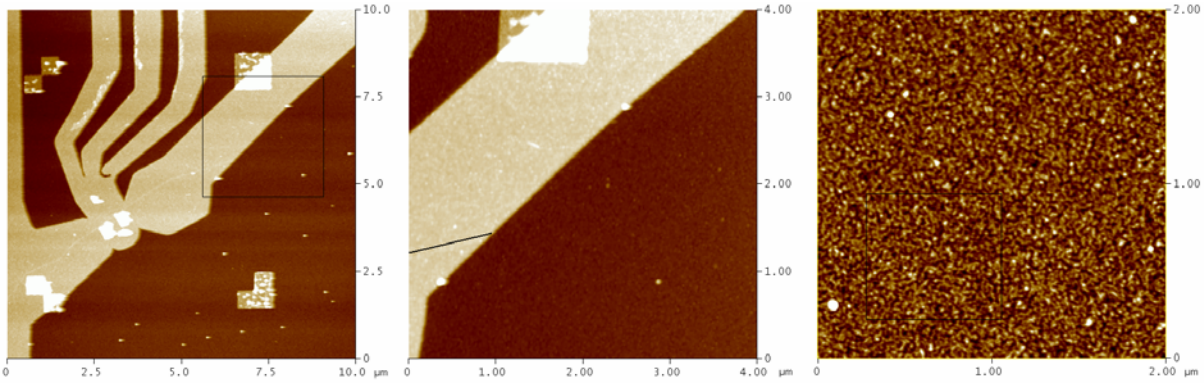

figure 3.4 AFM images of the surface of a fabricated sample. In the middle image, which is a close up of the left scan, a black line is drawn just above where the nanotube runs under the metal. The right image is a 2 x 2 µm scan of the silicon surface taken to determine the RMS.

After these scans the sample was put on the hotplate for 30 minutes at 250°C. In the AFM scan (figure 3.5 on the left) the nanotube can now be seen, as was mentioned before. The amount of residue on the surface is still quite large and since it is not so uniformly spread out over the surface anymore, the RMS has gone up to 2.4 nm. Because the sample was far from clean yet, it was heated up again. This time instead of a hotplate, the furnace was used in which the carbon nanotubes are grown on the samples (albeit in a different quartz tube). The sample was placed in the furnace for half an hour at a higher temperature of 350°C, to see whether the sample could

withstand such temperature and whether this might work better in terms of cleaning the surface. The image on the right of figure 3.5 shows an AFM scan of approximately the same area, after this second cleaning. The RMS of the area indicated by the black box is 0.65 nm, which is clearly an improvement over the uncleaned sample. Especially in this image it is obvious that there are a few spots around which a lot more residue is located than on the rest of the surface. When the scan on the left of figure 3.4 is compared to a scan after this second cleaning, it appears that these accumulations occur around features that were already clearly visible before cleaning (so they must be quite large). Why this happens is unclear, but it might be that resist is accumulating around imperfections on the original silicon surface.

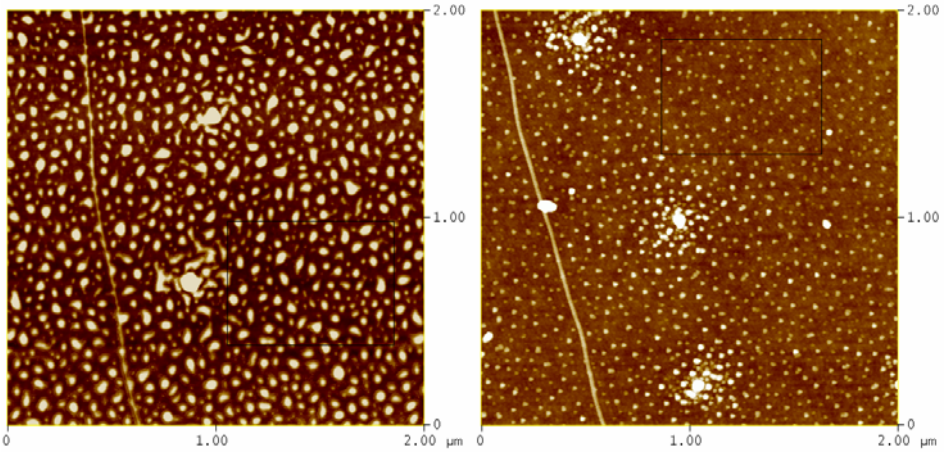

figure 3.5 The surface of the fabricated sample after cleaning. The left AFM scan is taken after 30 minutes on a hotplate at 250°C and the right image after another half hour in a furnace at 350°C.

Finally, in an attempt to remove the last bits of residue from the surface, the sample was again put in the furnace. This time it was set to 450°C and the sample was left in for an entire hour. Now something had happened to completely deform the metals on the surface, as can be seen on the right of figure 3.6.
Also the same area as in figure 3.5 was scanned (figure 3.6 on the left), which surprisingly showed very little improvement. The nanotube itself looks thinner, which could indicate that it is actually gone, leaving some residue in the area it had been. But then again this might just be related to the AFM tip or the scan rate (the scan in figure 3.5 was performed faster). Considering the heating time and temperature it is strange there is still residue on the surface. If it had all just been PMMA, the surface should have been clean for the most part. So something must have happened during the fabrication or cleaning stage.
The remaining residue could be something entirely different than PMMA, or it may be that the PMMA has reacted in some way to create a more thermally stable polymer. If the residue is something entirely different, it would probably have to originate from one of the solvents used in the fabrication process. Because there is such a lot of residue however, it seems more likely that the PMMA is altered in some way, probably by a reaction with oxygen or some contamination present. In the paper of Zeng et al. [6] it is also mentioned that the stability of PMMA can be

improved by additives. Though the chemicals mentioned there may not be present on our sample, there may very well other chemicals that have a similar effect.

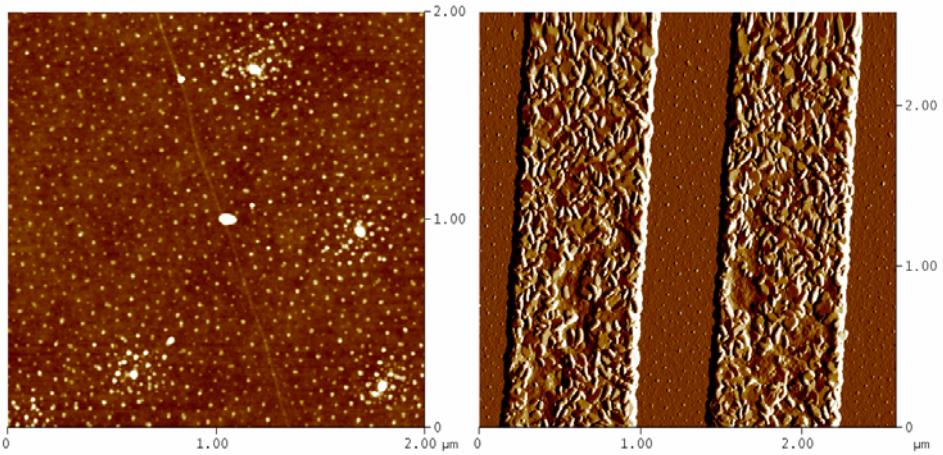

figure 3.6 The left image shows an AFM scan of the same area as in figure 3.5, after the sample has been put in the furnace for another hour at 450°C. On the right the amplitude image of two metal contacts on the same sample can be seen.

4 Effect on the electrical properties of devices

4.1 Single Electron Transistors

Besides using the AFM to investigate how the amount of residue on the surface is influenced by cleaning, also electrical measurements were performed. These measurements had to show what kind of effect the cleaning had. Hopefully the reduction of residue would have a positive effect on the electrical properties of the devices. Two different samples were used for measurements. One had a number of single electron transistors (SETs) on it, while the other was made with a large number of contacts on carbon nanotubes.
A sample with SETs on it had already been fabricated, so that was measured first. The electrical measurements consisted of simply determining the resistance of the SET. This was done by sweeping the applied voltage to the SET, and then measuring the resulting current. The sidegate was not used in these measurements.
Unfortunately, when the measurements before cleaning were performed, it turned out that three of the four SETs were not working. This left only one for determining what the effect is of heating the sample.
Initially the resistance was about 290 kΩ. The sample was then put on the hotplate for cleaning for 10 minutes at 280°C. After this, the resistance of the working SET was measured again, which had dropped to 180kΩ.
The second time the sample was heated another 10 minutes at again 280°C. This time a much smaller drop in resistance was measured to around 150kΩ.
For the third cleaning, the sample was put on the hotplate yet again for 10 minutes, but now at 300°C. The resistance then measured was 130kΩ.
Finally the sample was heated for the time of 1 hour at 300°C. Even though this was considerably longer than before, the resistance dropped only about 10kΩ to 120kΩ.
These measurements suggest that the effect of cleaning the samples by heating them is levelling out with longer heating periods. However, the initial change in resistance is unfortunately still very big, so it may be best to keep heating a sample with SETs to a minimum.

4.2 Nanotube devices

Not only SETs were considered, also a sample with CNT devices was fabricated to determine how these would react to heating. Because only room temperature measurements were performed no quantum dots were created. Instead one device consisted of two metal contacts connected to the CNT, with the doped silicon acting as a backgate (separated from the CNT by silicon oxide on the surface), thus creating a nanotube transistor. By making many contacts to the nanotubes on a sample, a large number of devices could be created. The design for the sample can be found in the appendix.
Since AFM scans for design had already been made after nanotube growth, no additional scans were made before fabrication. Then the sample was fabricated. The metal contacts were made of Cr/Au. Because in some parts of the sample there were some nanotubes that crossed at several locations on the surface, the sample was exposed to plasma in these locations to cut the nanotubes.
All the devices were measured with the probestation once the sample had been fabricated. For the measurement of a device a bias voltage of 10 mV was applied to one of the contacts. The current through the nanotube was then measured while the backgate voltage was varied. Care had to be taken not to ruin the devices by applying a too high backgate voltage or by sweeping the voltage too fast. Therefore a maximum backgate voltage of about 6V was used.
There were quite a number of devices that did not work, but there were still about 30 devices that did work. All of the nanotubes turned out to be semiconducting. Their quality varied greatly however in terms of noise and saturation current.

Before the sample was cleaned, a number of AFM scans were made to obtain a reference again for the amount of residue on the surface. For the roughness of the surface (away from any devices) a value of 0.7 nm was obtained. One of the places in which the nanotubes had been cut using plasma was also scanned. Surprisingly, this area seemed to have more residue on it than the unexposed areas. The right of figure 4.1 shows this AFM scan, while on the left the scan between the devices can be seen.

Why the area exposed to plasma has more residue on it is unclear, since the plasma should break up the polymer and leave a very clean substrate. The residue then presumably gets there during the lift-off process. It may be that even though the plasma should create a clean surface, at the same time a surface is created on which PMMA residue easily sticks.

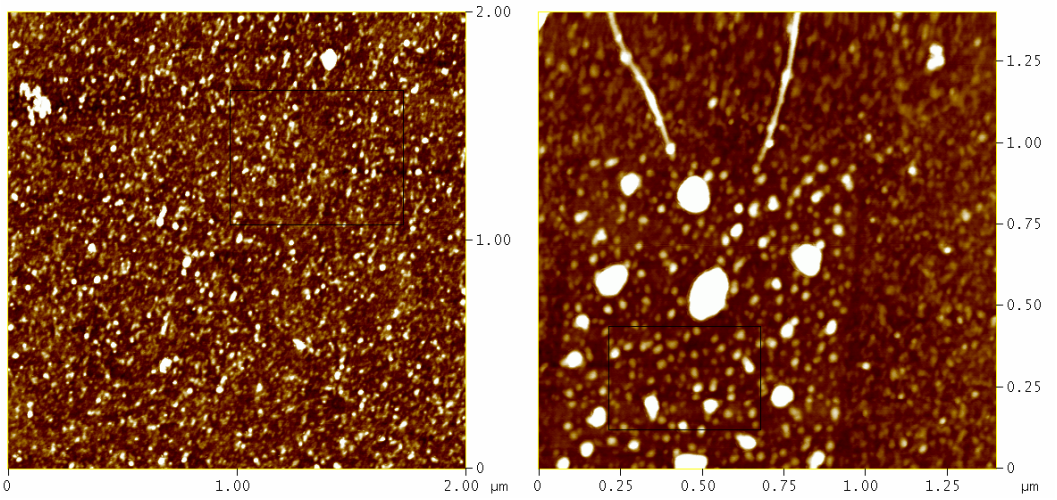

figure 4.1 Surface of the fabricated sample. The left image is an area without any tubes or contacts, whereas the right image shows an area where two intersecting nanotubes were cut with plasma. RMS of the left scan is 0.8 nm, and for the lower part of the area treated with plasma it is 1.6 nm.

Cleaning the sample was done at 300°C on the hotplate. The sample was left on there for 30 minutes.

The same areas as before cleaning were again scanned with the AFM. On the left of figure 4.2 the scan between the devices can be seen. It shows that the silicon surface between the devices now looked similar to that in figure 3.2a, the sample on which one layer of PMMA 350K had been deposited. At a value of 0.4 nm the RMS roughness is also equal to that sample. The area that had been exposed to the plasma to cut the nanotubes can be seen on the right side figure 4.2. It looks as if the substrate is starting to become visible between the large bumps, but other than that there does not seem to be a lot of improvement on this area. Also, the RMS is still about 1.6 nm in the area indicated by the black box.

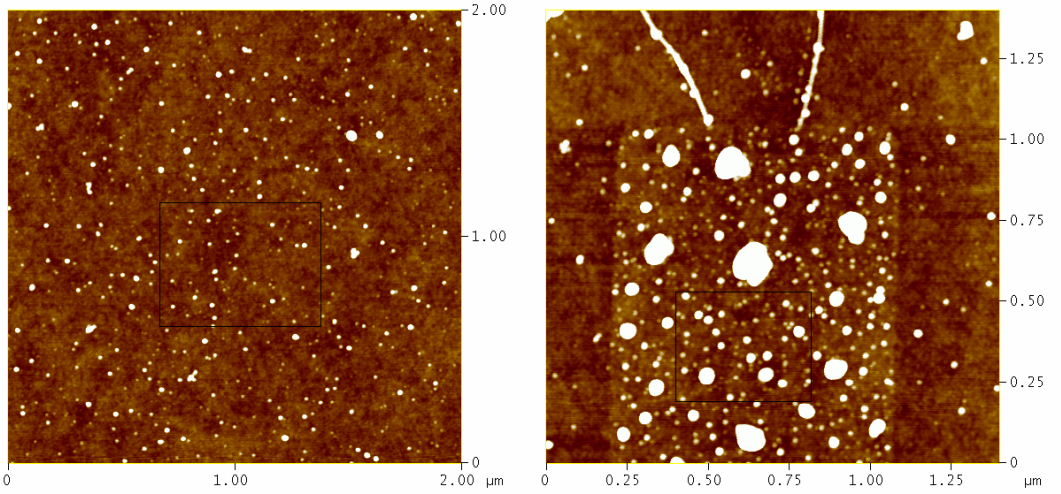

figure 4.2 Surface of the fabricated sample after heating in air at 300°C for 30 minutes. As in figure 4.1, the left shows an area without any tubes or contacts, while the right is the area where two intersecting nanotubes were cut with plasma. The area on the left has an RMS value of 0.4 nm and on the right it is 1.6 nm in the boxed area.

When the AFM scans were finished, electrical measurements were performed again. These were then compared to the measurements taken before baking. A summary of these results can be found in table 4.1. The devices were classified as one of three types according to their performance before the sample was heated. What these types were is explained below the table. Then the saturation current and the amount of noise are indicated for each device before cleaning as well as how this changed with the baking. All of the probestation measurements are included as graphs in the appendix.
The most apparent effect was that for all devices (as far as could be seen) the depletion region shifted towards higher backgate voltage after cleaning. For other characteristics the measurements were not that conclusive.
Devices that performed well (type I) generally got worse after the baking, because now a saturation current was visible. Some showed a decrease in noise, but because these devices already had little noise, not all of them really improved. When all the measured devices are considered, it seems that most of them decrease in noise.

As can be seen in the table as well, the samples were measured again after they had been cleaned for a second time. This time the sample was not put on a hotplate, but the furnace was used. It was placed in a quartz tube that is not used for nanotube growth and then argon was flown through the tube to create an inert environment. Just as with the hotplate the sample was heated for 30 minutes at 300°C.
Some AFM scans were again taken of the surface. Besides the area exposed to plasma that had been scanned before, also the areas around some of the devices were scanned.
This time definitely an improvement can be seen on the area exposed to plasma, because a few of the larger bumps have significantly decreased in height. The scan is displayed in the left of figure 4.3. The middle image show the area around device 1 from cvd4g1, and some noticeable features are present in this scan. First of all a nanotube seems to have moved over the surface, because there was not a connection between the two left contacts as can be seen now. Instead the tubes coming from under these contacts crossed somewhat left of this area and therefore they were cut with plasma. Besides this, a double tube can be seen between the two top contacts (which formed device 1). The lack of other double features and fact that two lines can be seen under the metal indicates that these are actually two tubes and that it is not just a scanning artefact. It might be that the tube where this device was created, was actually a nanotube rope. Whether this rope extended along the entire length is unclear, because the scan of device 4 (the two metal contacts right next to the first two) only shows a single line.
Another interesting scan was that of the contact between device 5 and 6. This can be seen on the left of Figure 4.4. It shows a surface that is a lot bumpier than that of other contacts, such as those from device 4 shown right next to it. It may be that this was caused by PMMA residue under the metal contact. The contact had an RMS roughness of 6 nm, while for the other contacts it was only 1.4-1.5 nm. This indicates that the probestation measurements are sensitive to the quality of the contacts, because especially device 5 was very noisy.

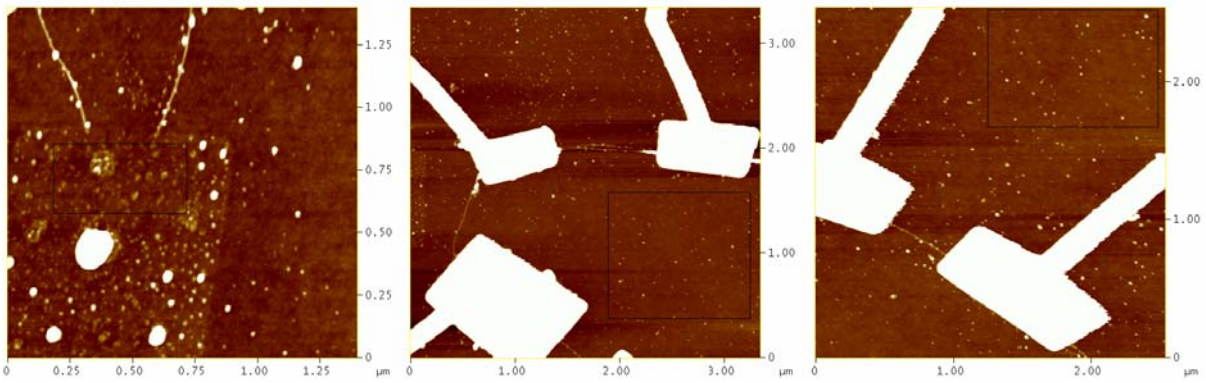

figure 4.3 Left: Scan of the area where two intersecting nanotubes were cut with plasma (same as in figures 4.1 and 4.2). Middle: scan of device 1 from cvd4g1 which contains a double tube. Left of the device it can be seen how two nanotubes moved towards each other after they were cut. Right: scan of device 4 from cvd4g1, which does not show.

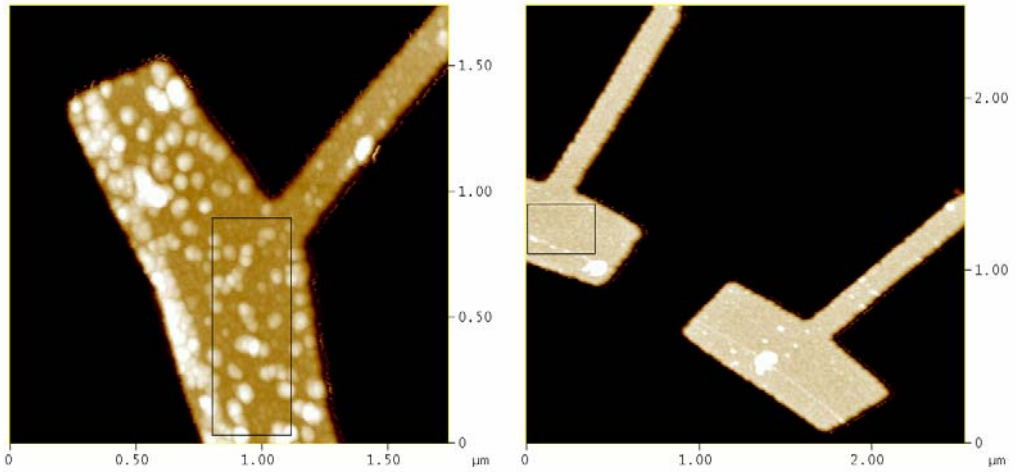

Figure 4.4 Left: AFM scan of the contact between devices 5 and 6. When it is compared to other contacts, such as the ones from device 4 (on the right), it is clearly rougher.

table 4.1 Overview of probestation measurements.

			before		After 1st		After 2nd	
		Type	I_{sat} (nA)	Noise	I_{sat} (nA)	Noise	I_{sat} (nA)	Noise
cvd4g1	1	I	- (>60)	A	45	-	26	-
	2	I	- (>120)	A	27	<	50	>
	3	I	- (>90)	A	30	-		
	4	II	140	A	6	<		
	5	II	7	B	8	<	2	-
	6	II	25	B	36	<		
	7	II	20	B	62	<	25	-
	8	II	18	B	32	-		
	10	III	<1	B	33	>		
	11	II	?	B	42	<		
	13	III	<1	B	95	-		
	14	III	1	B	40	-	2	-
	16	II	120	A	45	<		
	17	II *)	?	B	10	<		
	18	I	- (>100)	A	90	<	90	-
	19	II	14	B	11	<		
	20	II	30	B	35	<		
	21	II	35	B	13	<		
	22	III	0	B	9	>		
	23	I	- (>40)	A	- (>40)	-	2	-
cvd4g4	2	III	<1	B	1	-		
	3	III	<1	B	<1	<		
	6	III	<1	A	1/5 **)	-		
	15	II	15	B	1	<		
	16	III	<1	B	3	>		
	17	II	6	B	11	-		
	18	III	<1	B	0	<		
	19	II	17	A	<1	<		
	20	II	20	B	3	<		
	21	III	<1	B	8	>		

*) Between 1 and 2V the current seems to saturate, but then goes up again for lower voltages, while the noise is also higher at low backgate voltages.
**) On sweeping the backgate voltage from 6V back to 0V, the saturation current was about 5 nA, whereas at the start of the measurement it was 1 nA.

Type I: Smooth, steep current characteristic with no saturation visible yet in the measured regime (usually -3 to 6V).
Type II: Saturation has become visible, but there is still a significant current.
Type III: Very poor device with a saturation current typically less than 1 nA.
Bad looking, noisy graphs are classified with a 'B' under noise, while those with relatively low noise are labelled 'A'. For measurements after cleaning, it is indicated whether the noise is less ('<') than before, more ('>') or approximately equal ('-').

5 Conclusion

From the experiments that were performed to determine a suitable cleaning method we have learned several things.
First of all it became clear that the MAA resist leaves a very dirty surface. Even without fabrication there was residue over the entire surface, whereas in the other samples the silicon oxide surface was still clearly visible between the bits of residue. As a cleaning method, trying to dissolve the residue in hot dichloroethane turned out to be very ineffective. Baking the sample on hotplate on the other hand was highly effective. The PMMA samples only had a few small bits of residue left. For the PMGI sample the result was similar, only there was slightly more residue. A difference between the before and after baking scans of the MAA sample could definitely be seen, but there was still residue over the entire surface.

The electrical measurements performed on an SET showed that the effect of baking on the resistance of the SET diminished over time. Initially there was a significant drop in resistance. This may be due to oxygen migrating through the junction.

For the electrical measurements on the CNT transistors, there were very differing results. After the sample had first been heated in air, the depletion regions of all samples were found at higher backgate voltages. When the sample was again heated in a flow of inert gas (argon) the depletion regions were found at lower voltages again. This effect is therefore probably related to reactions with oxygen.
When the saturation current was considered the effect was not the same in all samples, in some it increased, in others it decreased. This could have been an effect related to the contacts on the tubes.
The noise generally seemed to decrease after baking. Most of the current curves got smoother after heating, but there were also some in which this was not the case. Again this might be closely related to the metal contacts.

Even after prolonged baking, fabricated samples still had some small bits of residue on their surface. This might have been caused by contamination with other substances, which could have been present in solvents. Contamination may also have come from glassware in the fabrication facility at DIMES. Also the PMMA may have undergone chemical changes to stabilize it. These two possible effects may have worked together; contaminations could have caused chemical stabilizing changes in the PMMA.

To see whether cleaning samples by baking them really can create quantum dots with low disorder, it is important to perform low temperature measurements. Unfortunately there was no time for that in this project. This may be a good subject for further research. To avoid any reactions with oxygen it is recommendable to heat the samples in an inert environment.

References

[1] P. Jarillo-Herrero, *Quantum transport in carbon nanotubes*, Ph.D. thesis (2005).
[2] S. Sapmaz, *Carbon nanotube quantum dots*, Ph.D. thesis (2006)
[3] S. Iijima, *Helical Microtubules of Graphitic Carbon*, Nature 354, 56-58 (1991).
[4] S. Iijima & T. Ichihashi, *Single-shell carbon nanotubes of 1-nm diameter*, Nature 363, 603-605 (1993).
[5] E.D. Minot, *Tuning the bandstructure of carbon nanotubes*, Ph.D. thesis (2004)
[6] W.R. Zeng, S.F. Li & W.K. Chow, *Review on Chemical Reactions of Burning Poly(methyl methacrylate) PMMA*, Journal of Fire Sciences 20, 401-433 (2002)
[7] R. Vilanove and F. Rondelez, *Scaling Description of Two-Dimensional Chain Conformations in Polymer Monolayers*, Physical Review Letters 45, 1502-1505 (1980)

Appendix

AFM scans before and after cleaning

Before spinning of resist

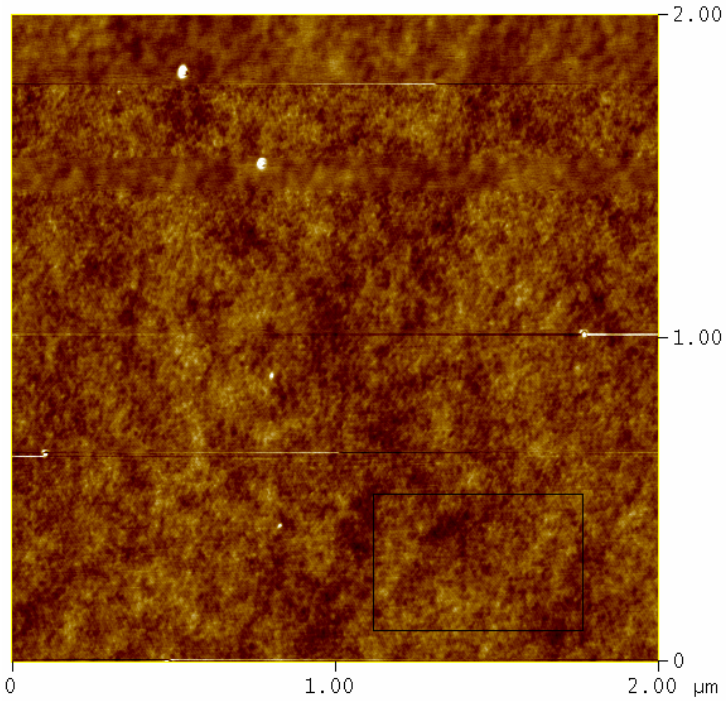

Sample 1a
prior to resist spinning

Image Statistics

Img. Z range	5.284 nm
Img. Raw mean	190.98 nm
Img. Rms (Rq)	0.236 nm
Img. Ra	0.183 nm
Img. Rmax	5.284 nm

Box Statistics

Z range	1.855 nm
Raw mean	190.98 nm
Rms (Rq)	0.235 nm
Mean roughness (Ra)	0.188 nm
Max height (Rmax)	1.804 nm

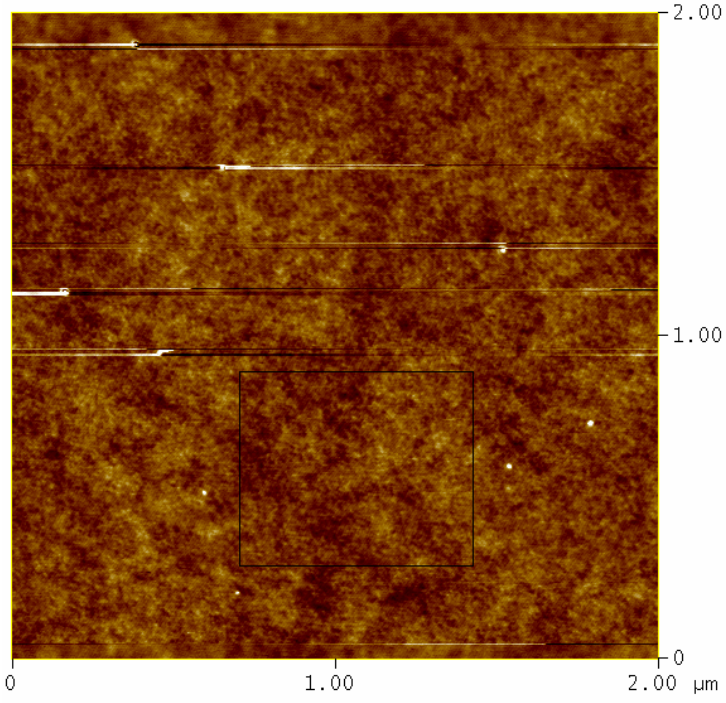

Sample 1a
prior to resist spinning

Image Statistics

Img. Z range	6.977 nm
Img. Raw mean	432.05 nm
Img. Rms (Rq)	0.256 nm
Img. Ra	0.189 nm
Img. Rmax	6.977 nm

Box Statistics

Z range	1.823 nm
Raw mean	432.03 nm
Rms (Rq)	0.218 nm
Mean roughness (Ra)	0.174 nm
Max height (Rmax)	1.746 nm

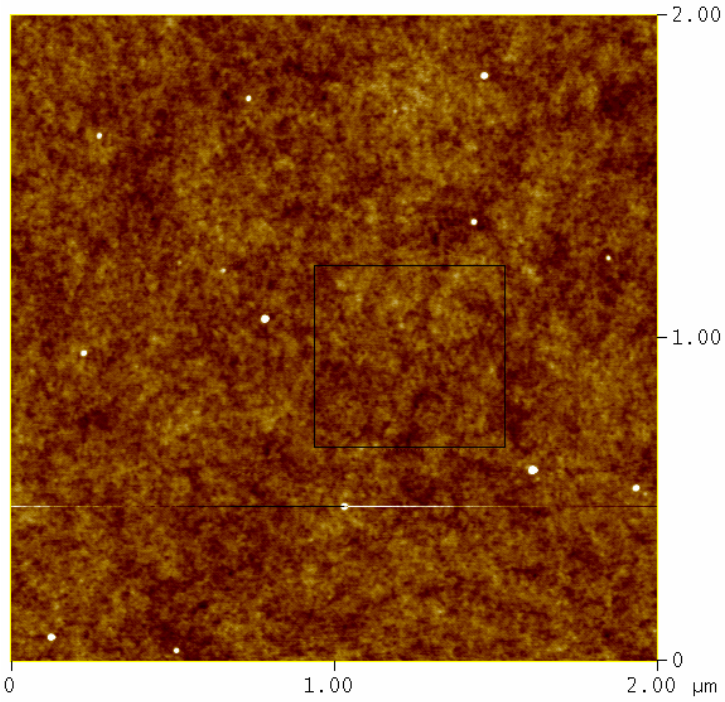

Sample 1b

prior to resist spinning

Image Statistics

Img. Z range	8.705 nm
Img. Raw mean	64.901 nm
Img. Rms (Rq)	0.240 nm
Img. Ra	0.179 nm
Img. Rmax	8.705 nm

Box Statistics

Z range	1.770 nm
Raw mean	64.902 nm
Rms (Rq)	0.215 nm
Mean roughness (Ra)	0.172 nm
Max height (Rmax)	1.856 nm

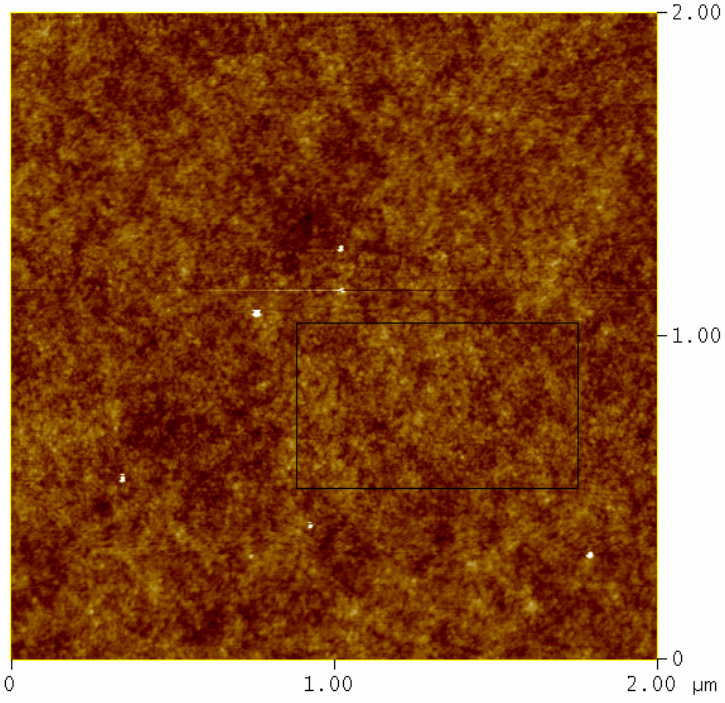

Sample 2a

prior to resist spinning

Image Statistics

Img. Z range	5.244 nm
Img. Raw mean	54.696 nm
Img. Rms (Rq)	0.226 nm
Img. Ra	0.177 nm
Img. Rmax	5.244 nm

Box Statistics

Z range	1.582 nm
Raw mean	54.738 nm
Rms (Rq)	0.212 nm
Mean roughness (Ra)	0.171 nm
Max height (Rmax)	1.578 nm

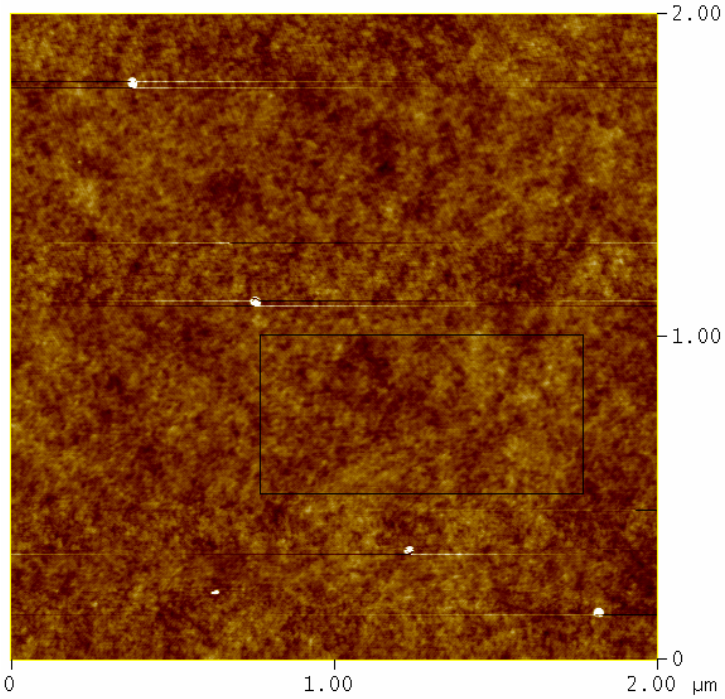

Sample 2b

prior to resist spinning

Image Statistics

Img. Z range	7.566 nm
Img. Raw mean	129.36 nm
Img. Rms (Rq)	0.238 nm
Img. Ra	0.176 nm
Img. Rmax	7.566 nm

Box Statistics

Z range	1.640 nm
Raw mean	129.38 nm
Rms (Rq)	0.208 nm
Mean roughness (Ra)	0.167 nm
Max height (Rmax)	1.569 nm

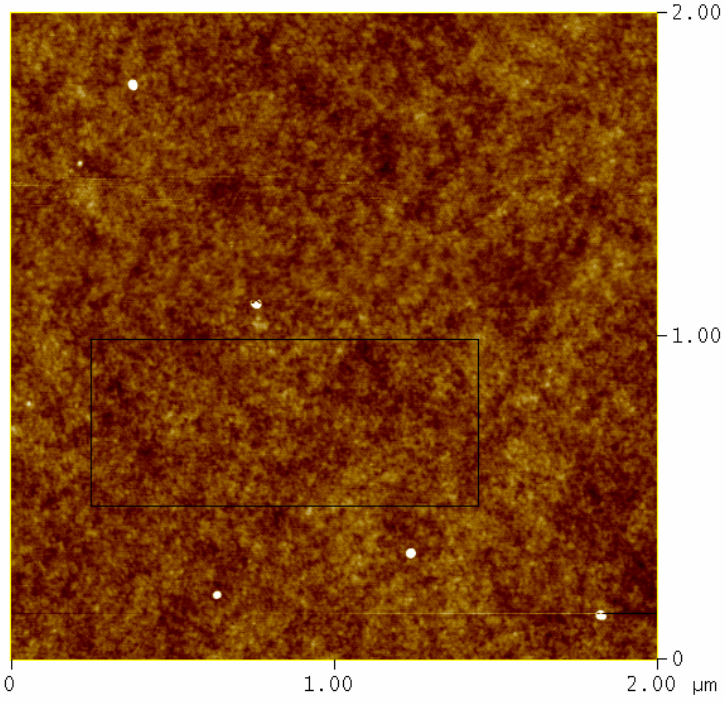

Sample 2b

prior to resist spinning

Image Statistics

Img. Z range	7.439 nm
Img. Raw mean	122.29 nm
Img. Rms (Rq)	0.243 nm
Img. Ra	0.182 nm
Img. Rmax	7.439 nm

Box Statistics

Z range	1.739 nm
Raw mean	122.27 nm
Rms (Rq)	0.221 nm
Mean roughness (Ra)	0.175 nm
Max height (Rmax)	1.725 nm

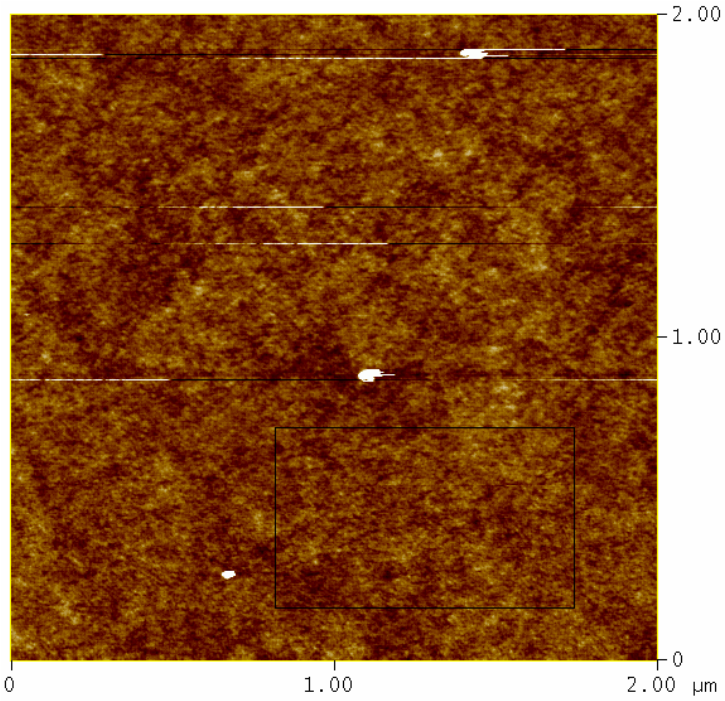

Sample 3a

prior to resist spinning

Image Statistics

Img. Z range	13.399 nm
Img. Raw mean	324.09 nm
Img. Rms (Rq)	0.319 nm
Img. Ra	0.210 nm
Img. Rmax	13.399 nm

Box Statistics

Z range	1.860 nm
Raw mean	278.26 nm
Rms (Rq)	0.238 nm
Mean roughness (Ra)	0.190 nm
Max height (Rmax)	1.902 nm

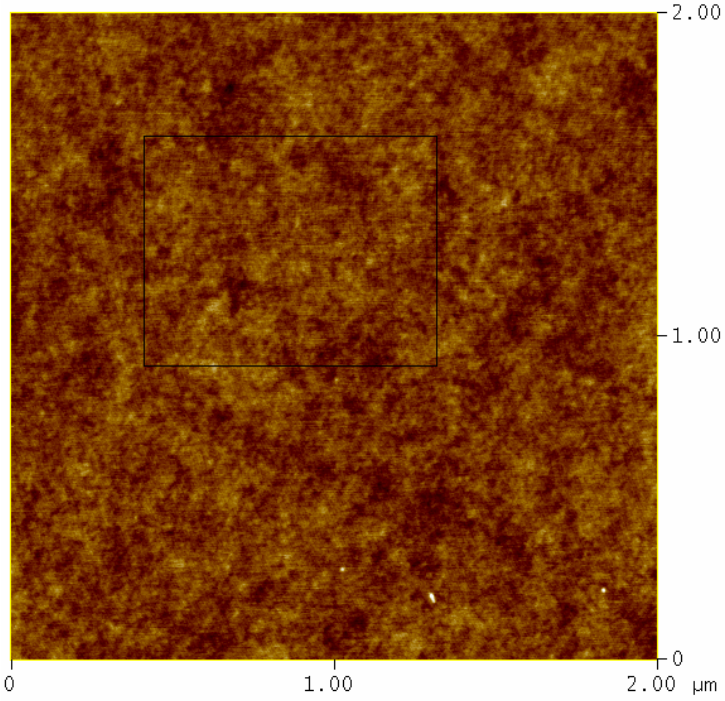

Sample 3b

prior to resist spinning

Image Statistics

Img. Z range	3.014 nm
Img. Raw mean	182.07 nm
Img. Rms (Rq)	0.219 nm
Img. Ra	0.174 nm
Img. Rmax	3.014 nm

Box Statistics

Z range	1.821 nm
Raw mean	182.10 nm
Rms (Rq)	0.218 nm
Mean roughness (Ra)	0.174 nm
Max height (Rmax)	1.805 nm

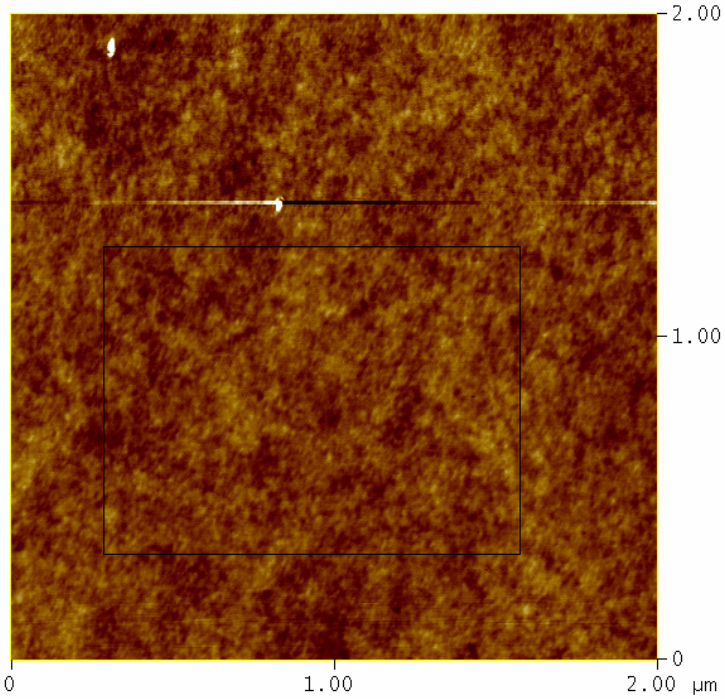

Sample 4a

prior to resist spinning

Image Statistics

Img. Z range	7.950 nm
Img. Raw mean	195.36 nm
Img. Rms (Rq)	0.232 nm
Img. Ra	0.176 nm
Img. Rmax	7.950 nm

Box Statistics

Z range	1.599 nm
Raw mean	195.36 nm
Rms (Rq)	0.200 nm
Mean roughness (Ra)	0.160 nm
Max height (Rmax)	1.570 nm

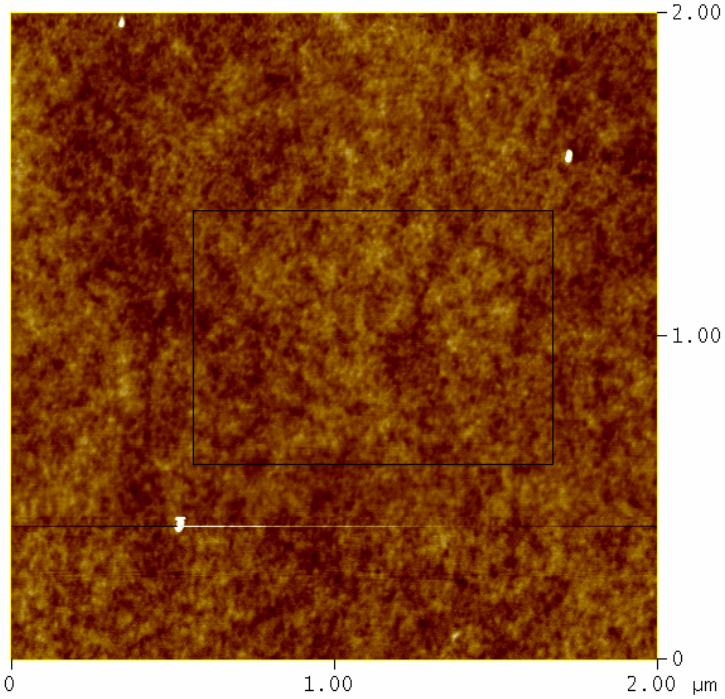

Sample 4a

prior to resist spinning

Image Statistics

Img. Z range	7.173 nm
Img. Raw mean	529.08 nm
Img. Rms (Rq)	0.230 nm
Img. Ra	0.175 nm
Img. Rmax	7.173 nm

Box Statistics

Z range	1.497 nm
Raw mean	529.11 nm
Rms (Rq)	0.201 nm
Mean roughness (Ra)	0.162 nm
Max height (Rmax)	1.454 nm

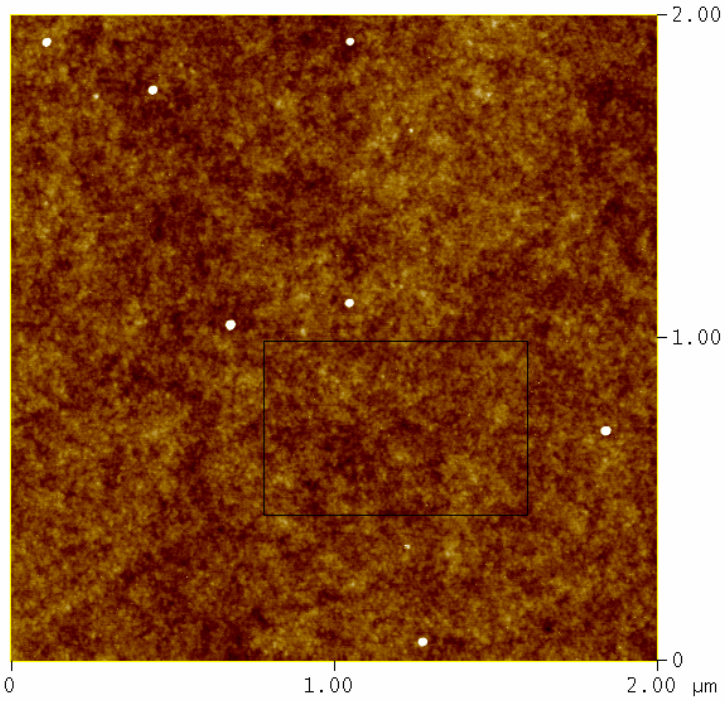

Sample 4b

prior to resist spinning

Image Statistics

Img. Z range	5.902 nm
Img. Raw mean	227.04 nm
Img. Rms (Rq)	0.246 nm
Img. Ra	0.184 nm
Img. Rmax	5.902 nm

Box Statistics

Z range	1.873 nm
Raw mean	227.01 nm
Rms (Rq)	0.216 nm
Mean roughness (Ra)	0.172 nm
Max height (Rmax)	1.854 nm

Before cleaning, after a layer of resist has been spun on and removed again

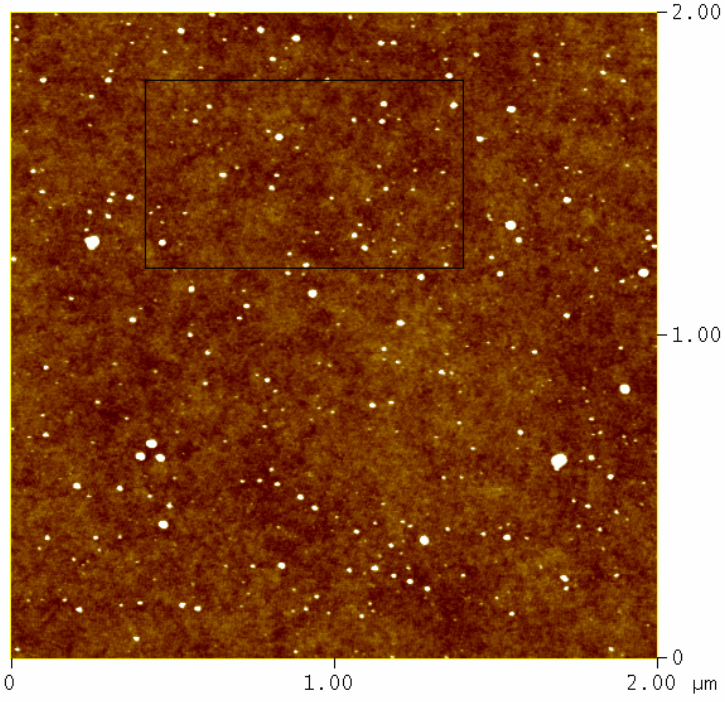

Sample 1a

resist used: PMMA 350K
no additional cleaning

Image Statistics

Img. Z range	15.263 nm
Img. Raw mean	393.39 nm
Img. Rms (Rq)	0.503 nm
Img. Ra	0.247 nm
Img. Rmax	15.262 nm

Box Statistics

Z range	9.025 nm
Raw mean	393.38 nm
Rms (Rq)	0.411 nm
Mean roughness (Ra)	0.231 nm
Max height (Rmax)	9.033 nm

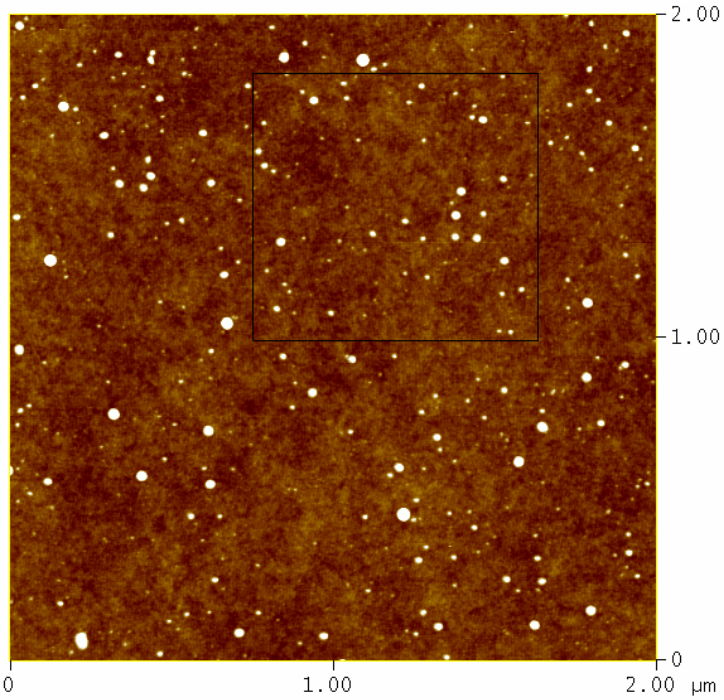

Sample 1b

resist used: PMMA 350K
no additional cleaning

Image Statistics

Img. Z range	16.485 nm
Img. Raw mean	146.76 nm
Img. Rms (Rq)	0.566 nm
Img. Ra	0.257 nm
Img. Rmax	16.490 nm

Box Statistics

Z range	9.039 nm
Raw mean	146.77 nm
Rms (Rq)	0.462 nm
Mean roughness (Ra)	0.239 nm
Max height (Rmax)	8.969 nm

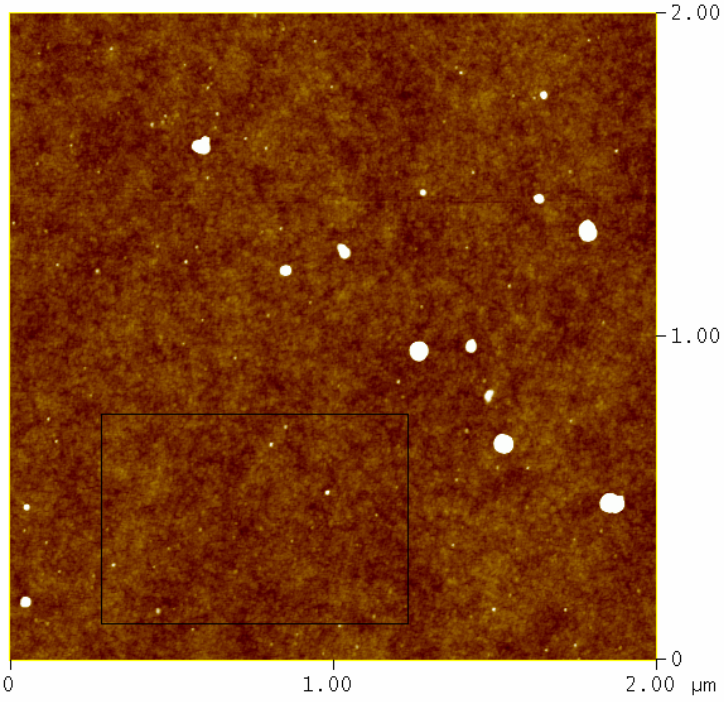

Sample 2a

resist used: PMGI
no additional cleaning

Image Statistics

Img. Z range	18.848 nm
Img. Raw mean	0.408 nm
Img. Rms (Rq)	0.630 nm
Img. Ra	0.235 nm
Img. Rmax	18.839 nm

Box Statistics

Z range	4.135 nm
Raw mean	-29.076 nm
Rms (Rq)	0.243 nm
Mean roughness (Ra)	0.188 nm
Max height (Rmax)	4.164 nm

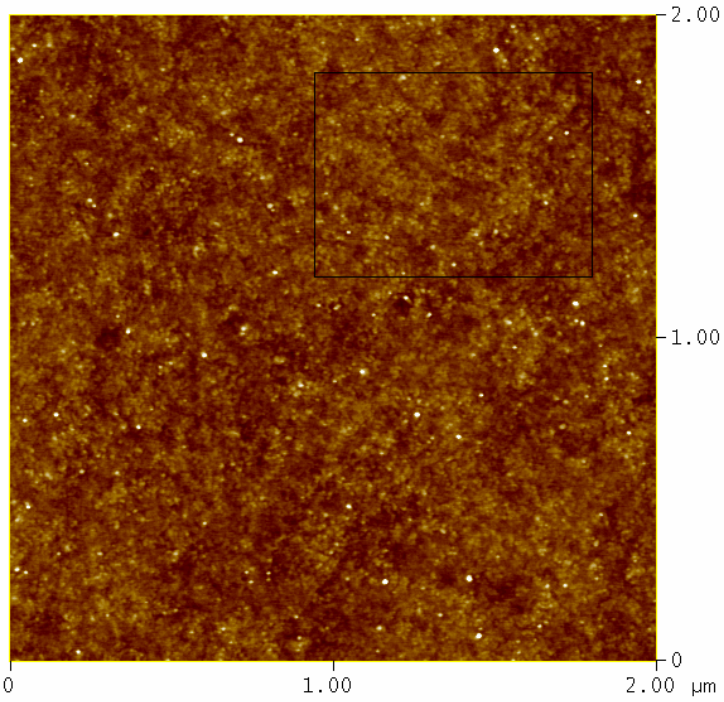

Sample 2c

resist used: PMGI
no additional cleaning

Image Statistics

Img. Z range	5.559 nm
Img. Raw mean	234.23 nm
Img. Rms (Rq)	0.360 nm
Img. Ra	0.275 nm
Img. Rmax	5.559 nm

Box Statistics

Z range	3.727 nm
Raw mean	234.27 nm
Rms (Rq)	0.343 nm
Mean roughness (Ra)	0.266 nm
Max height (Rmax)	3.729 nm

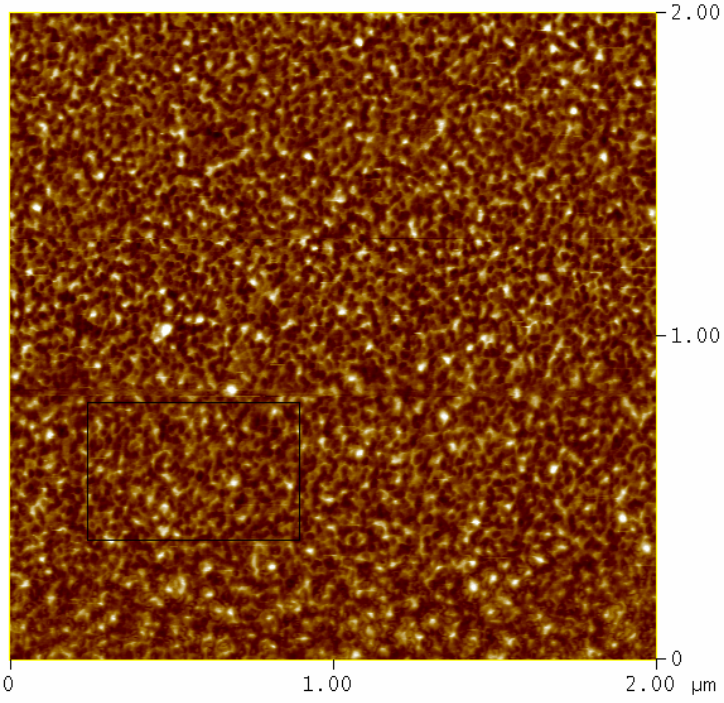

Sample 3a

resist used: MAA
no additional cleaning

Image Statistics

Img. Z range	19.888 nm
Img. Raw mean	85.646 nm
Img. Rms (Rq)	1.736 nm
Img. Ra	1.339 nm
Img. Rmax	19.888 nm

Box Statistics

Z range	12.383 nm
Raw mean	89.382 nm
Rms (Rq)	1.623 nm
Mean roughness (Ra)	1.261 nm
Max height (Rmax)	12.398 nm

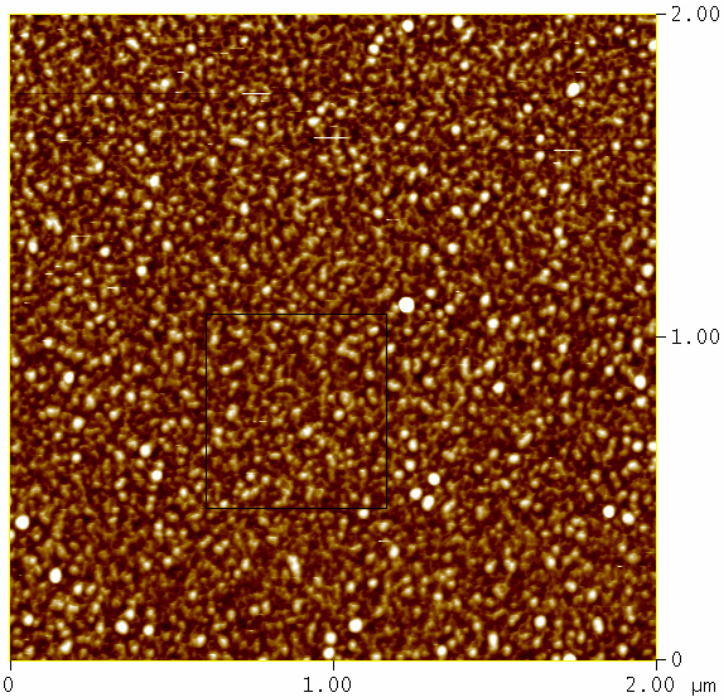

Sample 3b

resist used: MAA
no additional cleaning

Image Statistics

Img. Z range	64.543 nm
Img. Raw mean	229.46 nm
Img. Rms (Rq)	2.317 nm
Img. Ra	1.765 nm
Img. Rmax	64.543 nm

Box Statistics

Z range	13.940 nm
Raw mean	230.28 nm
Rms (Rq)	2.077 nm
Mean roughness (Ra)	1.661 nm
Max height (Rmax)	13.996 nm

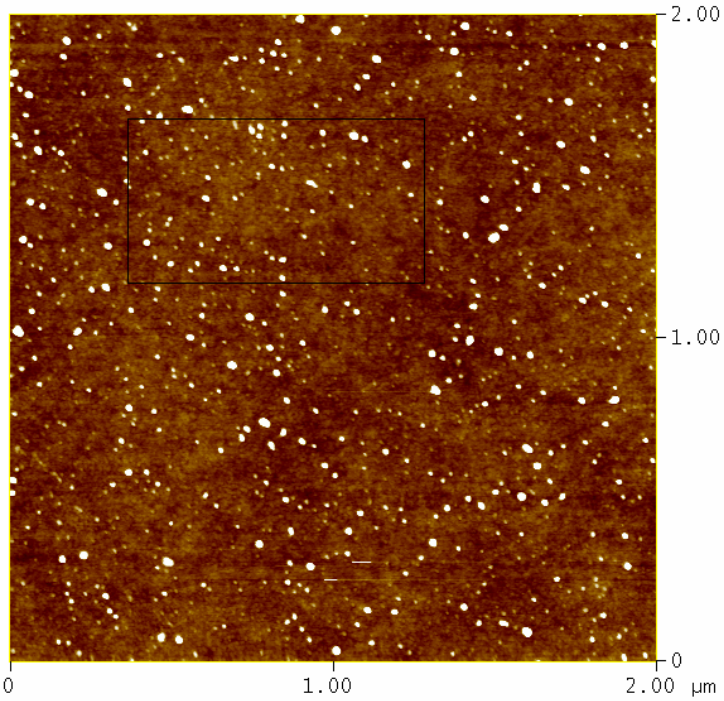

Sample 4a

resist used: PMMA 350K + PMMA 950K
no additional cleaning

Image Statistics

Img. Z range	21.865 nm
Img. Raw mean	-35.115 nm
Img. Rms (Rq)	0.739 nm
Img. Ra	0.340 nm
Img. Rmax	21.849 nm

Box Statistics

Z range	10.985 nm
Raw mean	-35.061 nm
Rms (Rq)	0.602 nm
Mean roughness (Ra)	0.302 nm
Max height (Rmax)	10.839 nm

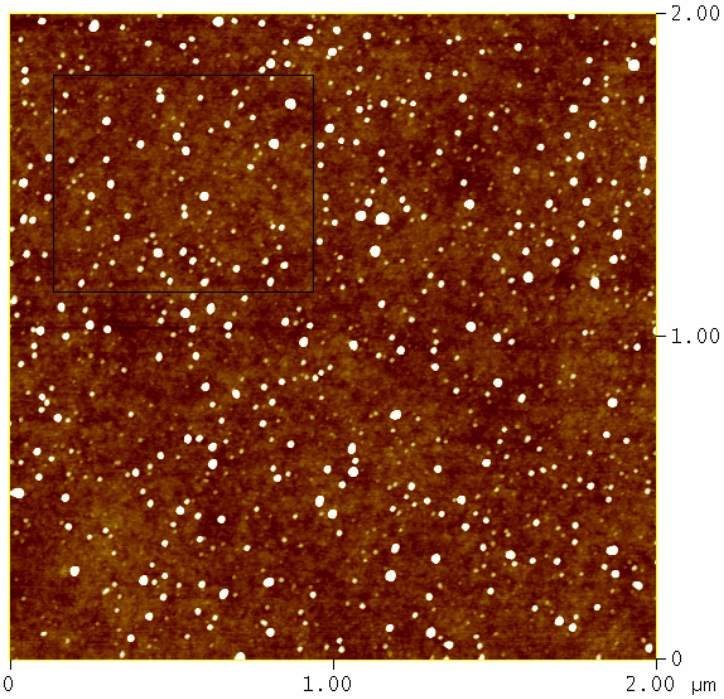

Sample 4b

resist used: PMMA 350K + PMMA 950K
no additional cleaning

Image Statistics

Img. Z range	14.639 nm
Img. Raw mean	98.804 nm
Img. Rms (Rq)	0.875 nm
Img. Ra	0.384 nm
Img. Rmax	14.621 nm

Box Statistics

Z range	11.287 nm
Raw mean	98.821 nm
Rms (Rq)	0.793 nm
Mean roughness (Ra)	0.345 nm
Max height (Rmax)	11.212 nm

After cleaning

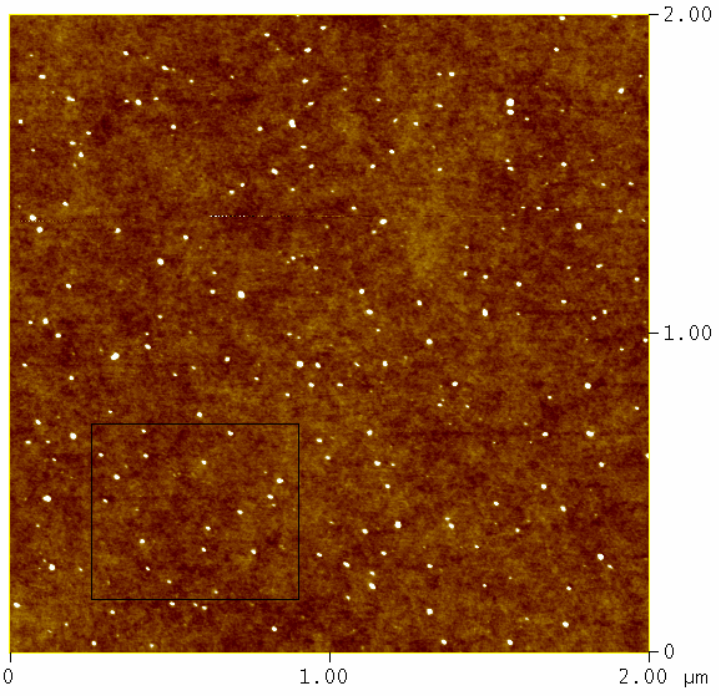

Sample 1a
resist used: PMMA 350k
cleaned in dichloroethane at 60°C for 30 minutes

Image Statistics

Img. Z range	13.539 nm
Img. Raw mean	145.65 nm
Img. Rms (Rq)	0.410 nm
Img. Ra	0.232 nm
Img. Rmax	13.539 nm

Box Statistics

Z range	6.485 nm
Raw mean	145.63 nm
Rms (Rq)	0.371 nm
Mean roughness (Ra)	0.219 nm
Max height (Rmax)	6.501 nm

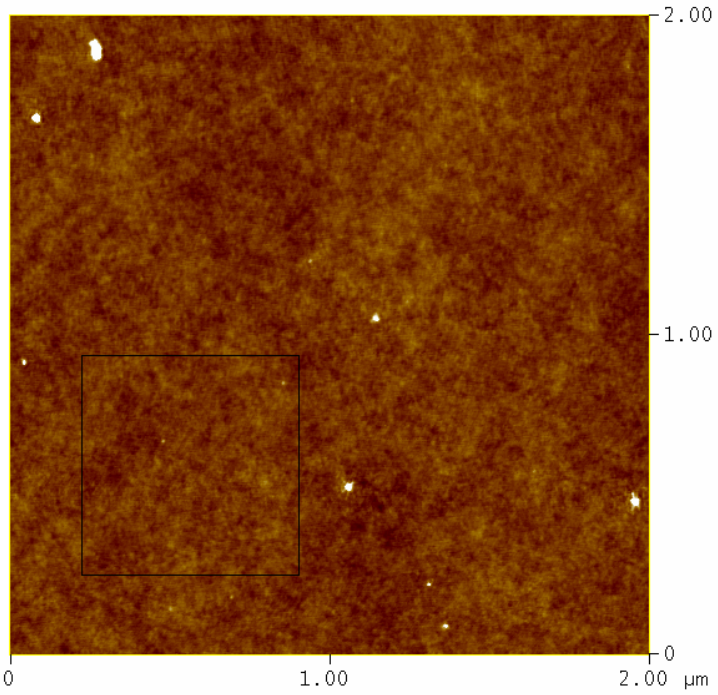

Sample 1b
resist used: PMMA 350k
Cleaned on hotplate at 250°C in air for 30 minutes

Image Statistics

Img. Z range	17.768 nm
Img. Raw mean	206.15 nm
Img. Rms (Rq)	0.342 nm
Img. Ra	0.188 nm
Img. Rmax	17.754 nm

Box Statistics

Z range	2.296 nm
Raw mean	206.16 nm
Rms (Rq)	0.216 nm
Mean roughness (Ra)	0.171 nm
Max height (Rmax)	2.244 nm

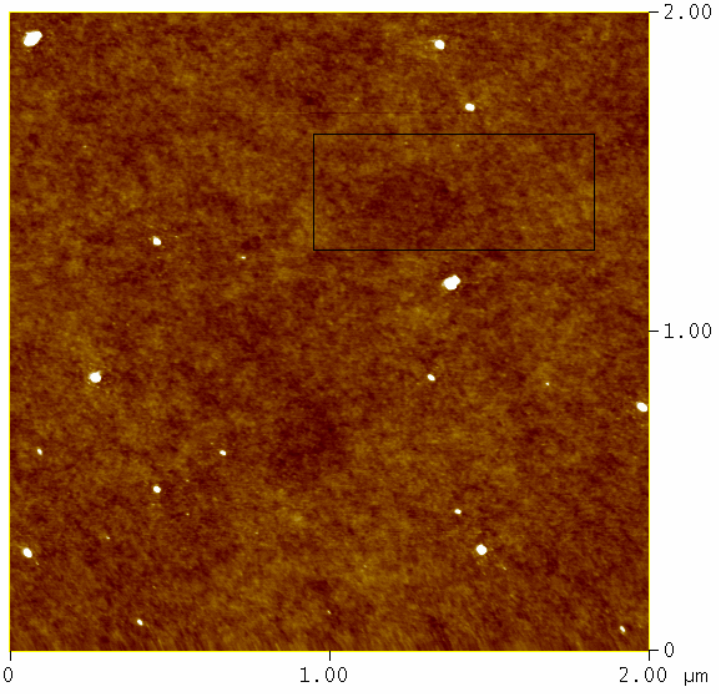

Sample 1b
resist used: PMMA 350k
cleaned on hotplate at 250°C in air for 30 minutes

Image Statistics

Img. Z range	16.218 nm
Img. Raw mean	194.44 nm
Img. Rms (Rq)	0.384 nm
Img. Ra	0.198 nm
Img. Rmax	16.217 nm

Box Statistics

Z range	2.251 nm
Raw mean	194.41 nm
Rms (Rq)	0.231 nm
Mean roughness (Ra)	0.185 nm
Max height (Rmax)	2.234 nm

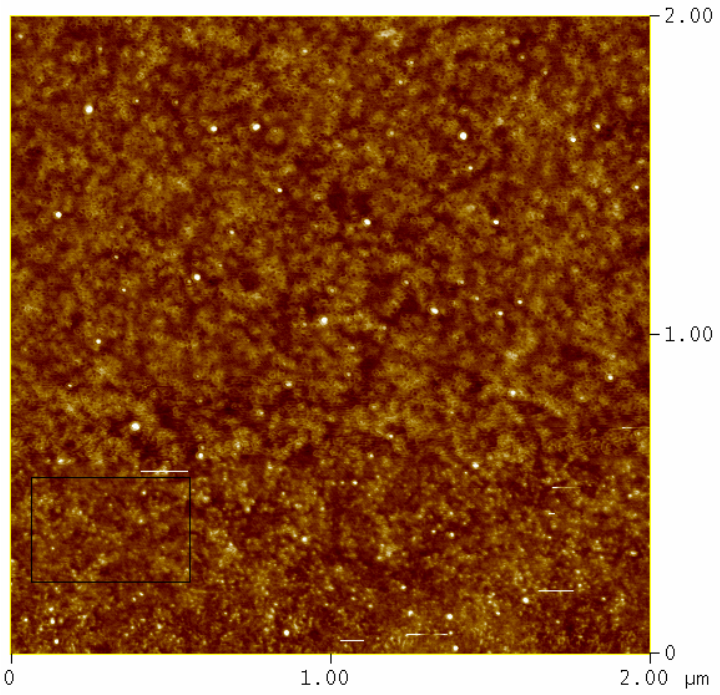

Sample 2a
resist used PMGI
cleaned in dichloroethane at 60°C for 30 minutes

Image Statistics

Img. Z range	32.143 nm
Img. Raw mean	72.623 nm
Img. Rms (Rq)	0.562 nm
Img. Ra	0.331 nm
Img. Rmax	32.128 nm

Box Statistics

Z range	3.614 nm
Raw mean	72.625 nm
Rms (Rq)	0.375 nm
Mean roughness (Ra)	0.290 nm
Max height (Rmax)	3.602 nm

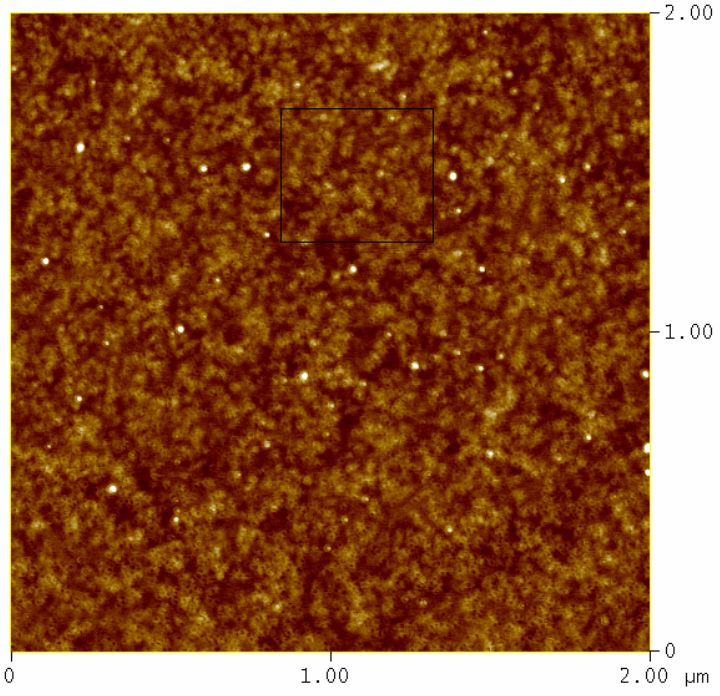

Sample 2a
resist used: PMGI
cleaned in dichloroethane at 60°C for 30 minutes

Image Statistics

Img. Z range	7.768 nm
Img. Raw mean	225.12 nm
Img. Rms (Rq)	0.419 nm
Img. Ra	0.328 nm
Img. Rmax	7.768 nm

Box Statistics

Z range	3.071 nm
Raw mean	225.13 nm
Rms (Rq)	0.381 nm
Mean roughness (Ra)	0.305 nm
Max height (Rmax)	3.077 nm

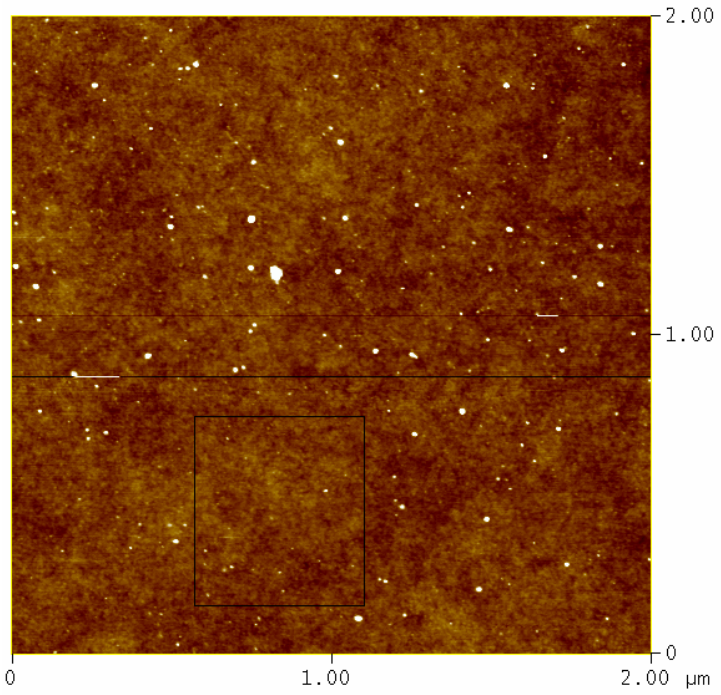

Sample 2a
resist used: PMGI
cleaned in dichloroethane at 60°C for 30 minutes

Image Statistics

Img. Z range	65.007 nm
Img. Raw mean	373.79 nm
Img. Rms (Rq)	0.564 nm
Img. Ra	0.232 nm
Img. Rmax	65.023 nm

Box Statistics

Z range	4.456 nm
Raw mean	373.83 nm
Rms (Rq)	0.248 nm
Mean roughness (Ra)	0.189 nm
Max height (Rmax)	4.405 nm

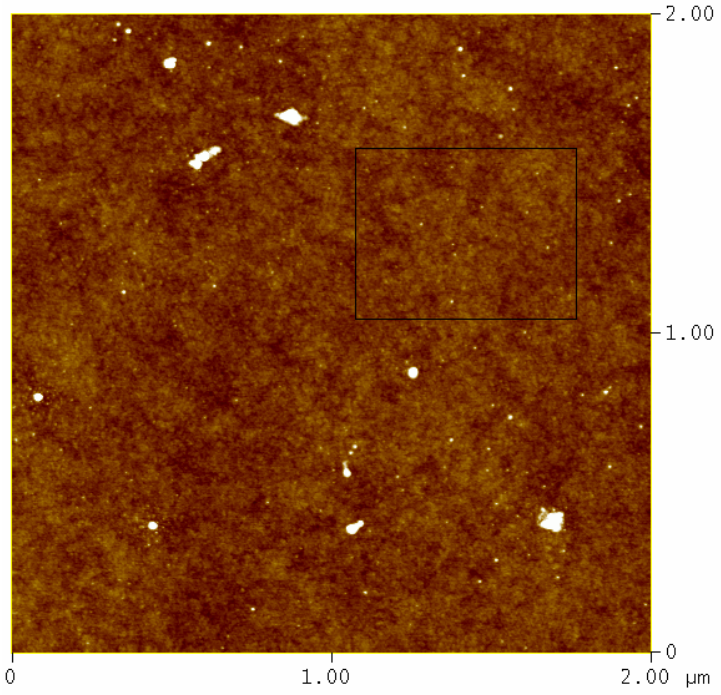

Sample 2b
resist used: PMGI
cleaned on hotplate at 250°C in air for 30 minutes

Image Statistics

Img. Z range	9.955 nm
Img. Raw mean	287.86 nm
Img. Rms (Rq)	0.363 nm
Img. Ra	0.218 nm
Img. Rmax	9.955 nm

Box Statistics

Z range	3.101 nm
Raw mean	287.90 nm
Rms (Rq)	0.236 nm
Mean roughness (Ra)	0.185 nm
Max height (Rmax)	3.106 nm

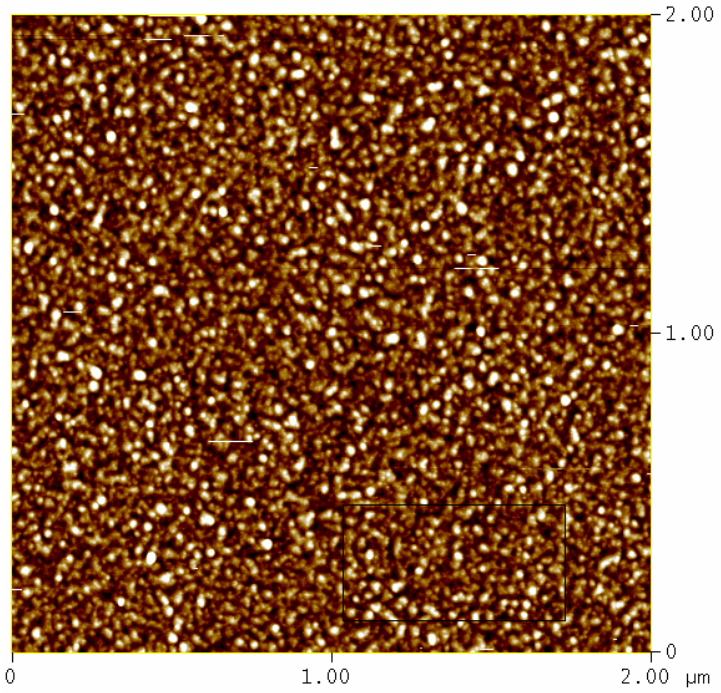

Sample 3a
resist used: MAA
cleaned in dichloroethane at 60°C for 30 minutes

Image Statistics

Img. Z range	79.272 nm
Img. Raw mean	0.737 nm
Img. Rms (Rq)	2.196 nm
Img. Ra	1.627 nm
Img. Rmax	79.251 nm

Box Statistics

Z range	14.159 nm
Raw mean	0.695 nm
Rms (Rq)	2.028 nm
Mean roughness (Ra)	1.610 nm
Max height (Rmax)	14.280 nm

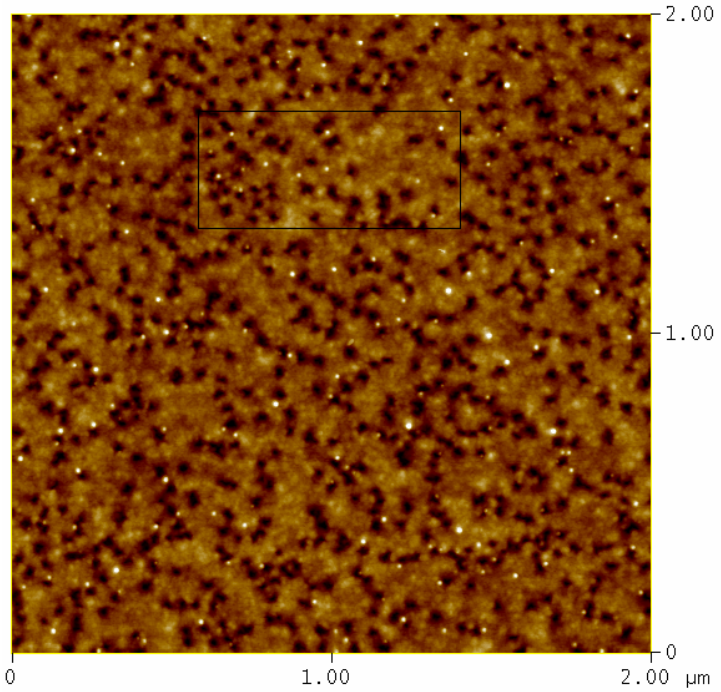

Sample 3b
resist used: MAA
cleaned on hotplate at 250°C in air for 30 minutes

Image Statistics

Img. Z range	12.819 nm
Img. Raw mean	218.30 nm
Img. Rms (Rq)	1.239 nm
Img. Ra	0.909 nm
Img. Rmax	12.819 nm

Box Statistics

Z range	10.233 nm
Raw mean	218.53 nm
Rms (Rq)	1.194 nm
Mean roughness (Ra)	0.860 nm
Max height (Rmax)	9.952 nm

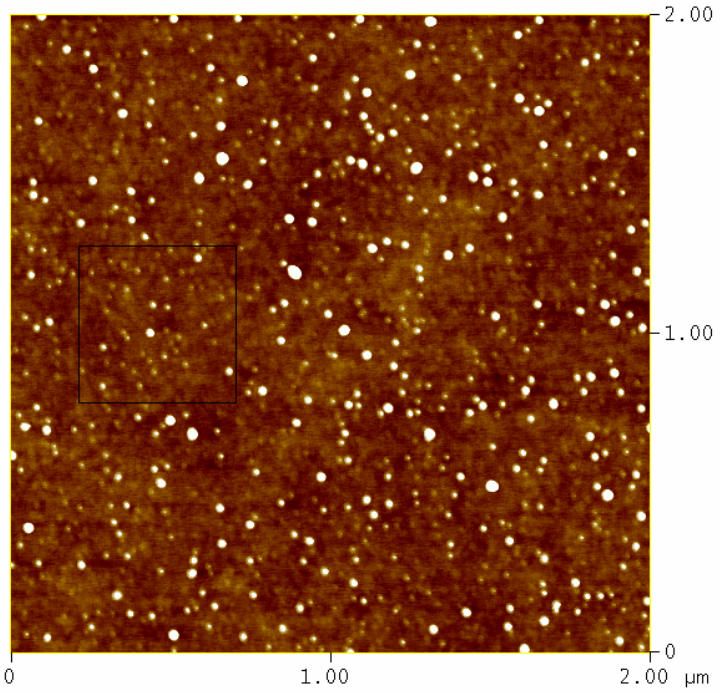

Sample 4a
resist used: PMMA 350k + PMMA 950k
cleaned in dichloroethane at 60°C for 30 minutes

Image Statistics

Img. Z range	15.916 nm
Img. Raw mean	-19.200 nm
Img. Rms (Rq)	0.750 nm
Img. Ra	0.344 nm
Img. Rmax	15.929 nm

Box Statistics

Z range	7.675 nm
Raw mean	-19.261 nm
Rms (Rq)	0.421 nm
Mean roughness (Ra)	0.239 nm
Max height (Rmax)	7.680 nm

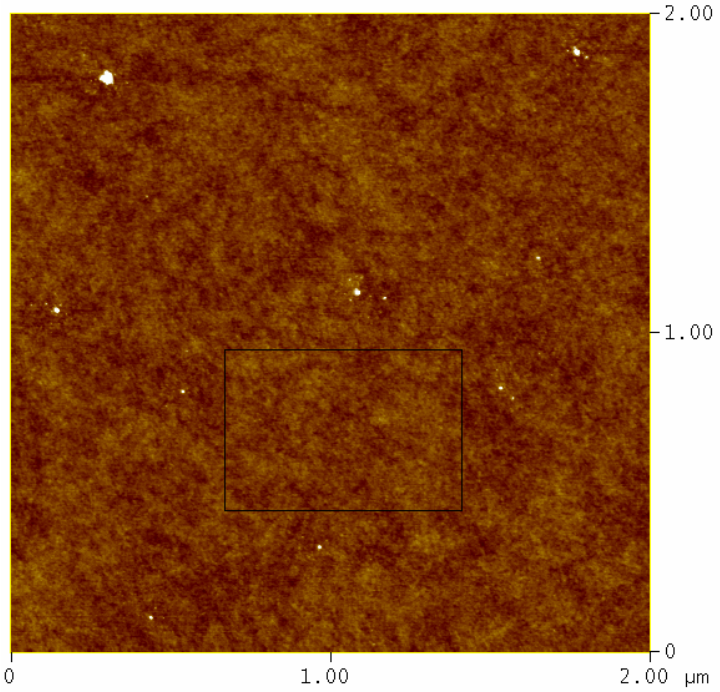

Sample 4b
resist used: PMMA 350k + PMMA 950k
cleaned on hotplate at 250°C in air for 30 minutes

Image Statistics

Img. Z range	9.079 nm
Img. Raw mean	244.14 nm
Img. Rms (Rq)	0.264 nm
Img. Ra	0.197 nm
Img. Rmax	9.079 nm

Box Statistics

Z range	1.740 nm
Raw mean	244.17 nm
Rms (Rq)	0.230 nm
Mean roughness (Ra)	0.184 nm
Max height (Rmax)	1.755 nm

Design for cvd4g

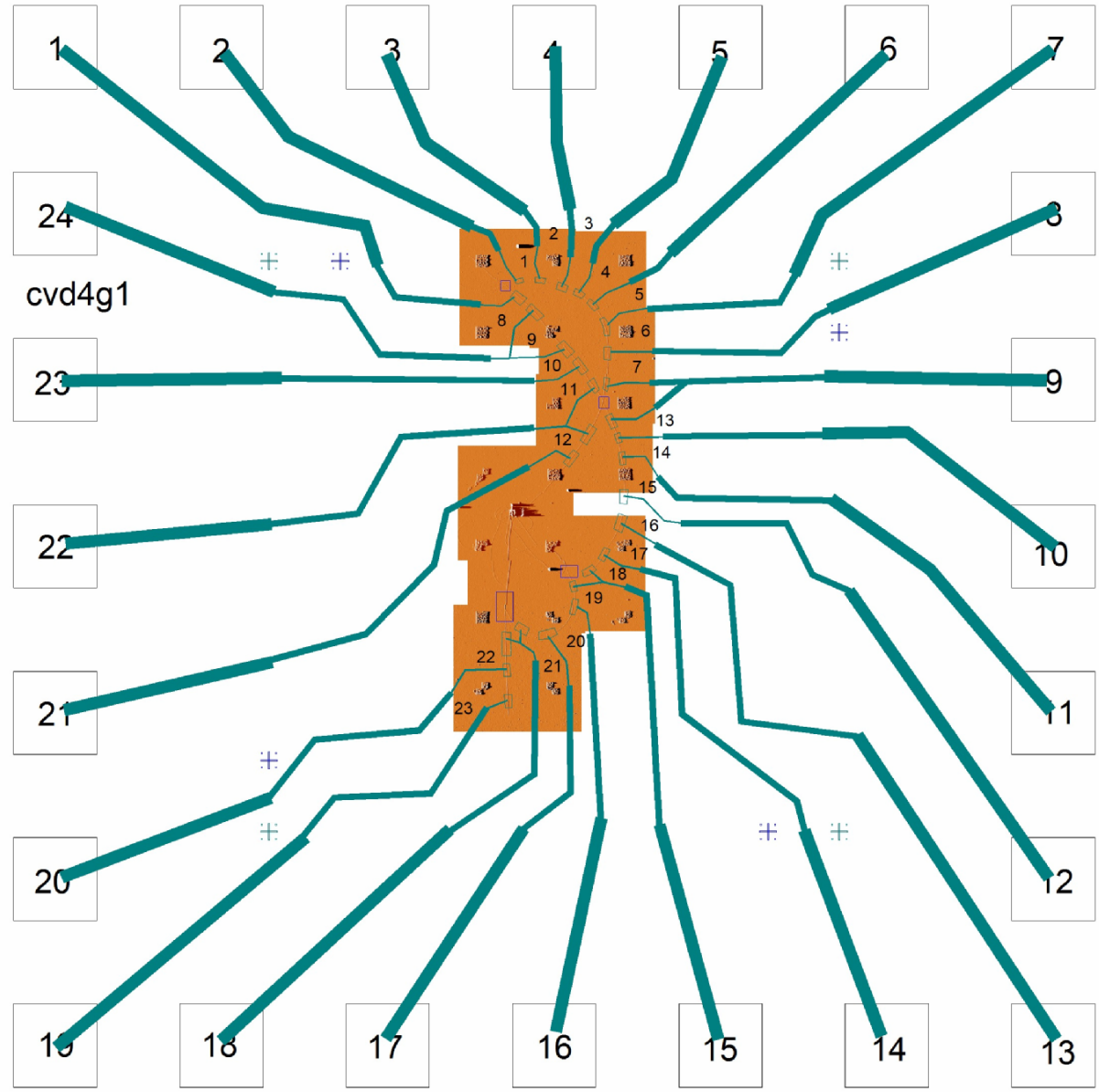

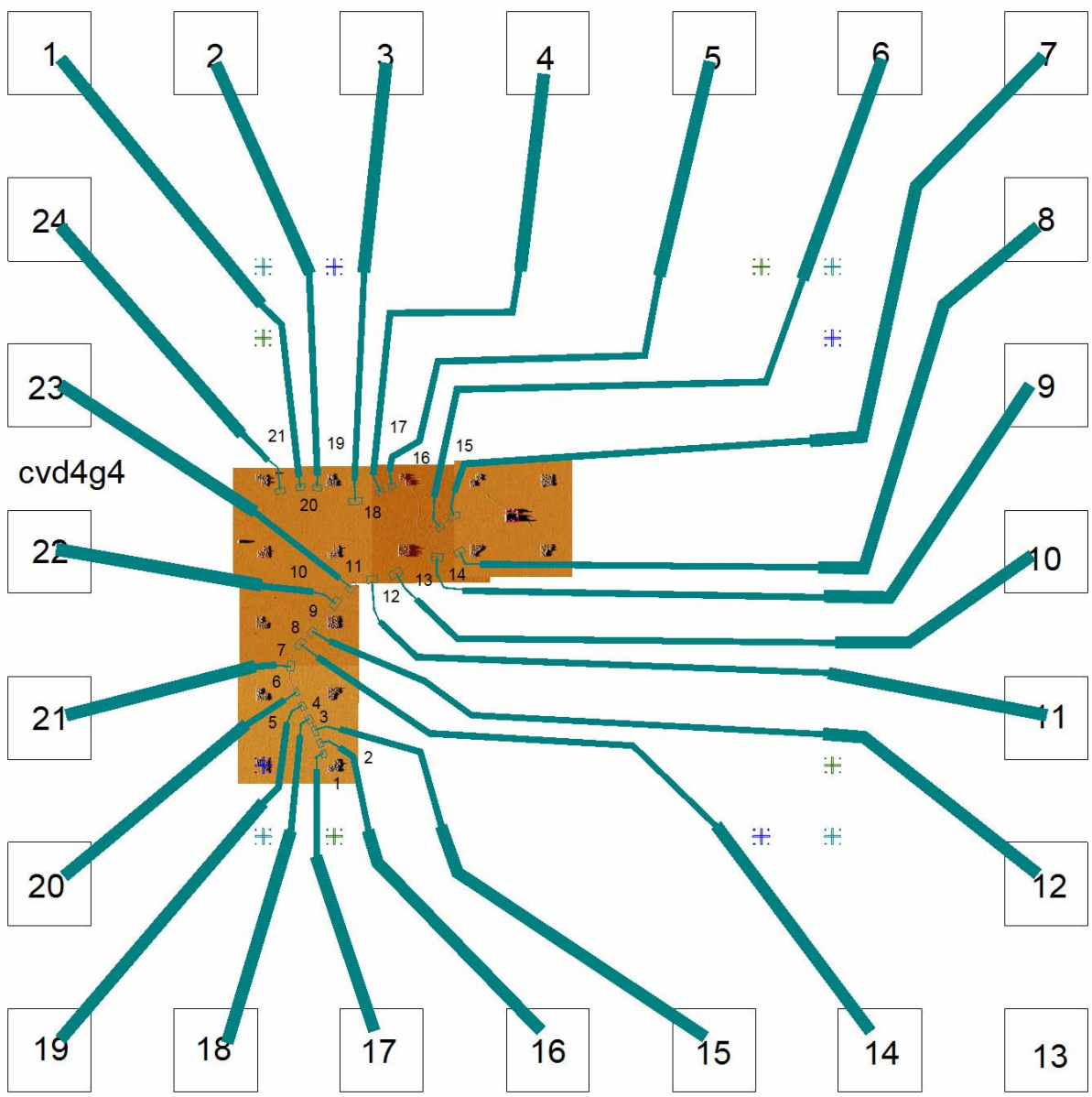
1
2
3
4
5
6
7
8
9
10
11
12
13
14
15
16
17
18
19
20
21
22
23
24
cvd4g4

Probestation measurements

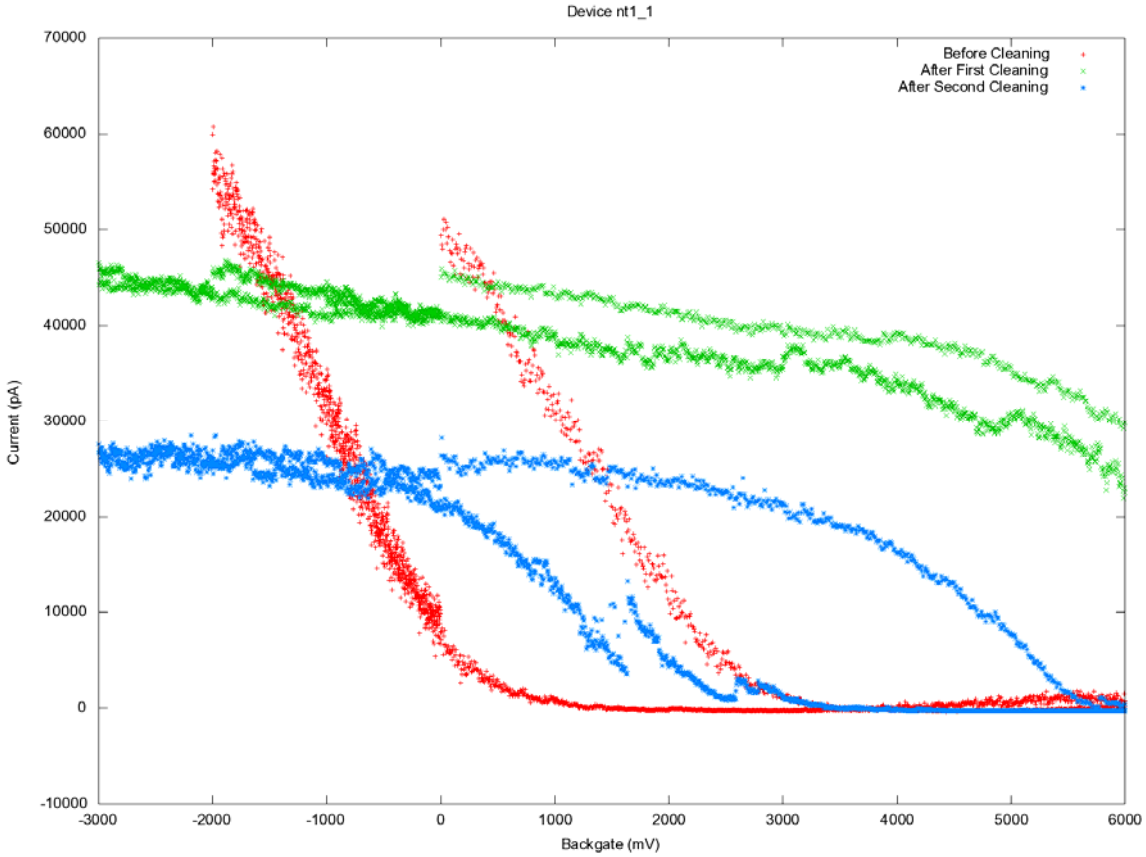

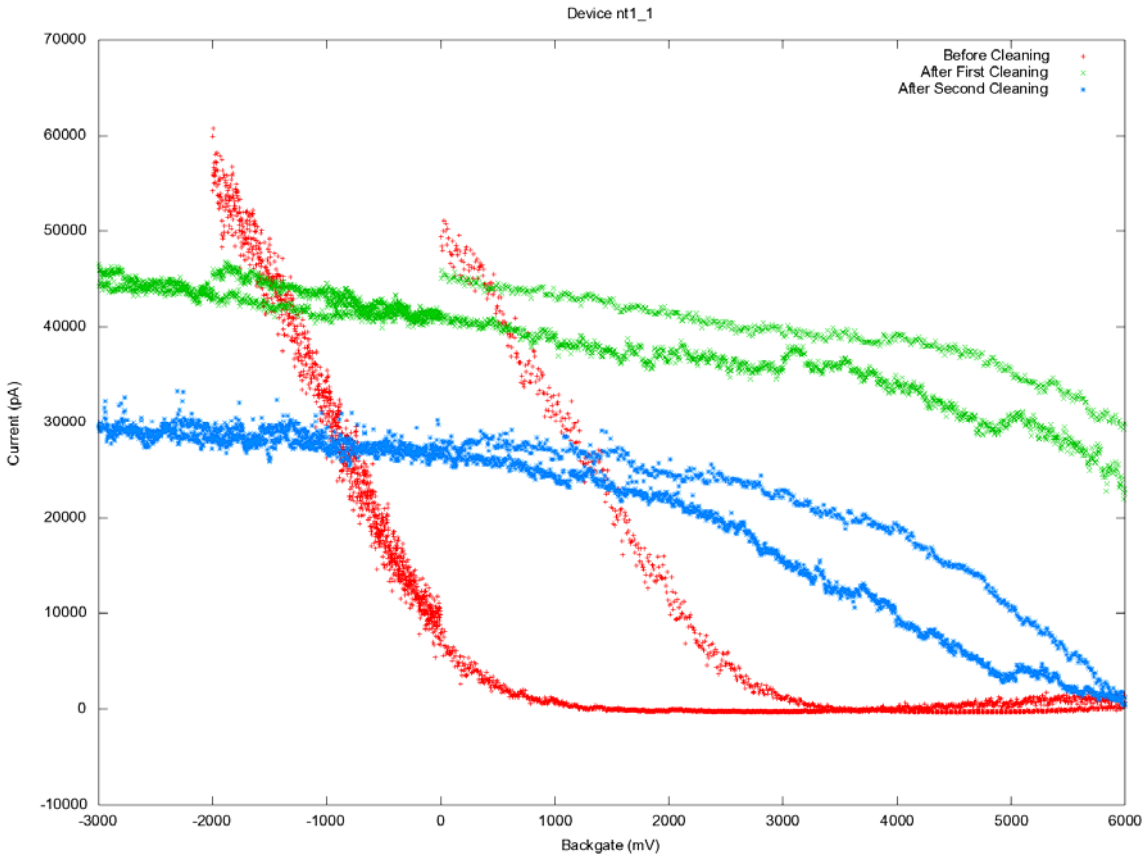

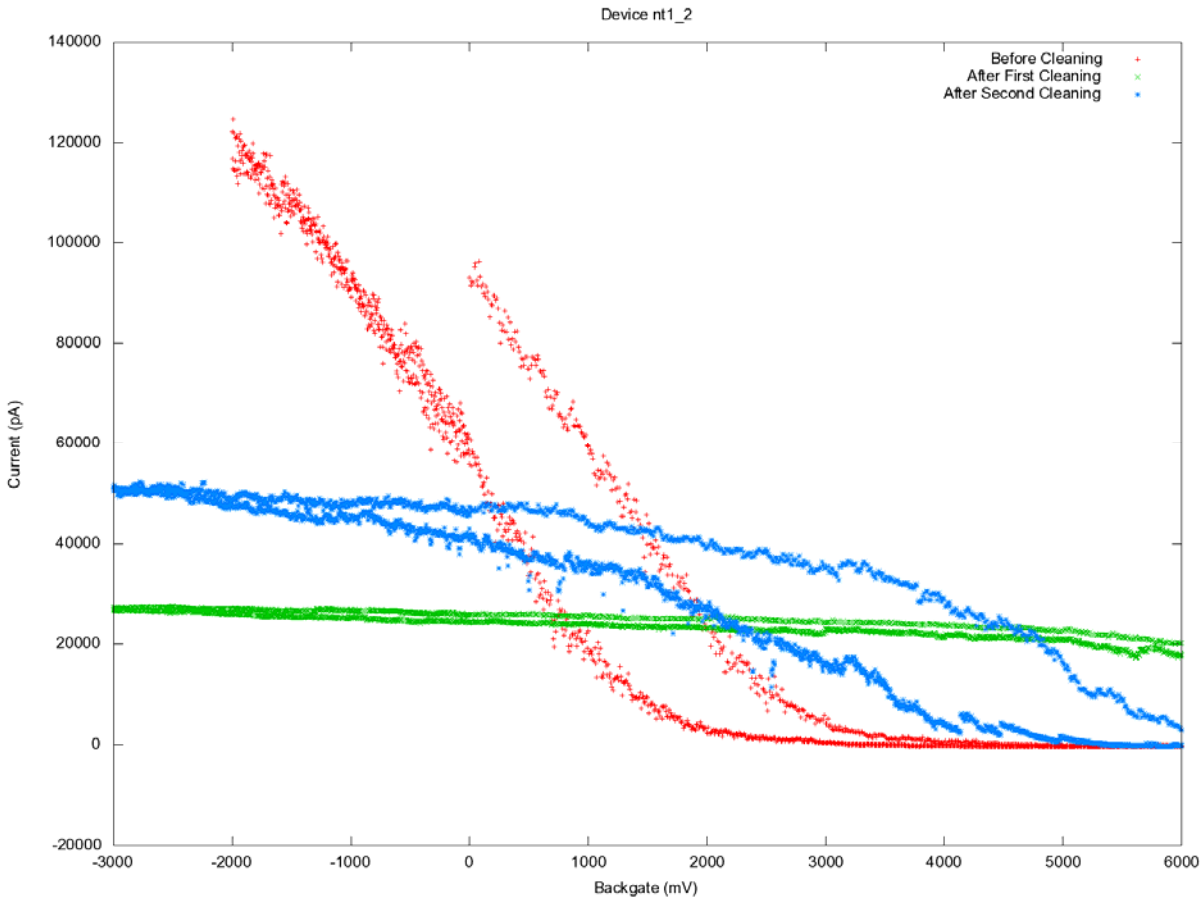
Device nt1_2
Before Cleaning
After First Cleaning
After Second Cleaning
Current (pA)
Backgate (mV)
140000
120000
100000
80000
60000
40000
20000
0
-20000
-3000
-2000
-1000
0
1000
2000
3000
4000
5000
6000

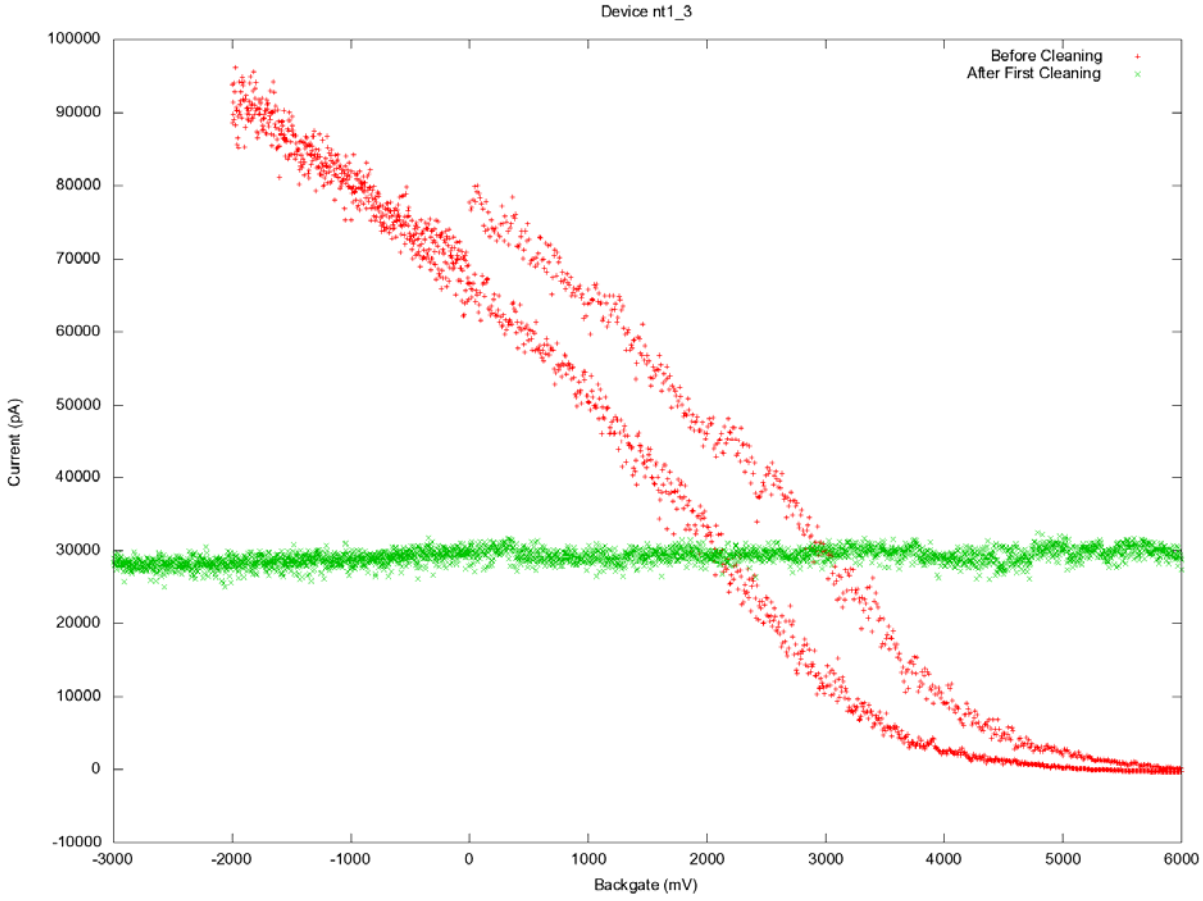
Device nt1_3
Before Cleaning
After First Cleaning
Current (pA)
Backgate (mV)
100000
90000
80000
70000
60000
50000
40000
30000
20000
10000
0
-10000
-3000
-2000
-1000
0
1000
2000
3000
4000
5000
6000

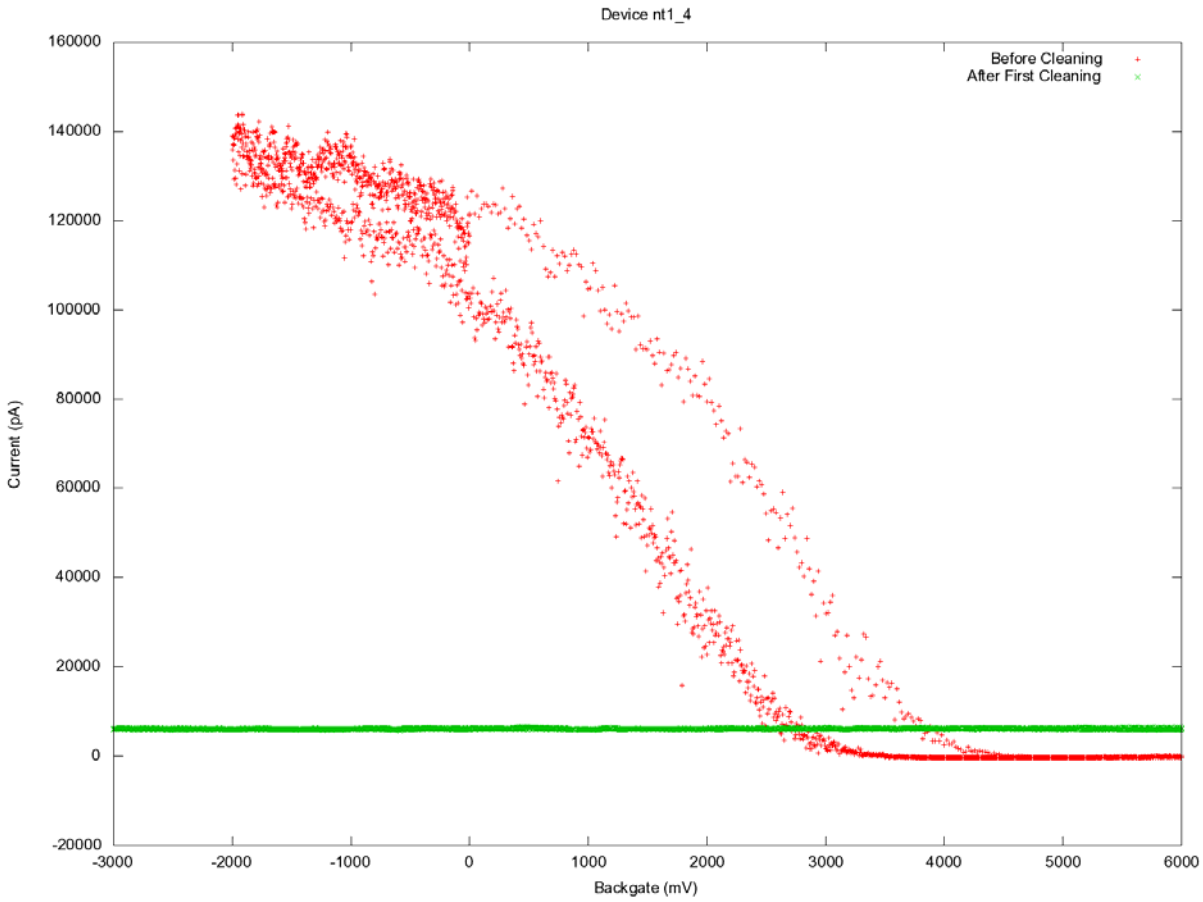
Device nt1_4
Before Cleaning
After First Cleaning
Current (pA)
Backgate (mV)
160000
140000
120000
100000
80000
60000
40000
20000
0
-20000
-3000
-2000
-1000
0
1000
2000
3000
4000
5000
6000

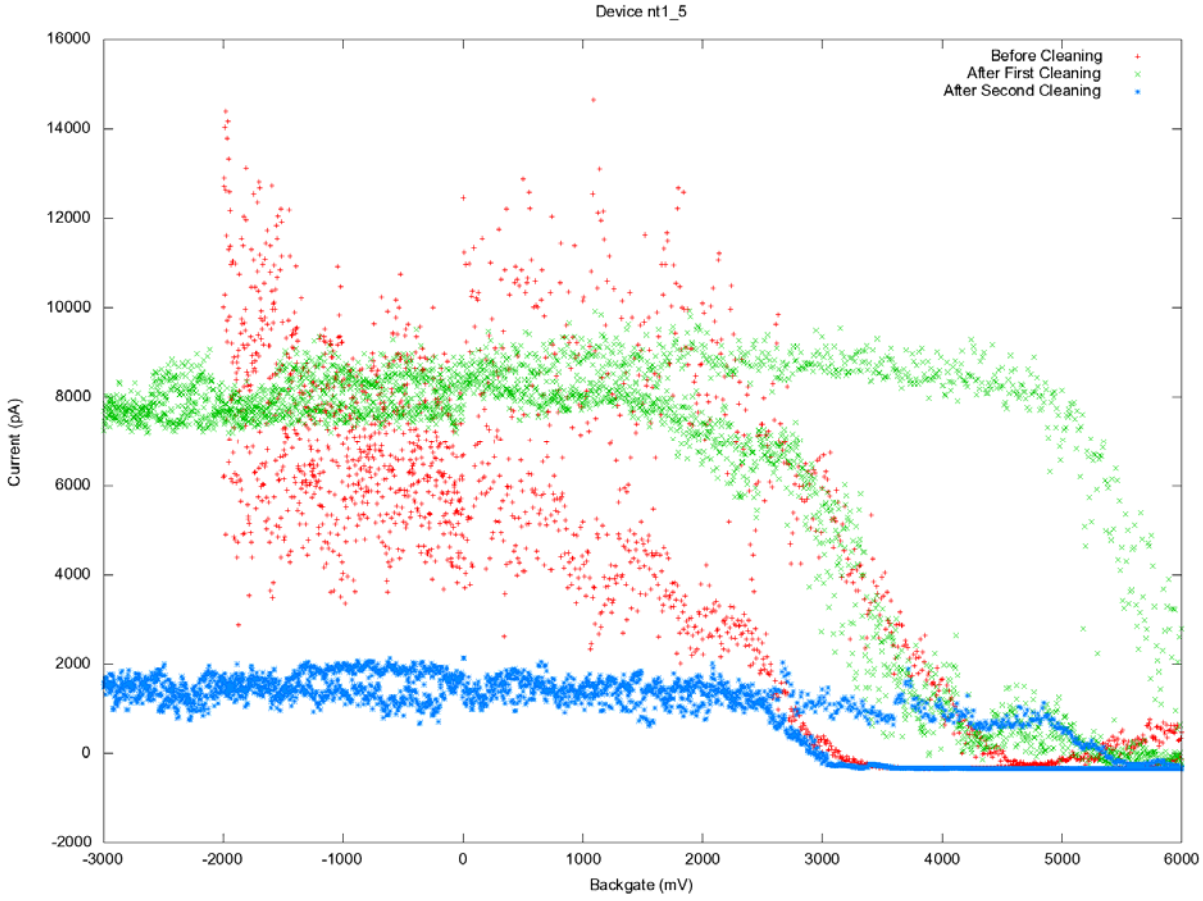
Device nt1_5
Before Cleaning
After First Cleaning
After Second Cleaning
Current (pA)
Backgate (mV)
16000
14000
12000
10000
8000
6000
4000
2000
0
-2000
-3000
-2000
-1000
0
1000
2000
3000
4000
5000
6000

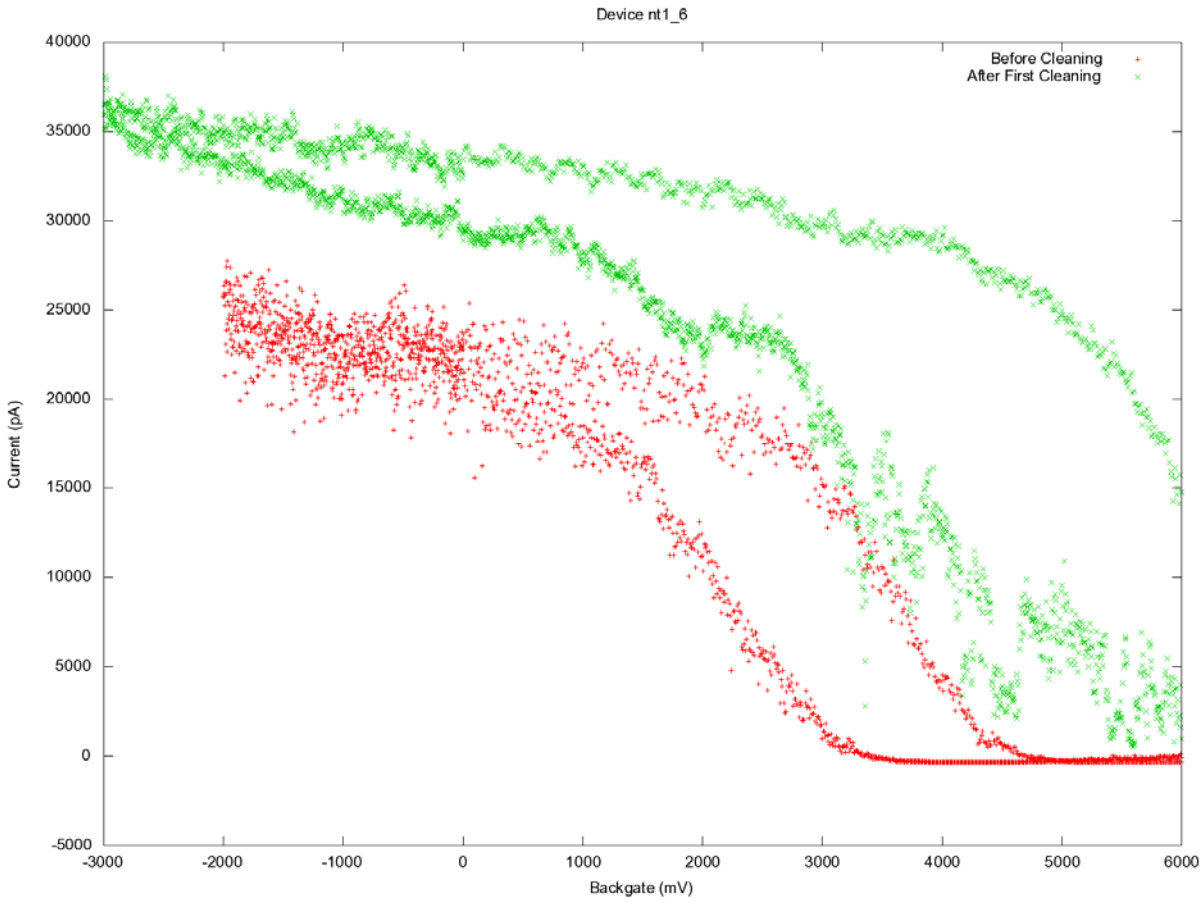
Device nt1_6
Before Cleaning
After First Cleaning
Current (pA)
Backgate (mV)
40000
35000
30000
25000
20000
15000
10000
5000
0
-5000
-3000
-2000
-1000
0
1000
2000
3000
4000
5000
6000

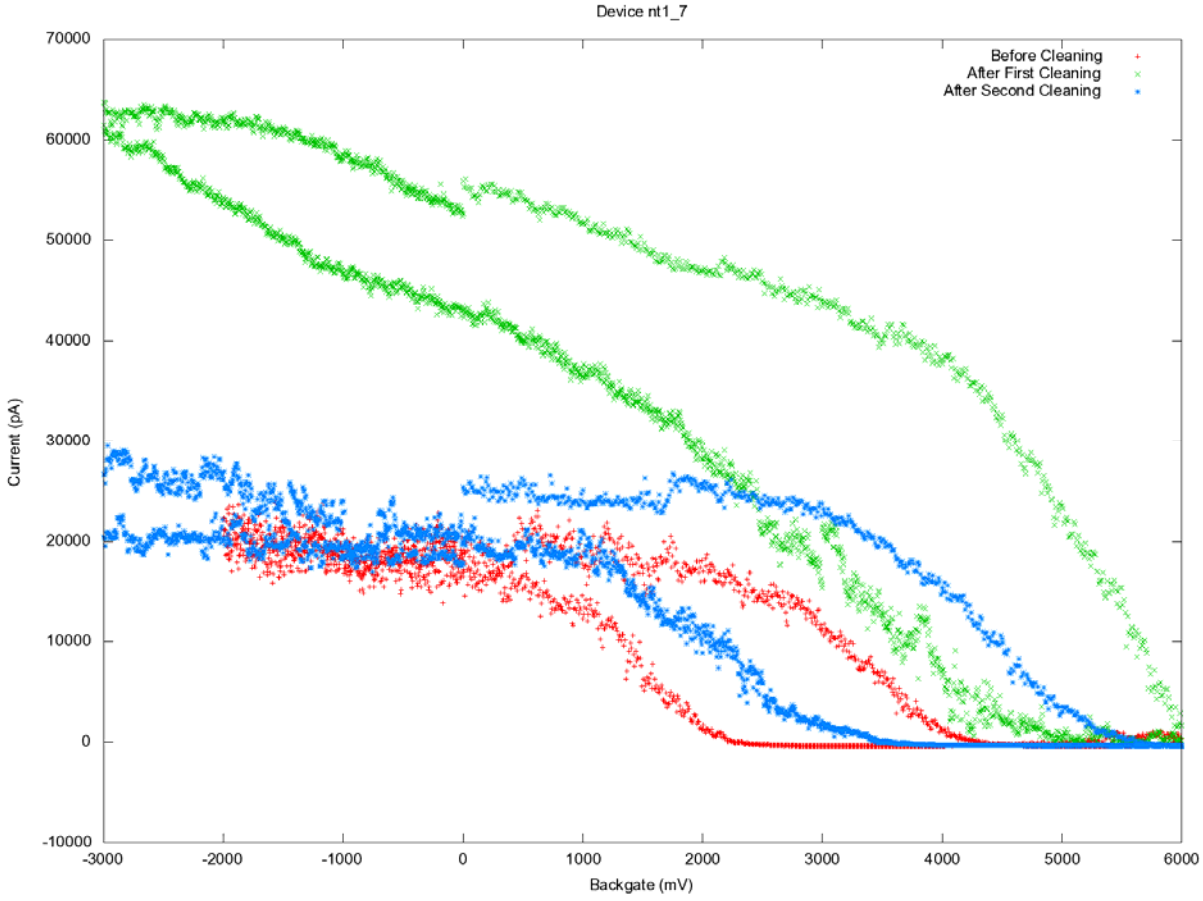
Device nt1_7
Before Cleaning
After First Cleaning
After Second Cleaning
Current (pA)
Backgate (mV)
70000
60000
50000
40000
30000
20000
10000
0
-10000
-3000
-2000
-1000
0
1000
2000
3000
4000
5000
6000

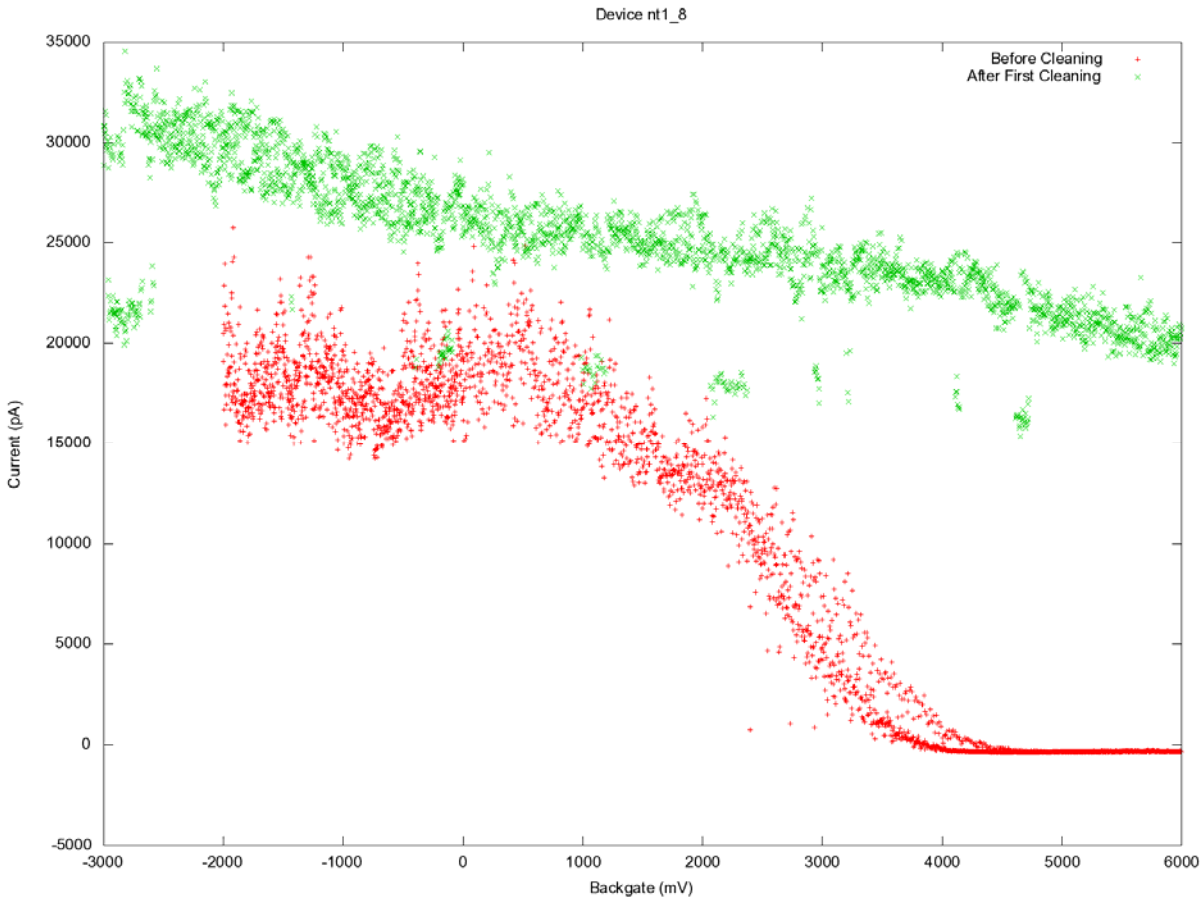
Device nt1_8
Before Cleaning
After First Cleaning
Current (pA)
Backgate (mV)
35000
30000
25000
20000
15000
10000
5000
0
-5000
-3000
-2000
-1000
0
1000
2000
3000
4000
5000
6000

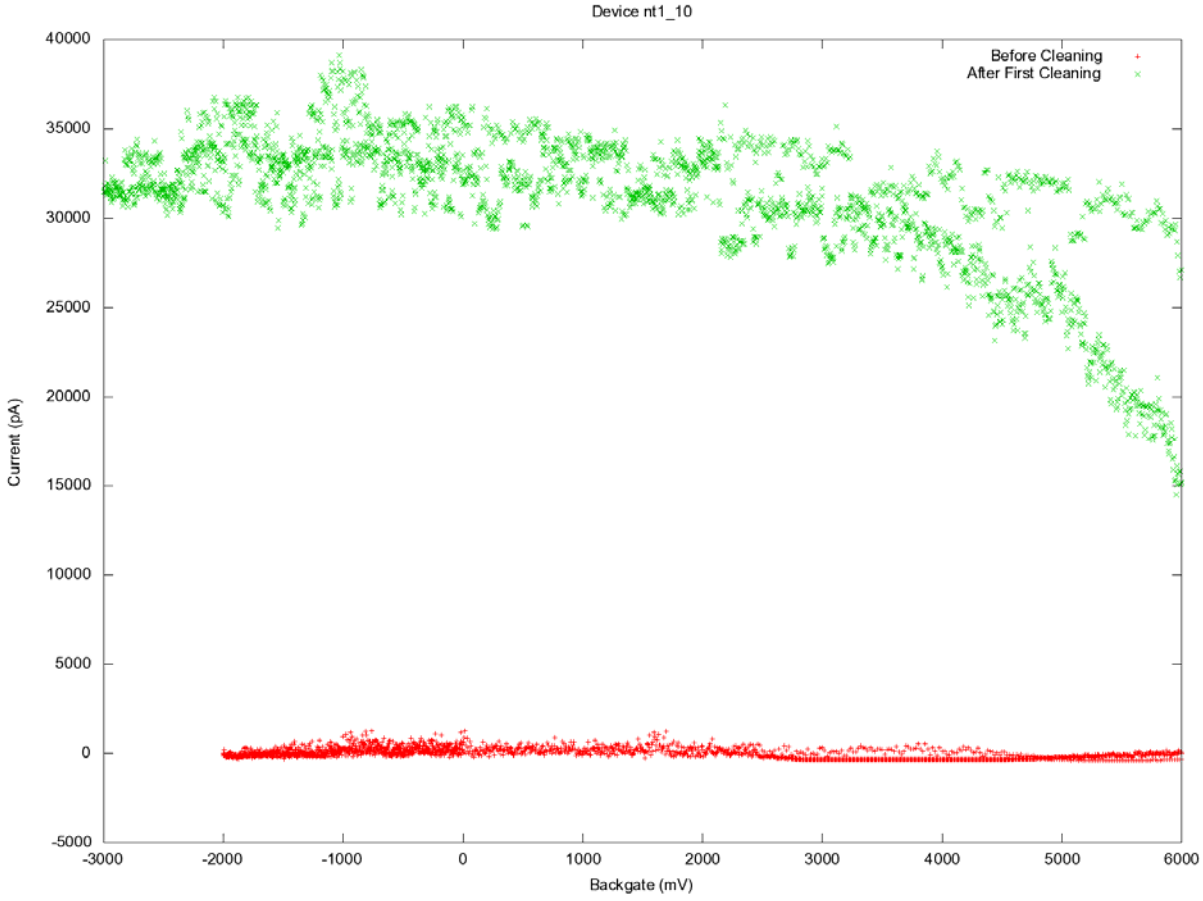
Device nt1_10
Before Cleaning
After First Cleaning
Current (pA)
Backgate (mV)
40000
35000
30000
25000
20000
15000
10000
5000
0
-5000
-3000
-2000
-1000
0
1000
2000
3000
4000
5000
6000

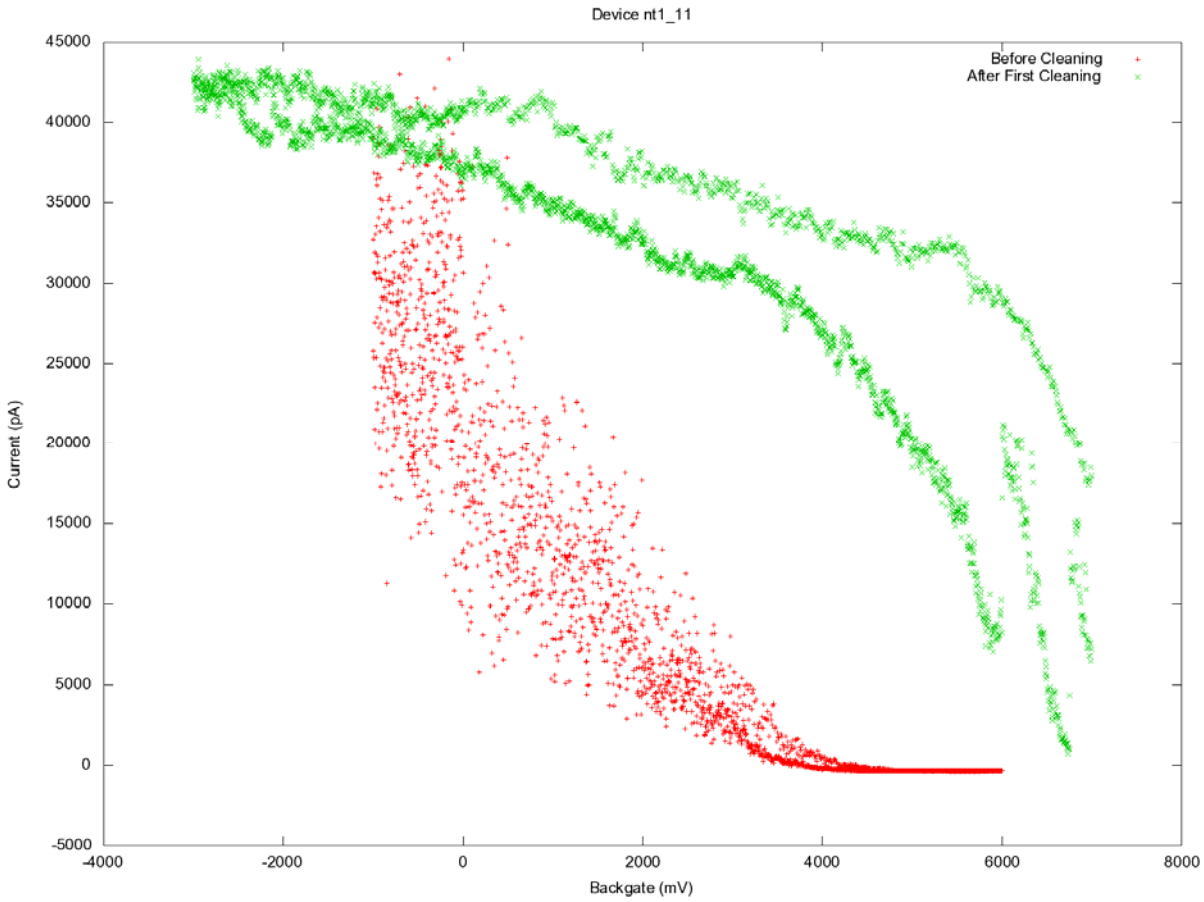
Device nt1_11
Before Cleaning
After First Cleaning
Current (pA)
Backgate (mV)
45000
40000
35000
30000
25000
20000
15000
10000
5000
0
-5000
-4000
-2000
0
2000
4000
6000
8000

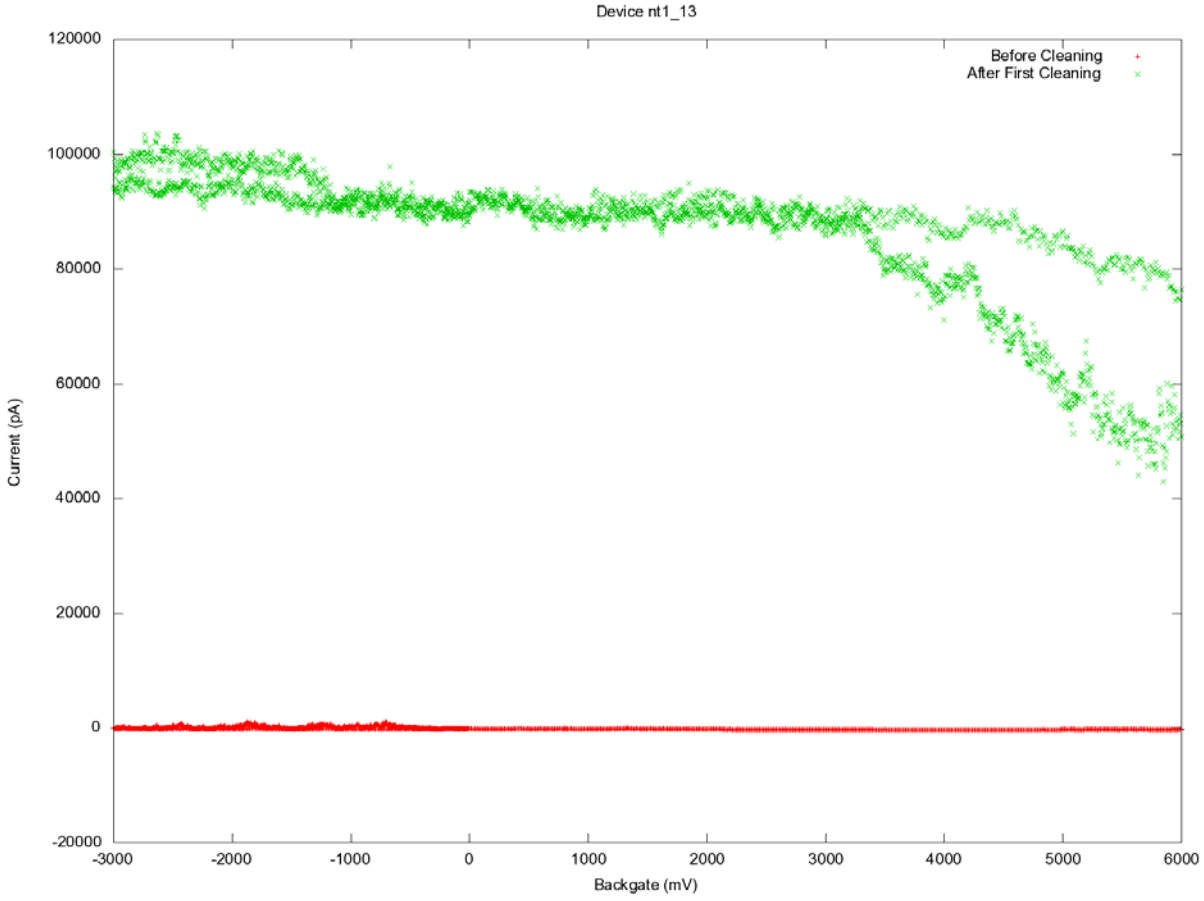
Device nt1_13
Before Cleaning
After First Cleaning
Current (pA)
Backgate (mV)
120000
100000
80000
60000
40000
20000
0
-20000
-3000
-2000
-1000
0
1000
2000
3000
4000
5000
6000

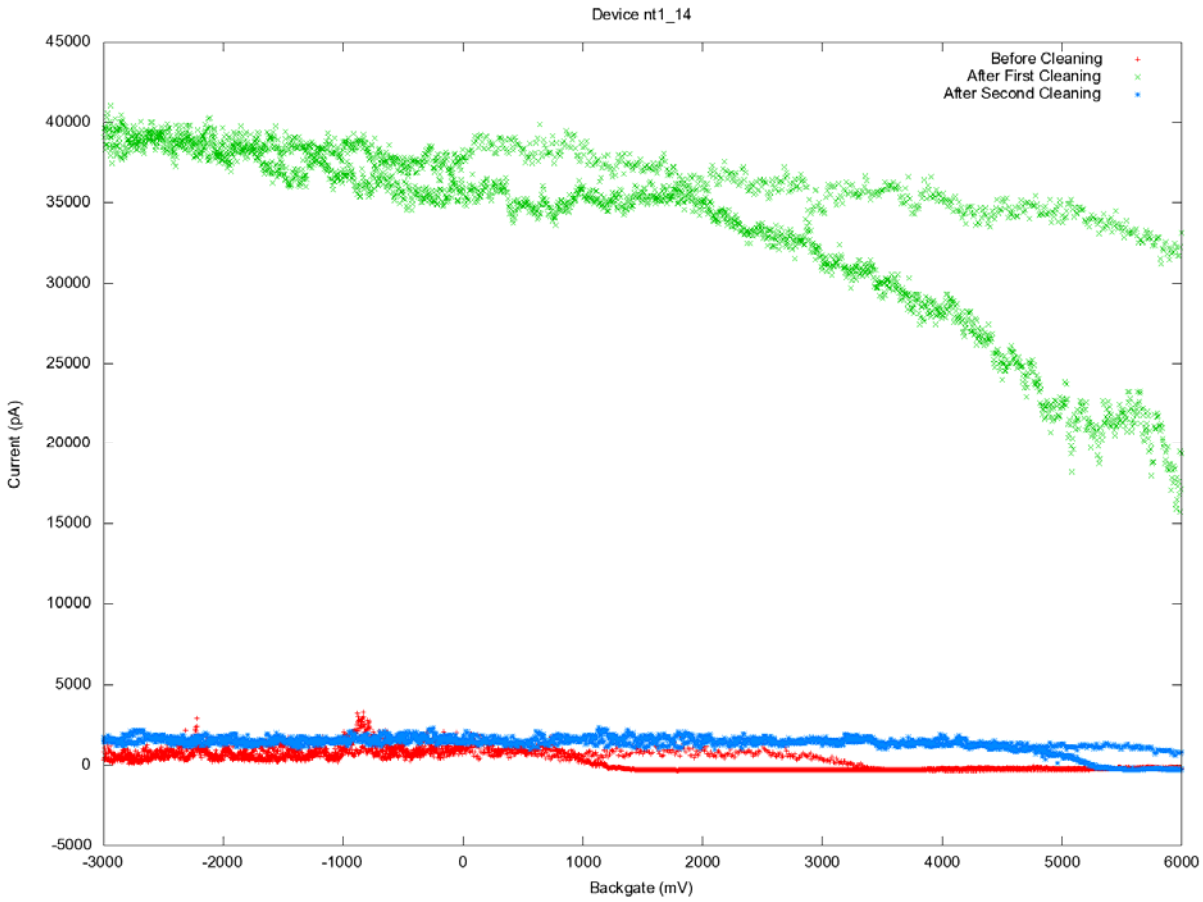
Device nt1_14
Before Cleaning
After First Cleaning
After Second Cleaning
Current (pA)
Backgate (mV)
45000
40000
35000
30000
25000
20000
15000
10000
5000
0
-5000
-3000
-2000
-1000
0
1000
2000
3000
4000
5000
6000

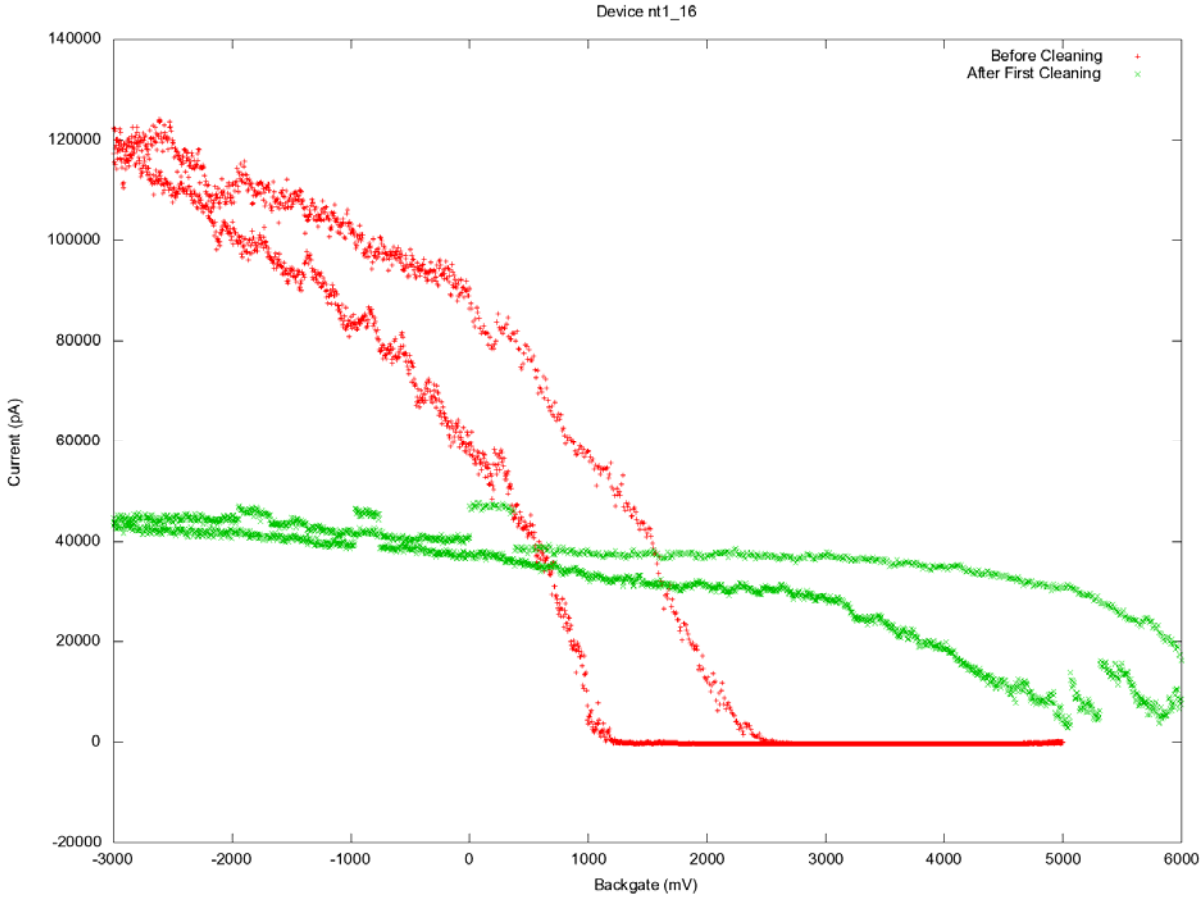
Device nt1_16
Before Cleaning
After First Cleaning
Current (pA)
Backgate (mV)
140000
120000
100000
80000
60000
40000
20000
0
-20000
-3000
-2000
-1000
0
1000
2000
3000
4000
5000
6000

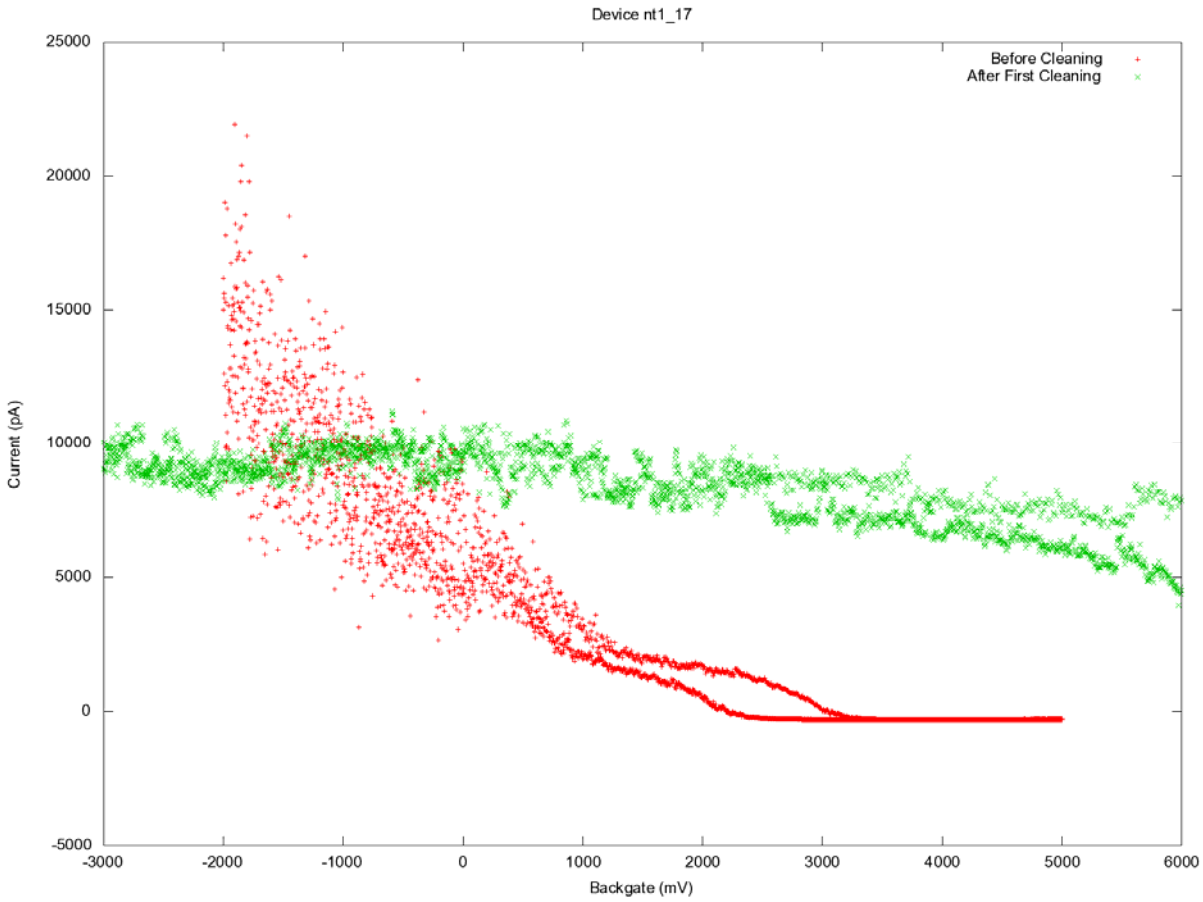
Device nt1_17
Before Cleaning
After First Cleaning
Current (pA)
Backgate (mV)
25000
20000
15000
10000
5000
0
-5000
-3000
-2000
-1000
0
1000
2000
3000
4000
5000
6000

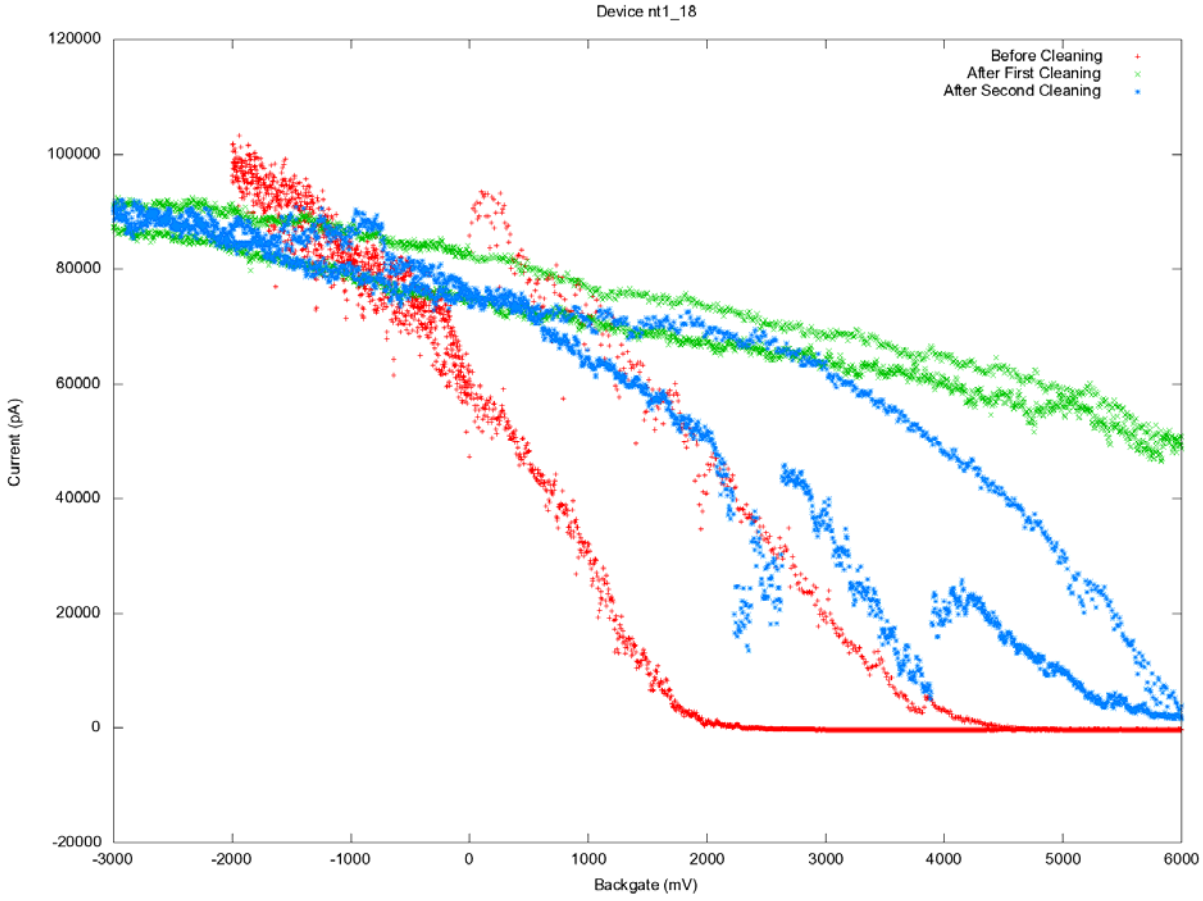
Device nt1_18
Before Cleaning
After First Cleaning
After Second Cleaning
Current (pA)
Backgate (mV)
120000
100000
80000
60000
40000
20000
0
-20000
-3000
-2000
-1000
0
1000
2000
3000
4000
5000
6000

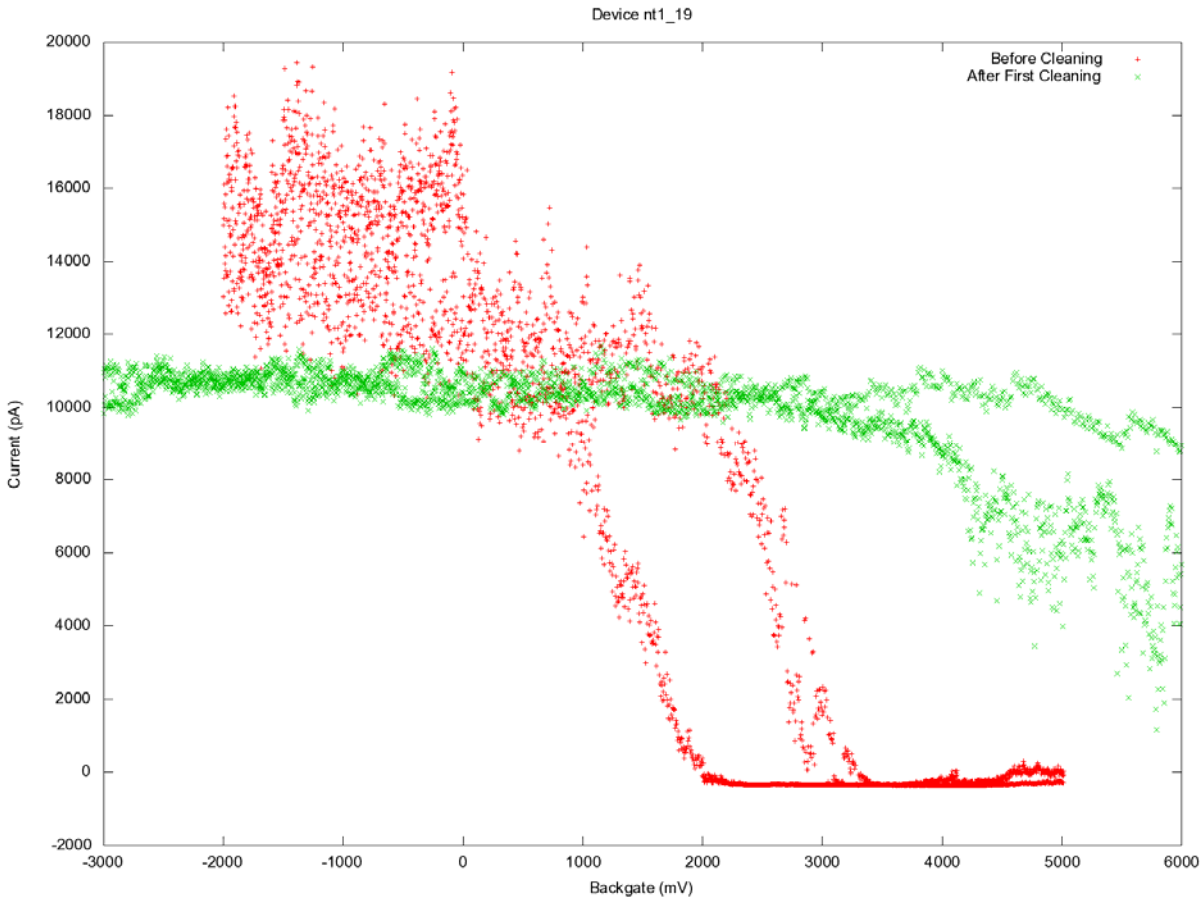
Device nt1_19
Before Cleaning
After First Cleaning
Current (pA)
Backgate (mV)
20000
18000
16000
14000
12000
10000
8000
6000
4000
2000
0
-2000
-3000
-2000
-1000
0
1000
2000
3000
4000
5000
6000

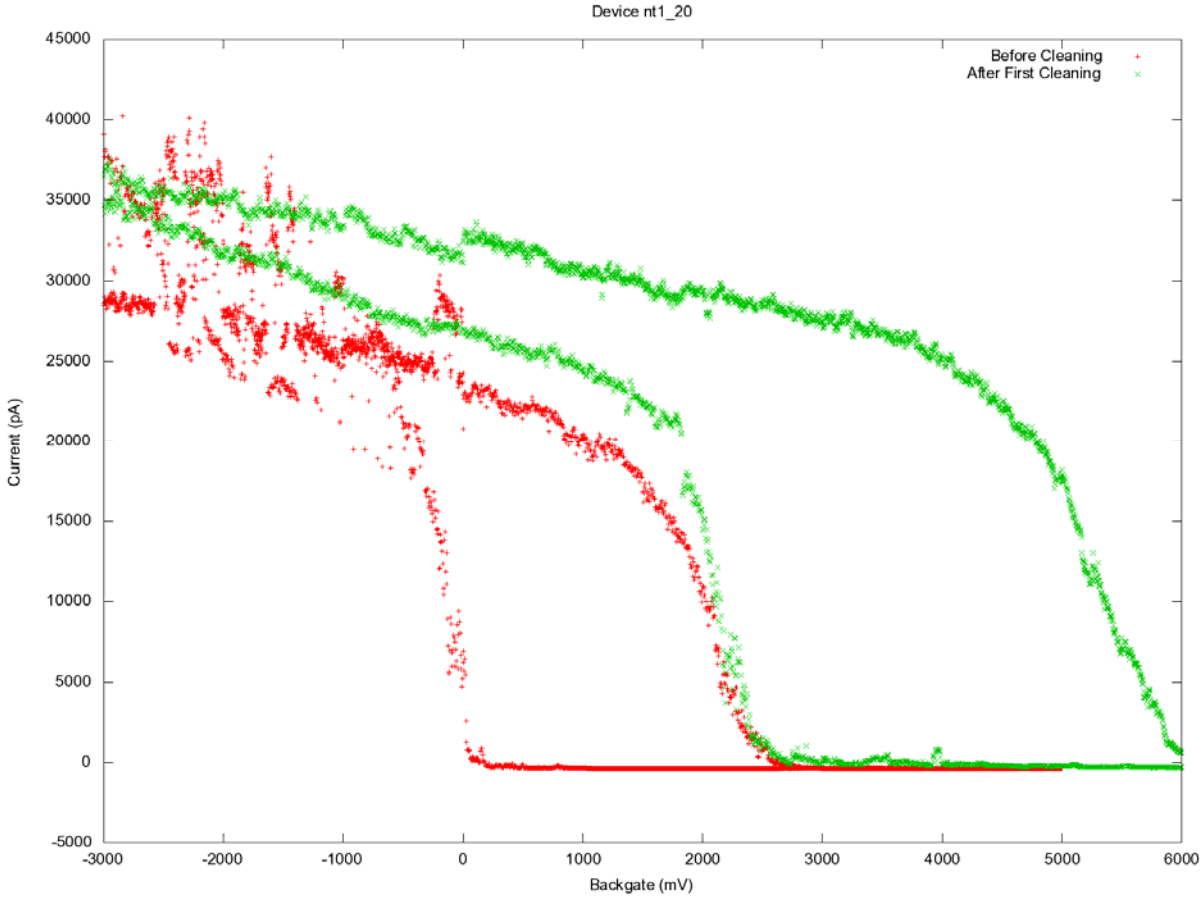
Device nt1_20
Before Cleaning
After First Cleaning
Current (pA)
Backgate (mV)
45000
40000
35000
30000
25000
20000
15000
10000
5000
0
-5000
-3000
-2000
-1000
0
1000
2000
3000
4000
5000
6000

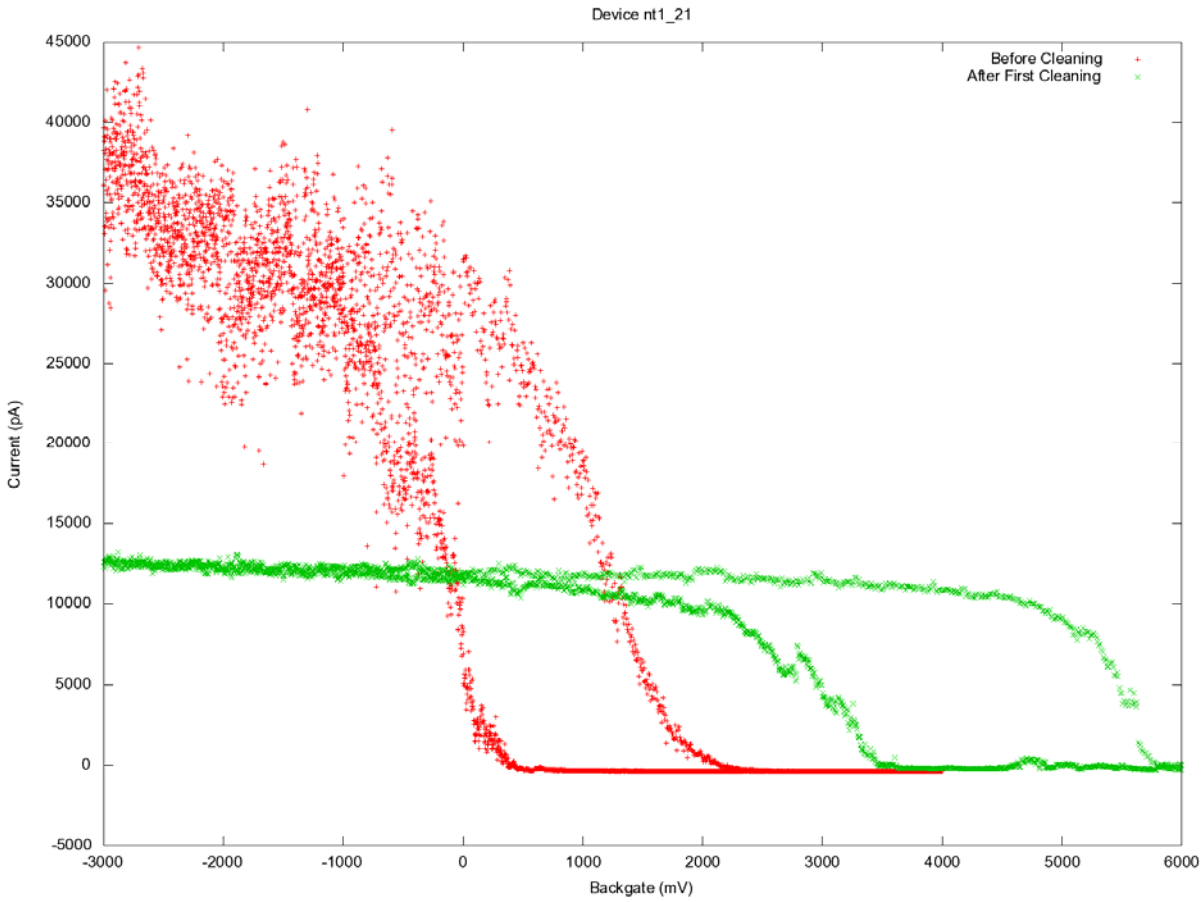
Device nt1_21
Before Cleaning
After First Cleaning
Current (pA)
Backgate (mV)
45000
40000
35000
30000
25000
20000
15000
10000
5000
0
-5000
-3000
-2000
-1000
0
1000
2000
3000
4000
5000
6000

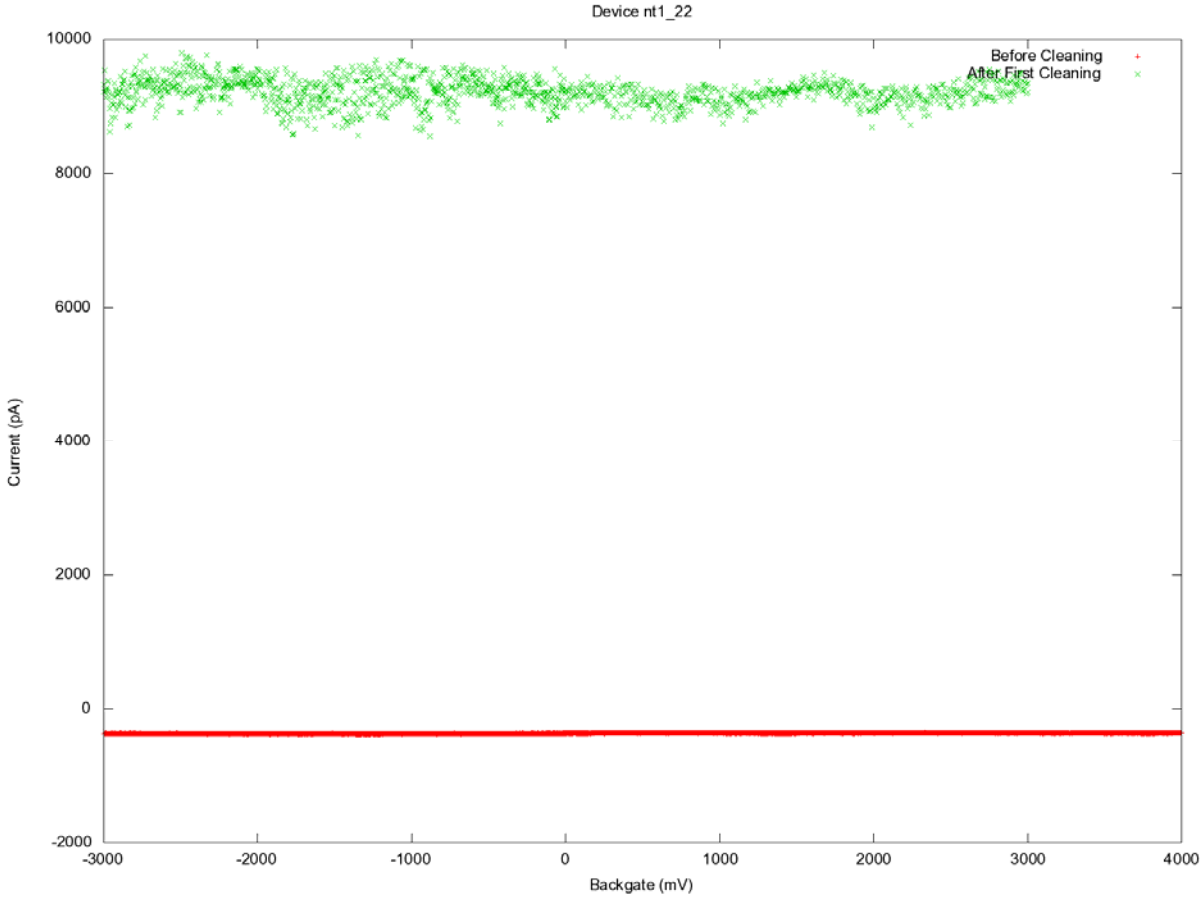
Device nt1_22
Before Cleaning
After First Cleaning
Current (pA)
Backgate (mV)
10000
8000
6000
4000
2000
0
-2000
-3000
-2000
-1000
0
1000
2000
3000
4000

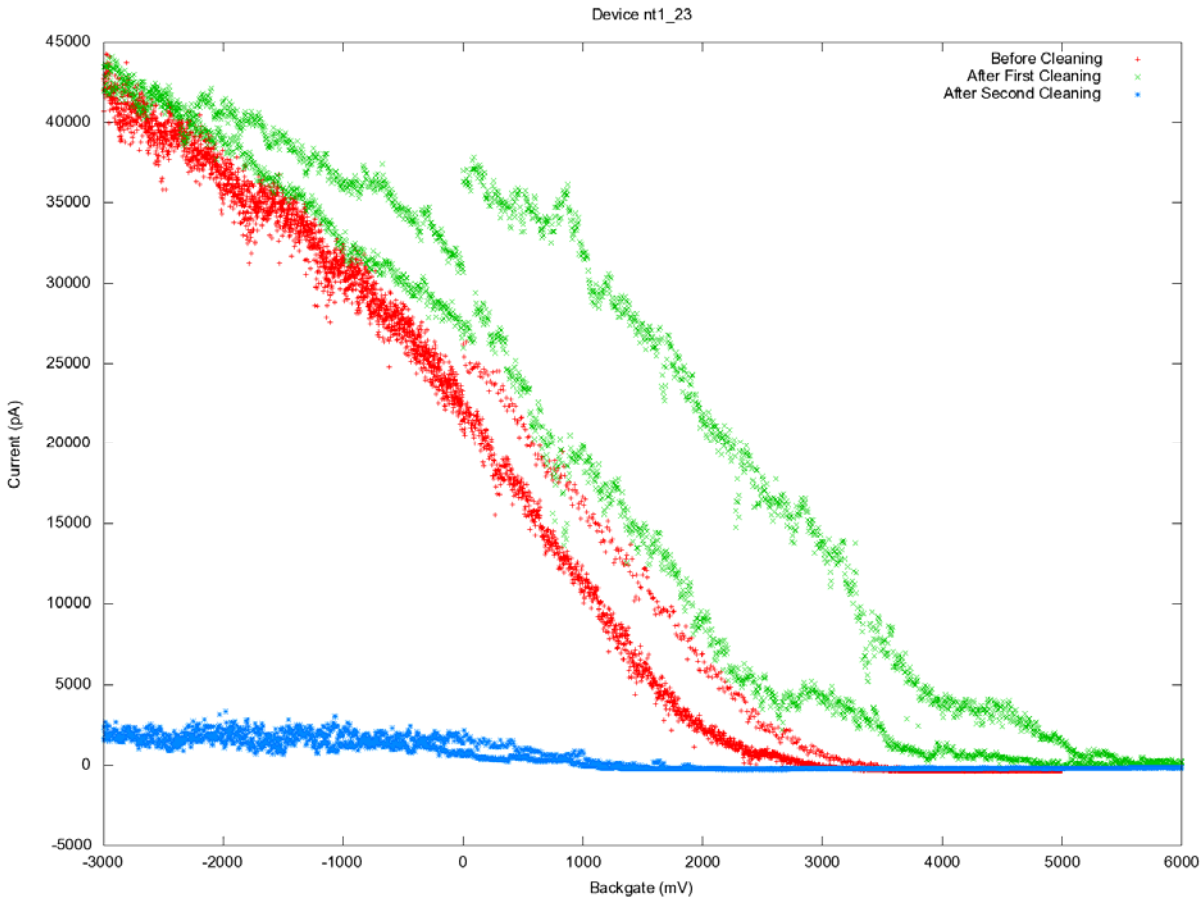
Device nt1_23
Before Cleaning
After First Cleaning
After Second Cleaning
Current (pA)
Backgate (mV)
45000
40000
35000
30000
25000
20000
15000
10000
5000
0
-5000
-3000
-2000
-1000
0
1000
2000
3000
4000
5000
6000

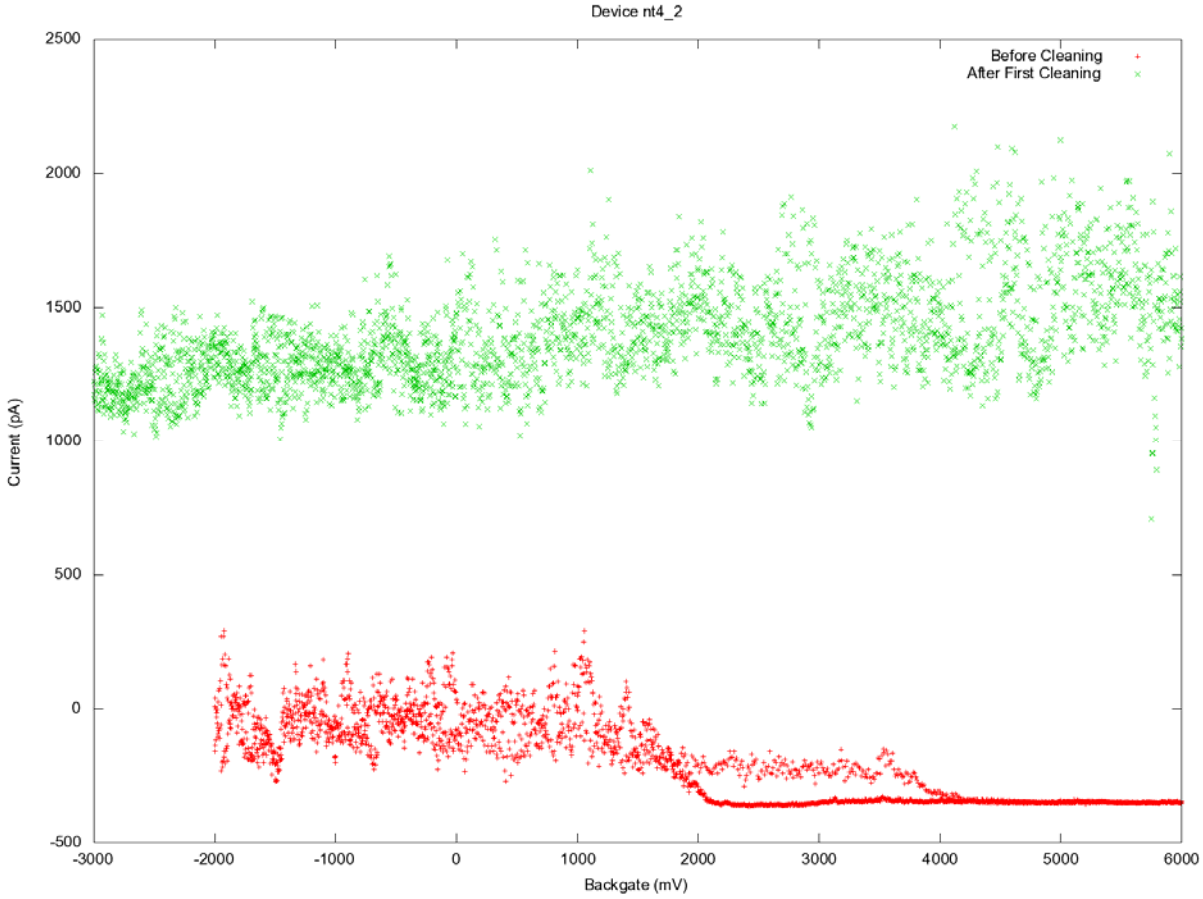
Device nt4_2
Before Cleaning
After First Cleaning
Current (pA)
Backgate (mV)
2500
2000
1500
1000
500
0
-500
-3000
-2000
-1000
0
1000
2000
3000
4000
5000
6000

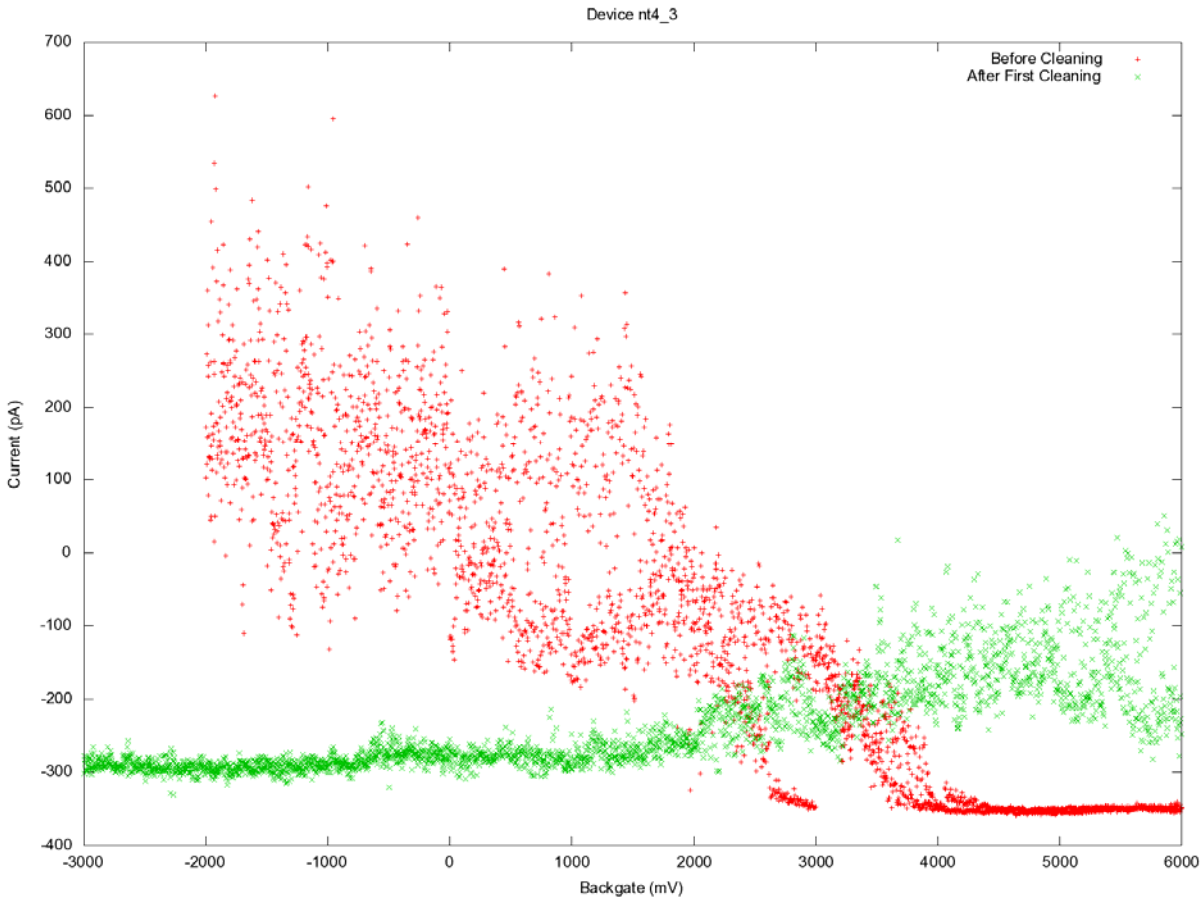
Device nt4_3
Before Cleaning
After First Cleaning
Current (pA)
Backgate (mV)
700
600
500
400
300
200
100
0
-100
-200
-300
-400
-3000
-2000
-1000
0
1000
2000
3000
4000
5000
6000

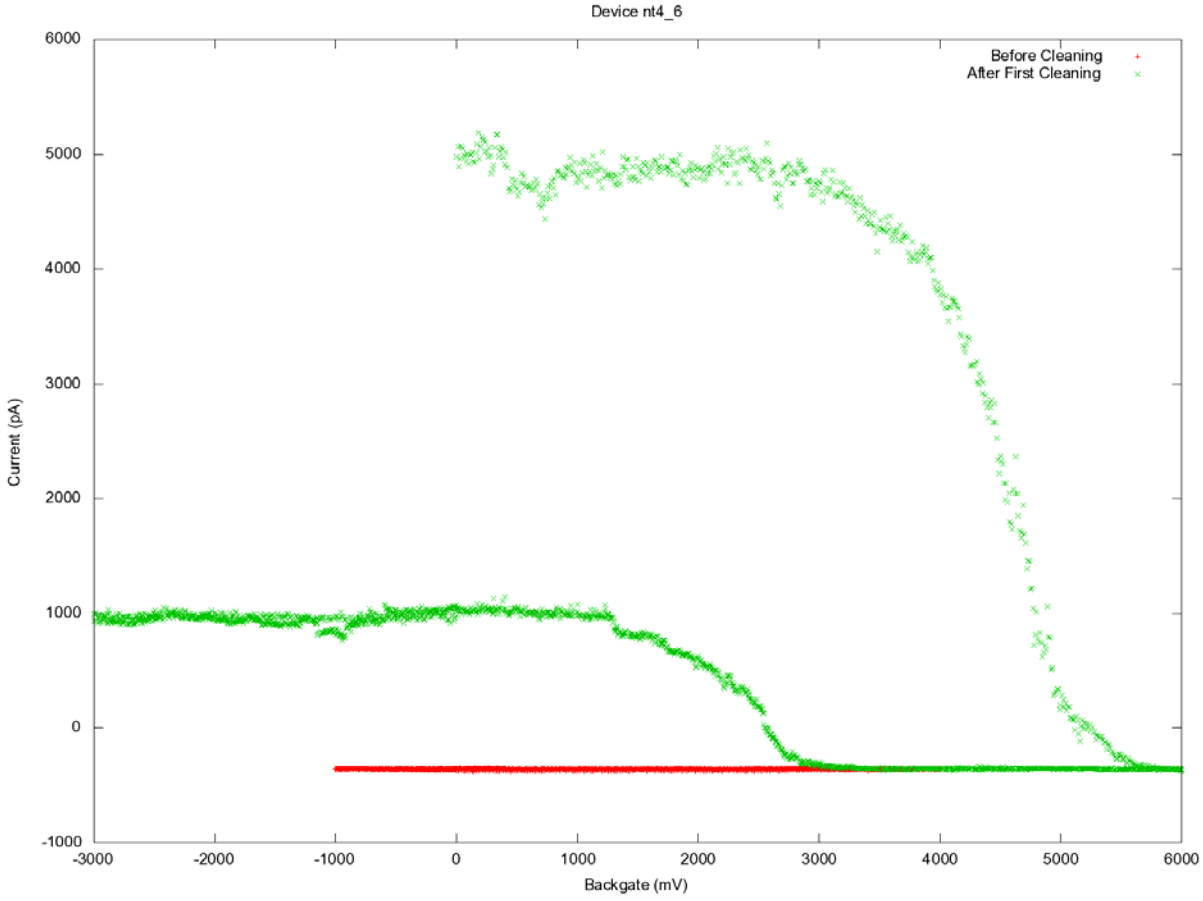
Device nt4_6
Before Cleaning
After First Cleaning
Current (pA)
Backgate (mV)
6000
5000
4000
3000
2000
1000
0
-1000
-3000
-2000
-1000
0
1000
2000
3000
4000
5000
6000

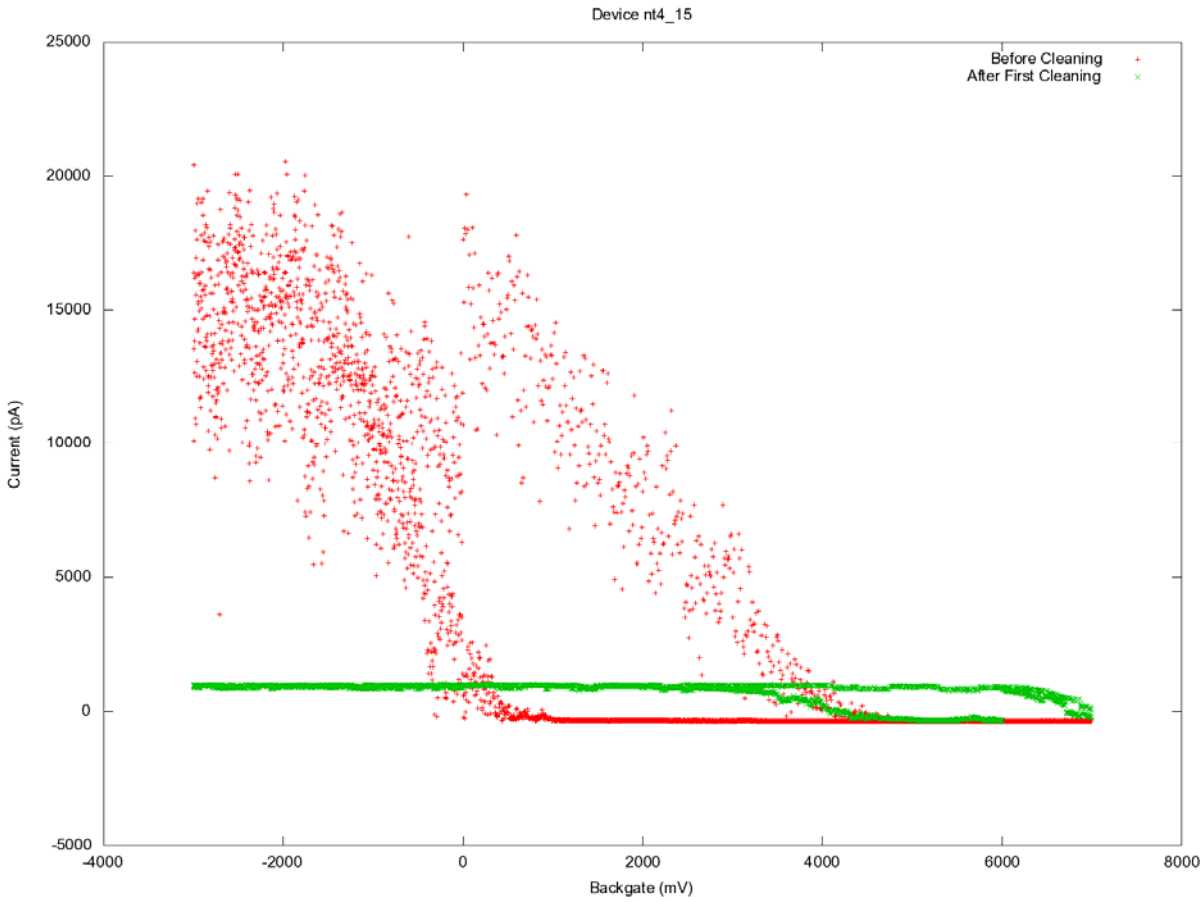
Device nt4_15
Before Cleaning
After First Cleaning
Current (pA)
Backgate (mV)
25000
20000
15000
10000
5000
0
-5000
-4000
-2000
0
2000
4000
6000
8000

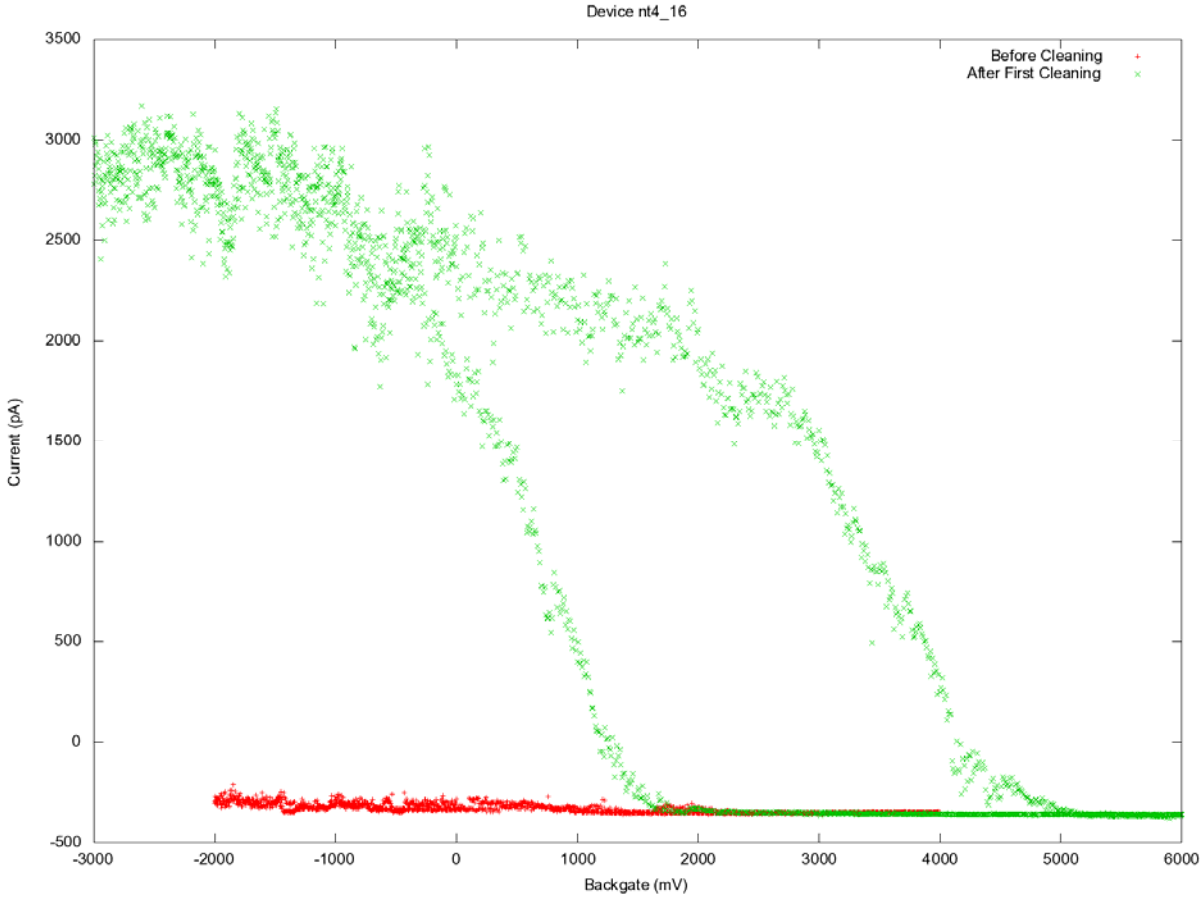
Device nt4_16
Before Cleaning
After First Cleaning
Current (pA)
Backgate (mV)
3500
3000
2500
2000
1500
1000
500
0
-500
-3000
-2000
-1000
0
1000
2000
3000
4000
5000
6000

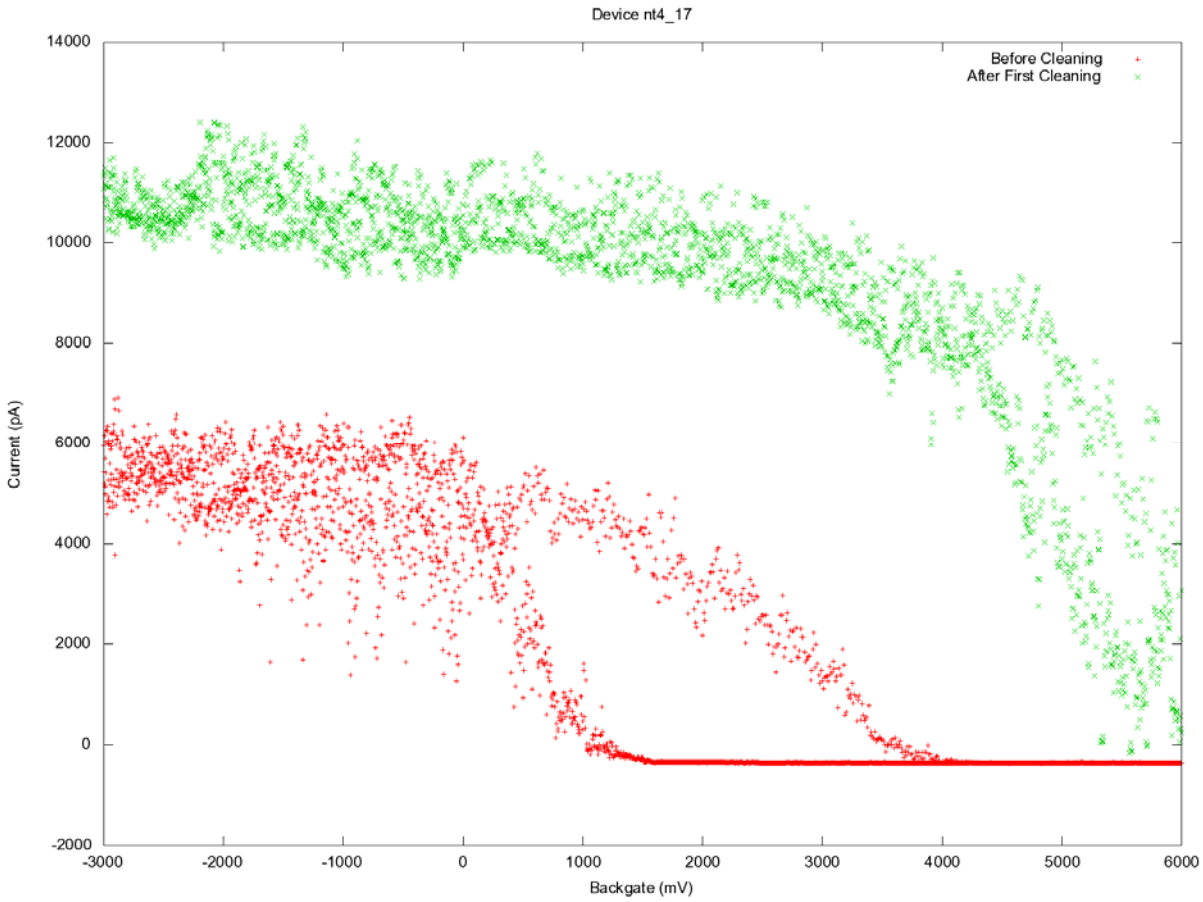
Device nt4_17
Before Cleaning
After First Cleaning
Current (pA)
Backgate (mV)
14000
12000
10000
8000
6000
4000
2000
0
-2000
-3000
-2000
-1000
0
1000
2000
3000
4000
5000
6000

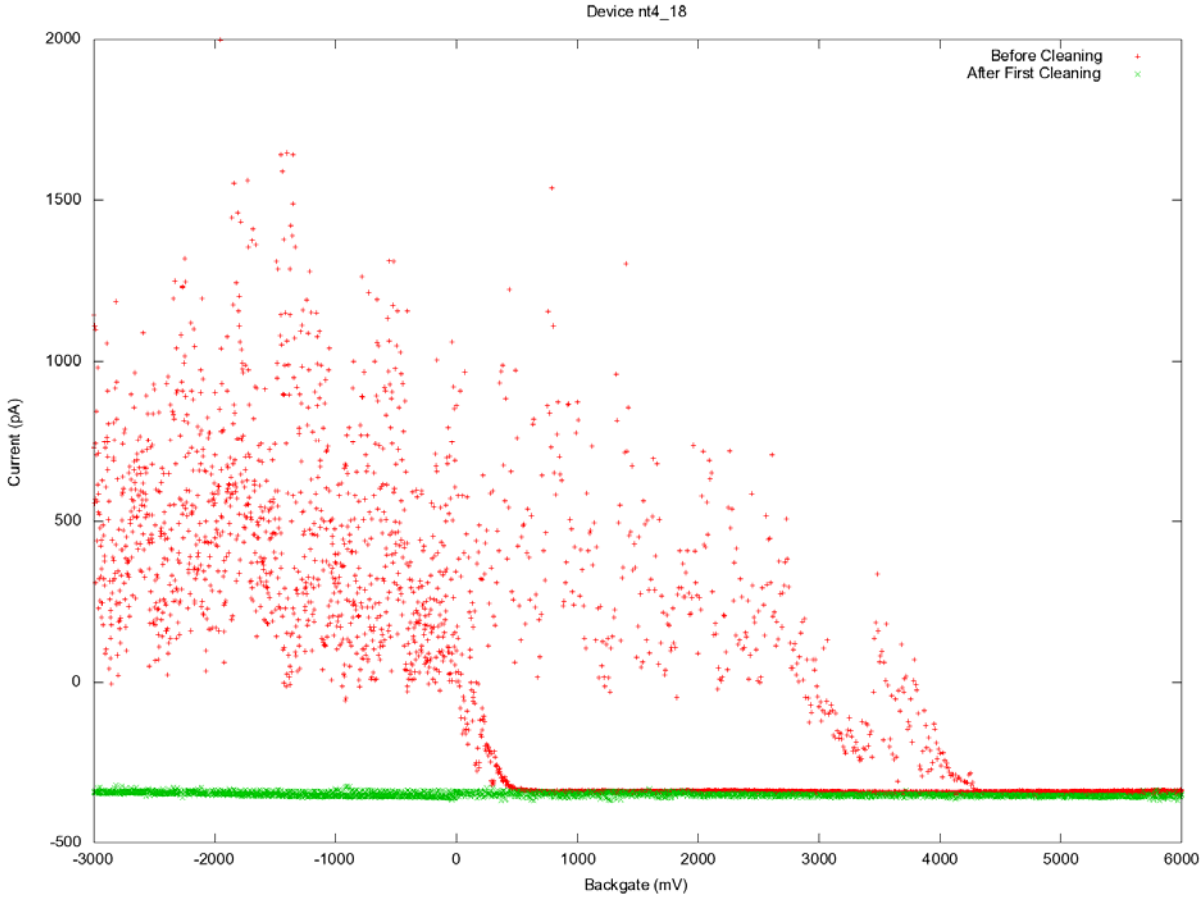
Device nt4_18
Before Cleaning
After First Cleaning
Current (pA)
Backgate (mV)
2000
1500
1000
500
0
-500
-3000
-2000
-1000
0
1000
2000
3000
4000
5000
6000

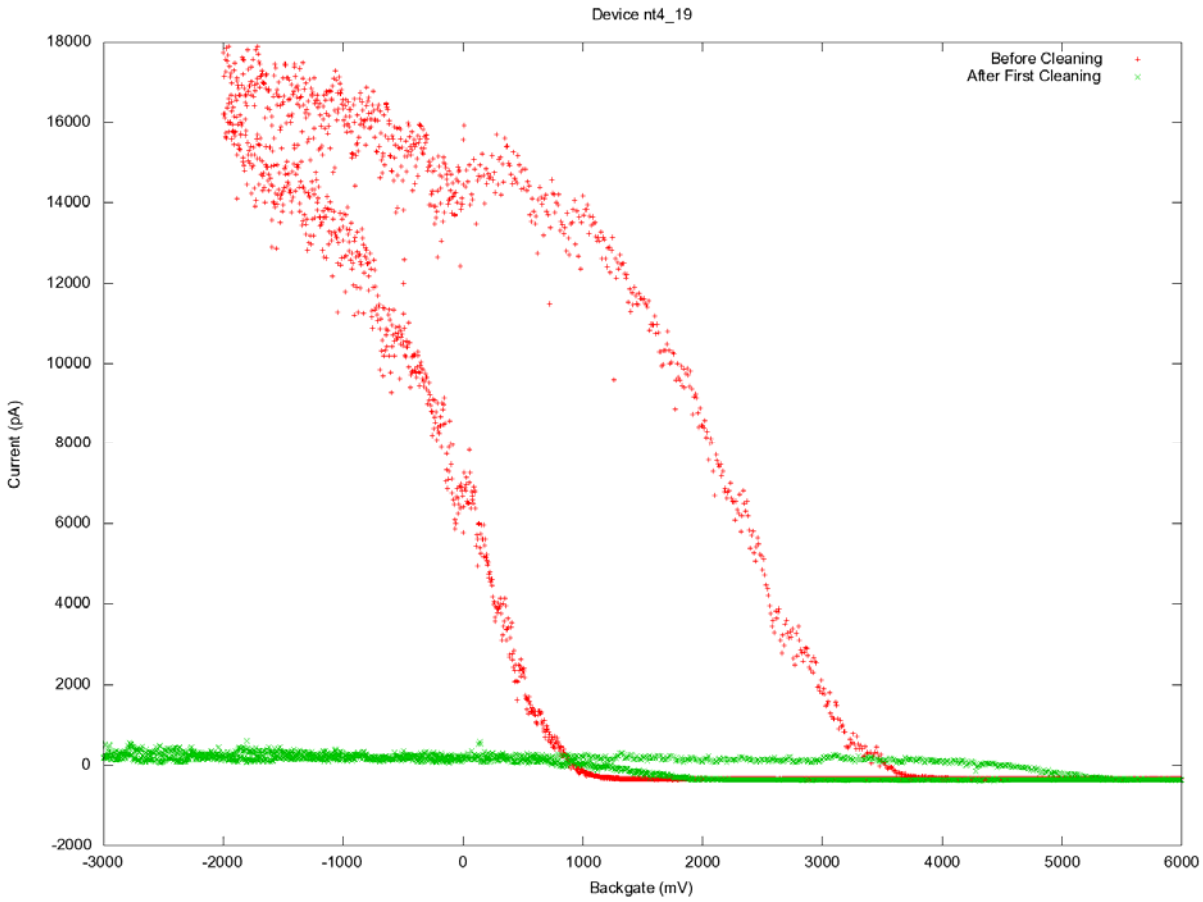
Device nt4_19
Before Cleaning
After First Cleaning
Current (pA)
Backgate (mV)
18000
16000
14000
12000
10000
8000
6000
4000
2000
0
-2000
-3000
-2000
-1000
0
1000
2000
3000
4000
5000
6000

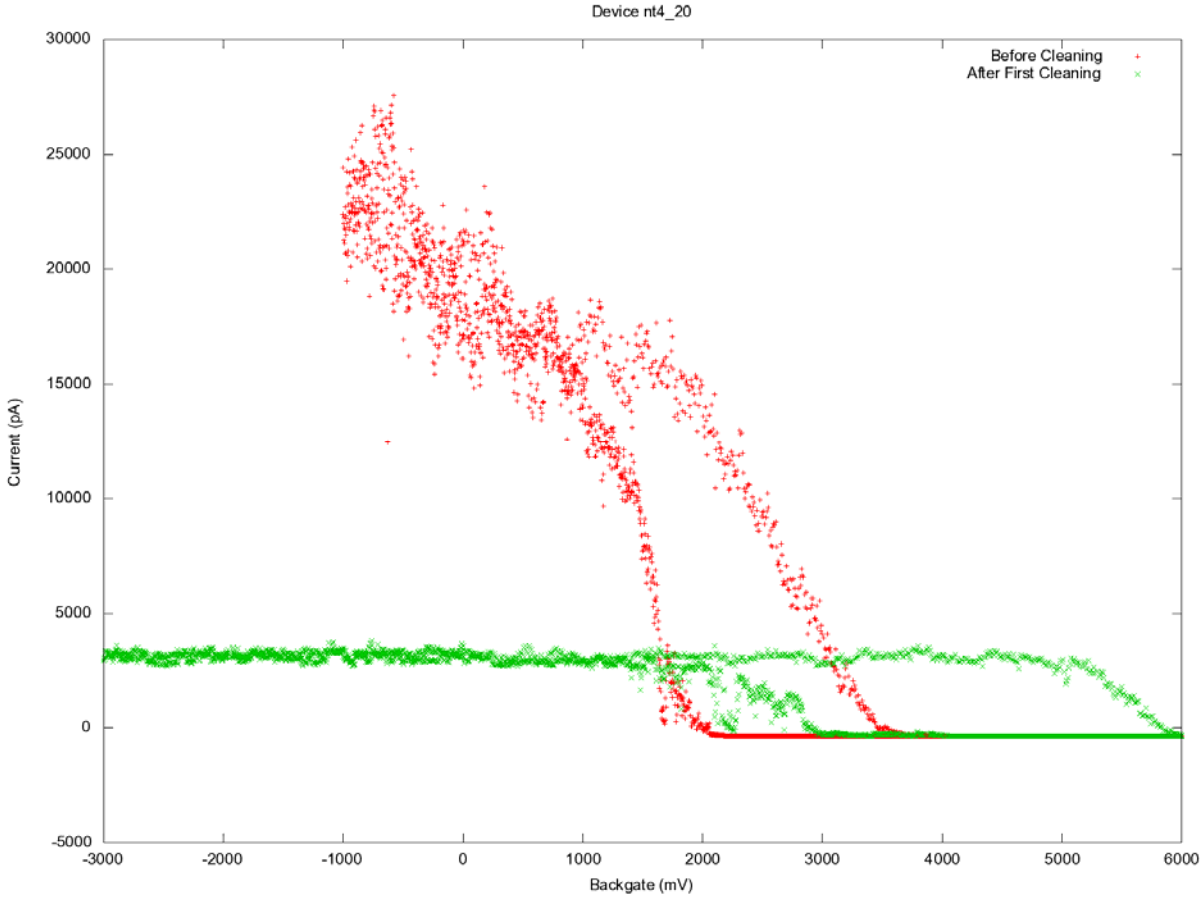
Device nt4_20
Before Cleaning
After First Cleaning
Current (pA)
Backgate (mV)
30000
25000
20000
15000
10000
5000
0
-5000
-3000
-2000
-1000
0
1000
2000
3000
4000
5000
6000

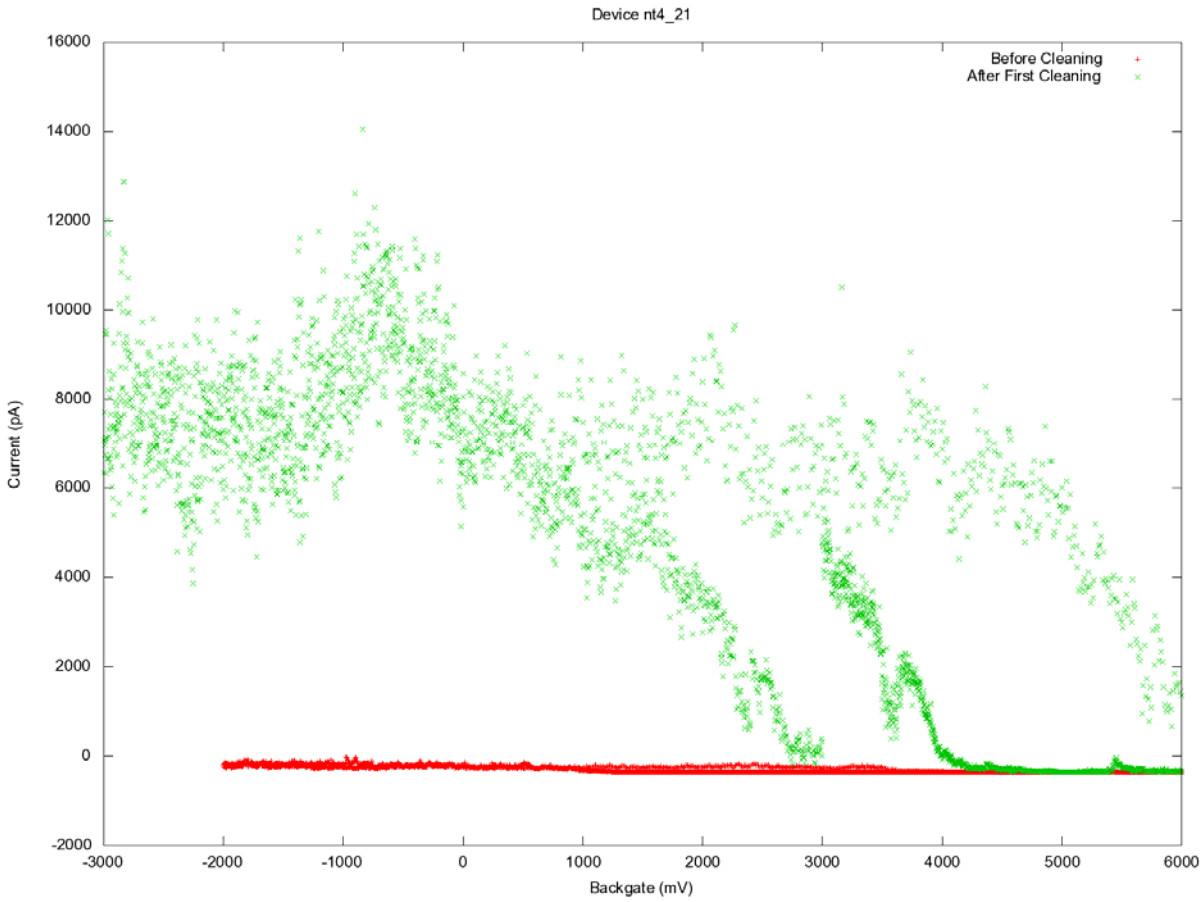
Device nt4_21
Before Cleaning
After First Cleaning
Current (pA)
Backgate (mV)
16000
14000
12000
10000
8000
6000
4000
2000
0
-2000
-3000
-2000
-1000
0
1000
2000
3000
4000
5000
6000